IITM Earth System Model: Goals, Priorities, Future Plans

R. Krishnan
Indian Institute of Tropical Meteorology, Pune, India

Workshop on CLIMATE STUDIES

TIFR - International Centre for Theoretical Sciences (TIFR-ICTS), Bengaluru

1–3 March 2022

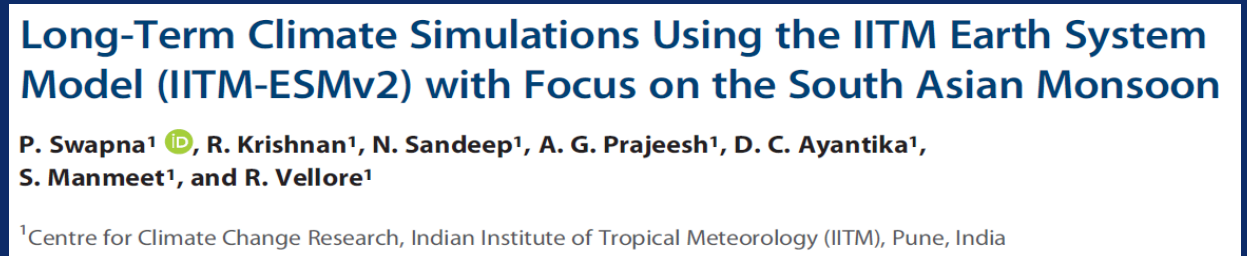

Long-Term Climate Simulations Using the IITM Earth System Model (IITM-ESMv2) with Focus on the South Asian Monsoon

P. Swapna[1], R. Krishnan[1], N. Sandeep[1], A. G. Prajeesh[1], D. C. Ayantika[1], S. Manmeet[1], and R. Vellore[1]

[1]Centre for Climate Change Research, Indian Institute of Tropical Meteorology (IITM), Pune, India

Numerical modelling & prediction linked to scales of weather & climate phenomena

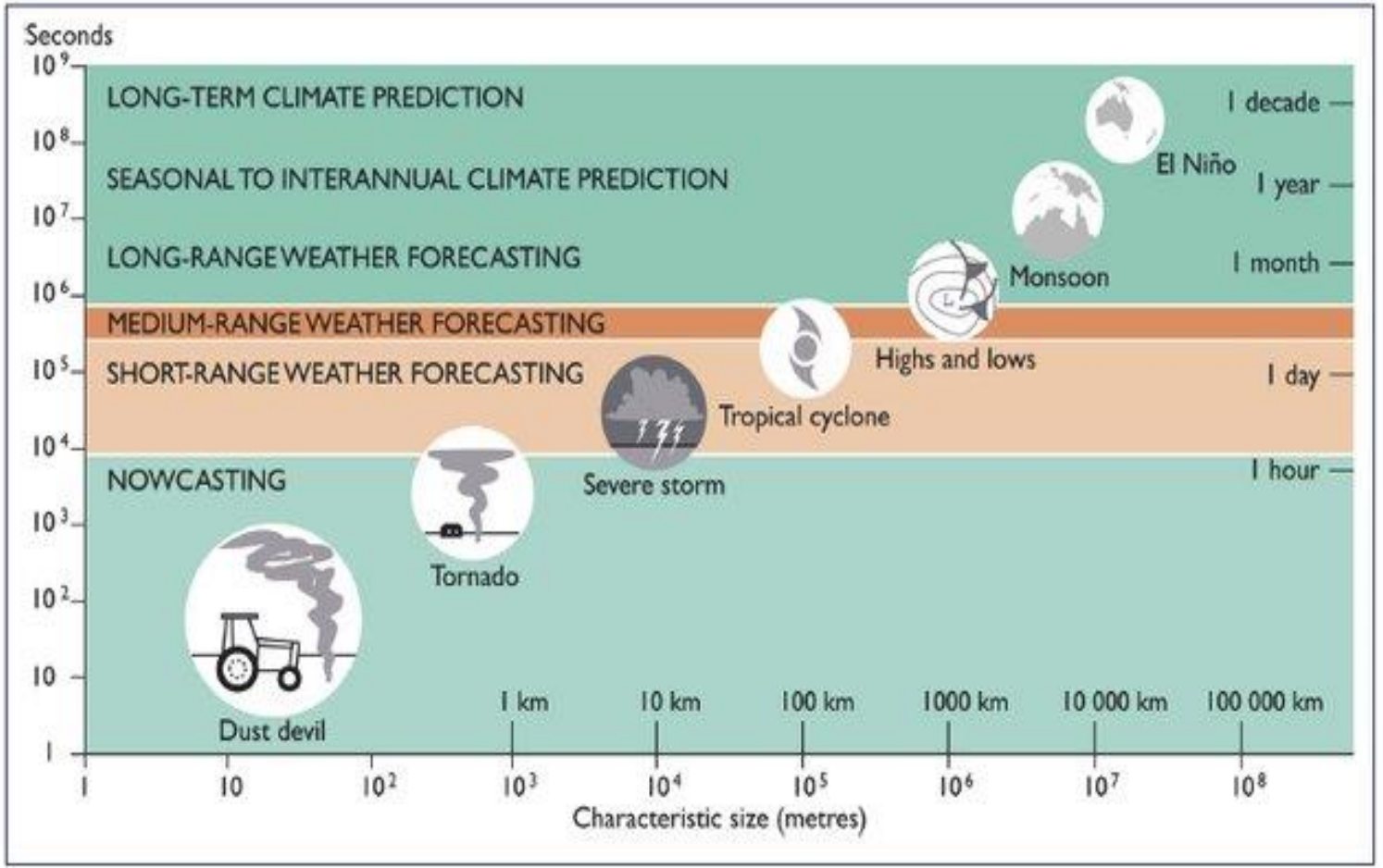

Introduction: Numerical Weather Prediction (NWP)

Basic ideas for NWP were developed more than a century ago

- **Vilhem Bjerknes**, Norway (1904) – Weather predictions should be based on well-established laws of Physics and regarded as a deterministic problem. A sufficiently accurate knowledge of the **atmospheric initial state** should allow prediction of future states
- **L.F. Richardson (U.K)** (1922) World War 1, attempts to solve the equations numerically (by hand), but his solution was a failure

Several obstacles had to be overcome first

- Fuller understanding of atmospheric dynamics
- Regular radiosondes and later satellites provided initial conditions
- Stable finite difference schemes were developed
  - **ENIAC:** Electronic Numerical Integrator and Computer, University of Pennsylvania
  - **Jule Charney, John von Neumann, Fjortoft (1950)** – Numerical integration of barotropic vorticity equation. Quasi-geostrophic approximation & hydrostatic balance – (eliminates acoustic and gravity waves, but retains planetary waves). First numerical model of the atmosphere.
  - **Rossby & Team (1950)**: First successful real-time weather forecast (see Harper et al. 2007).
  - **Phillips N.A. (1956):** The general circulation of the atmosphere: A numerical experiment. Depict monthly and seasonal pattern of circulation in troposphere. **Starting of general circulation models and climate models (e.g., GFDL, Princeton).**
  - **Lorenz E.N. (1963):** Discovery of deterministic chaos. A simple model (3-variable) of convection showed two regimes with chaotic transition between them. Even with a perfect model and almost perfect initial conditions, the forecast loses all skill in a finite time interval. A butterfly flap in Brazil can change the forecast in Texas in one or two weeks. Limits to predictability of weather.
- Powerful electronic computers provided means of carrying the massive calculations required
- Massive increase in computing power

Science of Climate Change

Joseph Fourier (1824): Concept of glass bowl effect

John Tyndall (1859): Demonstrates and explains the physical basis of what we now call as greenhouse effect. The atmosphere admits the entrance of the solar heat, but checks its exit and the result is a tendency to accumulate heat the surface of the planet.

Svante Arrhenius (1896): Quantifies the changes in surface temperature (approx 5^{o}C) to be expected from a doubling of CO_2

Guy Callendar (1938): States that human's activities lead to increased surface temperatures

Charles Keeling (1928-2005): Mauna Loa facility detection of atmospheric composition change (1957 – present)

Manabe and Strickler (1964): Thermal equilibrium of an atmosphere with a convective adjustment. Radiative convective models (RCM) to compute the states of thermal equilibrium, as well as pure radiative equilibrium, of the atmosphere.

Manabe and Wetherald (1967): Thermal equilibrium of the atmosphere with a given distribution of relative humidity. Doubling the existing CO2 content of the atmosphere has the effect of increasing the surface temperature by about 2.3^{o}C for the atmosphere with realistic distribution of relative humidity and by about 1.3^{o}C for that with realistic distribution of absolute humidity. First clear demonstration of **Water Vapour Feedback.** **Nobel Prize in Physics (2021) for Climate Science – Syukuro Manabe & Klaus Hasselmann**

THE CONVERSATION

Academic rigour, journalistic flair

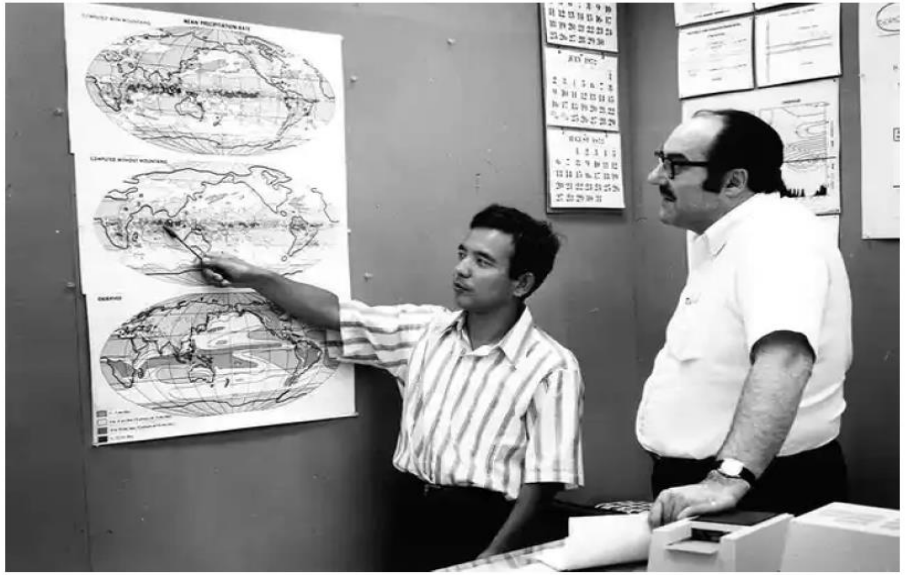

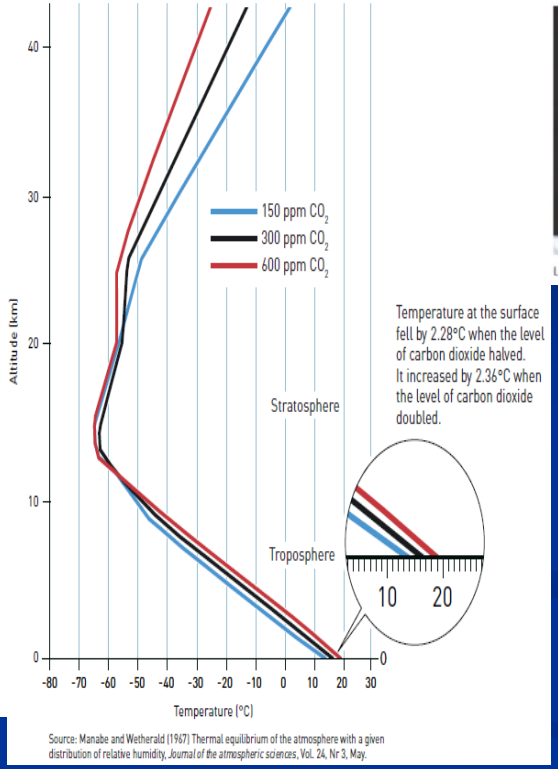

Source: Manabe and Wetherald (1967) Thermal equilibrium of the atmosphere with a given distribution of relative humidity, *Journal of the atmospheric sciences*, Vol. 24, Nr 3, May.

Laureate: Manabe receives his Nobel Prize, October 2021. EPA-EFE

Manabe modelled the links between temperature, altitude and CO2 levels. Johan Jamestad / Royal Swedish Academy of Sciences / Manabe and Wetherald (1967). J. Atmos. Sci.,

Syukuro Manabe & his colleague Joseph Smagorinsky in 1972 The most influential climate science paper of all time – Piers Forster, University of Leeds

Thermal Equilibrium of the Atmosphere with a Given Distribution of Relative Humidity

SYUKURO MANABE AND RICHARD T. WETHERALD

Carbon dioxide heats the atmosphere: Increased levels of carbon dioxide lead to higher temperature in the lower atmosphere, while the upper atmosphere gets colder. Manabe thus confirmed that the variation in temperature is due to increased levels of carbon dioxide; if it was caused by increased solar radiation, the entire atmosphere should have warmed up

Physical principals governing flow

$$d\overline{\mathbf{V}}/dt + fk \times \overline{\mathbf{V}} + \nabla\overline{\phi} = \mathbf{F}, \qquad \textit{(horizontal momentum)}$$

$$d\overline{T}/dt - \kappa\overline{T}\omega/p = Q/c_p, \qquad \textit{(thermodynamic energy)}$$

$$\nabla \cdot \overline{\mathbf{V}} + \partial\overline{\omega}/\partial p = 0, \qquad \textit{(mass continuity)}$$

$$\partial\overline{\phi}/\partial p + R\overline{T}/p = 0, \qquad \textit{(hydrostatic equilibrium)}$$

$$d\overline{q}/dt = S_q. \qquad \textit{(water vapor mass continuity)}$$

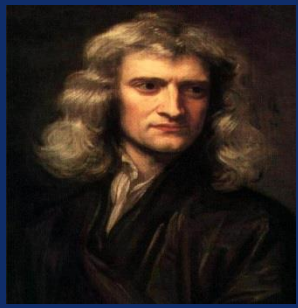

Isaac Newton

Harmless looking terms F, Q, S_q > "physics"

Courtesy: Kamal Puri

PHYSICAL PROCESSES OF IMPORTANCE TO WEATHER PREDICTION

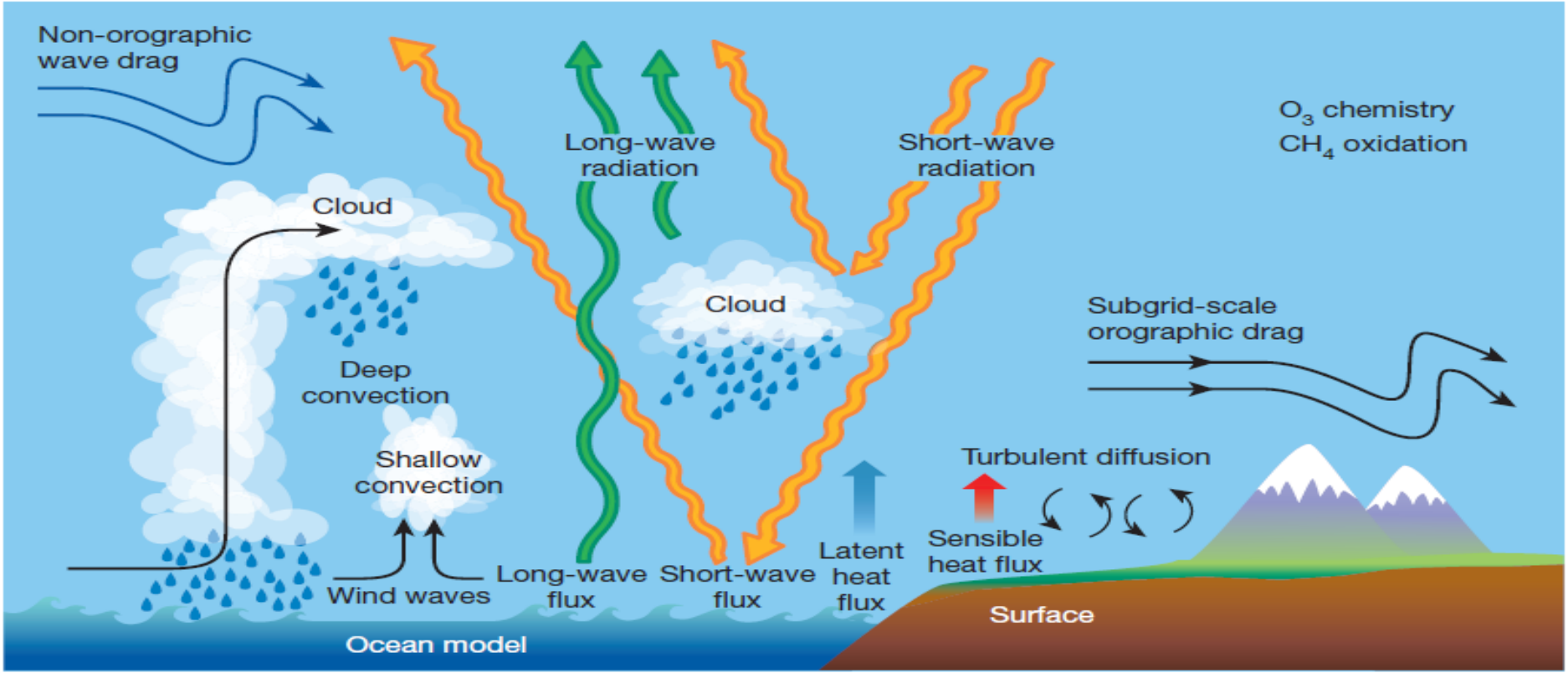

The physical processes shown above are not explicitly resolved in current NWP models, but they are represented via parameterizations describing their contributions to the resolved scales in terms of mass, momentum and heat transfers

Source: Bauer, Thorpe & Brunet, Nature (2015)

Basis of a weather / climate model

Equations of motions & laws of thermodynamics to predict rate of change of: *T, P, V, q, etc.*

10 Million equations: 100,000 Points × 100 Levels × 10 variables

Time step ~ 10 minutes

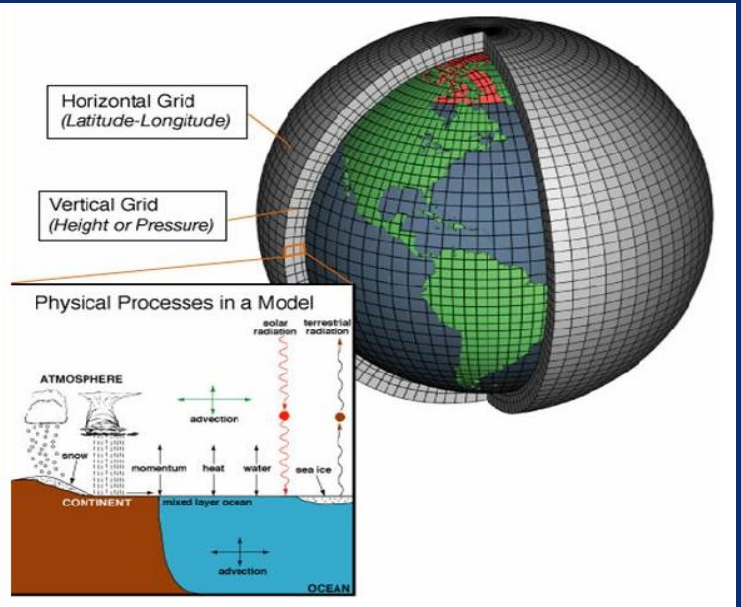

Representation of atmosphere: temperature, wind, moisture, pressure on a grid

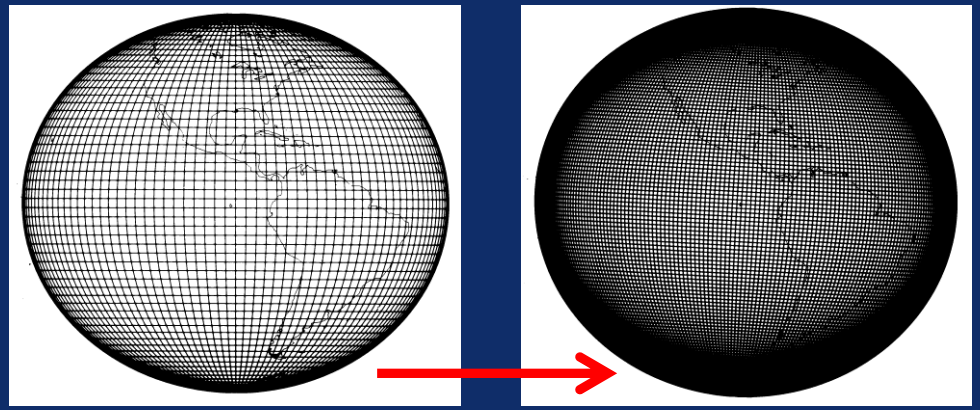

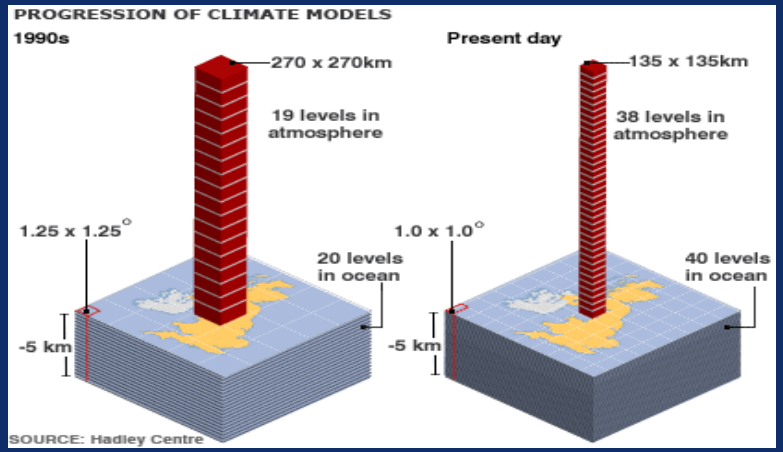

Courtesy:

Kamal Puri

Formulation of Atmospheric General Circulation Models

Grid-point method : The atmospheric dynamical variables in space and time are solved on a finite difference grid

Spectral method: Here, the atmospheric dynamical fields over the globe are represented in the form of waves using spherical harmonics. The spectral technique comes under the class of Galerkin methods and is very useful in numerically solving linear and nonlinear (partial) differential equations

- Haurwitz (1940) initiated the use of the spherical harmonics to solve two-dimensional non-divergent vorticity equation in the spherical domain.
- Silberman (1954) extended the treatment of nonlinear advection terms using the interaction coefficient method, which requires large memory allocations and therefore it was an undesirable proposition.
- Later Platzman (1960), Baer and Platzman (1961), and Kubota et al. (1961), Ellsaesser (1966), Robert (1966) and others analysed many of the mathematical characteristics of spectral technique.
- Eliasen et al. (1970) and Orszag (1970) independently developed the transform method for evaluation of the nonlinear terms. The transform method ultimately popularized the spectral method for studies of general circulation and numerical weather prediction at the operational and research centers (Bourke, 1972, 1974, 1977; Eliasen and Machenhauer, 1974, Sela, 1980).

Spectral Representation

$$f(\lambda,\mu,\sigma,t) = a\sum_{m=-J}^{J}\sum_{l=|m|}^{K} f_l^{\,m} P_l^m(\mu) e^{im\lambda}$$

$l > |k|$

$\mu = \sin\phi$

$f_l^{\,m}$ are the spherical harmonic coefficients, also known as spectral coefficients (complex in nature)

$P_l^m(\mu)$ Associated *Legendre* polynomial, of degree *l* and order *m*; *a* is the radius of the earth; *m* represents zonal wave number; *l – m* denotes meridional wave number; *J* is the wave number truncation; *K* is the highest degree of associated *Legendre* polynomial (depends on the truncation scheme). Describes the north-south variation of the spherical harmonic wave

$e^{im\lambda}$ Describes the east-west variation

Laplace equation in spherical coordinates

$$\frac{d}{d\mu}\left((1-\mu^2)\frac{dY}{d\mu}\right)+\frac{1}{1-\mu^2}\frac{\partial^2 Y}{\partial\lambda^2}+n(n+1)Y=0,$$

where λ is longitude, $\mu = \sin\theta$, with θ being latitude.

$$\nabla^2 u = \frac{\partial^2 u}{\partial x^2}+\frac{\partial^2 u}{\partial y^2}+\frac{\partial^2 u}{\partial z^2}=0.$$

Laplace equation in Cartesian coordinates

Solution of Laplace's equation on a sphere is of the form

$Y_n^m(\mu,\lambda) = P_n^m(\mu)e^{im\lambda}$. $Y_n^m(\mu,\lambda)$ is a *spherical harmonic* of order m and degree n. The factor $e^{im\lambda}$ describes the east-west variation, and the factor $P_n^m(\mu)$ describes the north-south variation of the spherical harmonic wave $Y_n^m(\mu,\lambda)$. Some useful mathematical

An Efficient, One-Level, Primitive-Equation Spectral Model

1972

WILLIAM BOURKE—*Commonwealth Meteorology Research Centre, Melbourne, Victoria, Australia*

A Multi-Level Spectral Model. I. Formulation and Hemispheric Integrations

1974

WILLIAM BOURKE

Australian Numerical Meteorology Research Centre, Melbourne, Australia 3001

(Manuscript received 5 March 1974, in revised form 6 August 1974)

A Global Spectral Model for Simulation of the General Circulation

1978

BRYANT J. MCAVANEY, WILLIAM BOURKE AND KAMAL PURI

Australian Numerical Meteorology Research Centre, P.O. Box 5089AA, Melbourne, Australia 3001

$$\frac{d\mathbf{V}}{dt} = -f\mathbf{k}\times\mathbf{V} - \nabla\Phi - RT\nabla \ln p_* + \mathbf{F}$$

$$\frac{dT}{dt} = \frac{RT}{c_p}\left(\frac{\dot{\sigma}}{\sigma} - \frac{\partial\dot{\sigma}}{\partial\sigma} - \nabla\cdot\mathbf{V}\right)$$

$$\frac{d \ln p_*}{dt} = -\nabla\cdot\mathbf{V} - \frac{\partial\dot{\sigma}}{\partial\sigma}$$

$$\frac{\partial\Phi}{\partial\sigma} = -\frac{RT}{\sigma}.$$

Here the vertical coordinate system of Phillips is employed; the vertical coordinate being defined as $\sigma = p/p_*$ where p_* denotes the surface pressure and p the pressure within the atmospheric fluid. $\mathbf{V}$ is the horizontal wind vector with eastward and northward components of u and v respectively, T is the absolute temperature, Φ is the geopotential height, f is the

With the further substitutions $U = u\cos\phi$, $V = v\cos\phi$, Eqs. (5) to (8) may be expanded in part into spherical polar coordinates yielding, where λ denotes longitude, ϕ denotes latitude and a the radius is taken to be constant

$$\frac{\partial}{\partial t}\nabla^2\psi = -\frac{1}{a\cos^2\phi}\left(\frac{\partial A}{\partial\lambda} + \cos\phi\frac{\partial B}{\partial\phi}\right) - 2\Omega\left(\sin\phi\nabla^2\chi + \frac{V}{a}\right) \quad (13)$$

$$\frac{\partial}{\partial t}\nabla^2\chi = \frac{1}{a\cos^2\phi}\left(\frac{\partial B}{\partial\lambda} - \cos\phi\frac{\partial A}{\partial\phi}\right) + 2\Omega\left(\sin\phi\nabla^2\psi - \frac{U}{a}\right) - \nabla^2(E + \Phi' + RT_0 q) \quad (14)$$

$$\frac{\partial T}{\partial t} = -\frac{1}{a\cos^2\phi}\left(\frac{\partial}{\partial\lambda}UT' + \cos\phi\frac{\partial}{\partial\phi}VT'\right) + T'\nabla^2\chi + \gamma\dot{\sigma} + \frac{RT}{c_p}\{\overline{\nabla^2\chi} + (\mathbf{V} + \overline{\mathbf{V}})\cdot\nabla q\} \quad (15)$$

$$\frac{\partial q}{\partial t} = \overline{\mathbf{V}}\cdot\nabla q + \overline{\nabla^2\chi}. \quad (16)$$

Here

$$A = \xi U + \dot{\sigma}\frac{\partial V}{\partial\sigma} + \frac{RT'}{a}\cos\phi\frac{\partial q}{\partial\phi} - \frac{g}{p_*}\frac{\partial\tau_y}{\partial\sigma}, \quad (17)$$

$$B = \xi V - \dot{\sigma}\frac{\partial U}{\partial\sigma} - \frac{RT'}{a}\frac{\partial q}{\partial\lambda} + \frac{g}{p_*}\frac{\partial\tau_x}{\partial\sigma}, \quad (18)$$

$$E = \frac{U^2 + V^2}{2\cos^2\phi}. \quad (19)$$

Advantages

- Accurate evaluation of the nonlinear advection terms

- Nice conservation properties (eg. Spectral methods of solving barotropic non-divergent models conserve area-averaged mean square kinetic energy and mean square vorticity – two quantities that fail to be conserved with some finite different methods).

- Ease of modelling flow over the entire globe. Mapping of the sphere in spectral models automatically makes a more uniform grid spacing that is common with finite difference models.

- One of the problems with finite difference approach is that near the poles, constant longitudinal increments, yield small geographical east-west distances between grid-points, and these very small distances limit the time step due to CFL criterion. The spectral technique is free from polar singularities

- Easy implementation of semi-implicit time integration schemes

- Fewer computations as compared to grid-point models at the same horizontal resolution.

- Accurate and stable numerics

Disadvantages

- Difficulties in handling discontinuity – Gibbs phenomena. In Fourier spectral methods, spurious oscillations can arise near discontinuities of a function. Use of filters helps to mitigate the effects of Gibbs oscillations

- Spurious / unphysical negative mixing ratios (e.g. water vapour) can arise due to finite truncation. Corrections applied.

Rhomboidal truncation

$$f(\lambda,\mu,\sigma,t) = a\sum_{m=-J}^{J}\sum_{l=|m|}^{|m|+J} f_l^{\,m} P_l^m(\mu) e^{im\lambda}$$

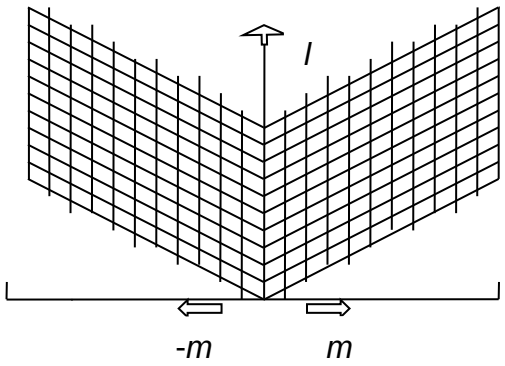

Triangular truncation

$$f(\lambda,\mu,\sigma,t) = a\sum_{m=-J}^{J}\sum_{l=|m|}^{J} f_l^{\,m} P_l^m(\mu) e^{im\lambda}$$

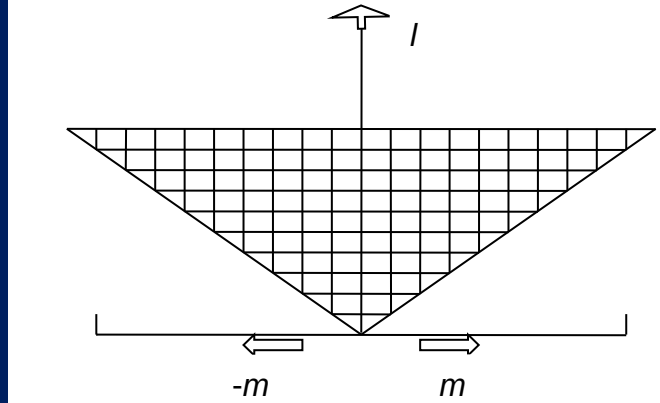

- Aliasing : If we have *2N + 1* grid points, we represent them into N waves by analyzing them into a maximum of *N-Fourier* (N-sine and N-cosine) components. If one tries to resolve more than N waves out of 2N +1 data points, a false representation (aliasing) of lower wave numbers into higher wave numbers occurs. So, the number of grid-points should be chosen such that the computations are free from aliasing.
- In addition to alias free computations, the FFT computations require that the number of grid points along the zonal direction satisfy $N = N_o 2^p$ (where N_o = 1 or 3 or 5 and p is positive). For example: for T42 truncation, N=42 thus $N_{\_Nlon} = 3N+1 \leq 128$. Note that $128=2^7$.
- For *Legendre* transform in the meridional (North-South) direction we need to have more than $N_{\_Nlat} = (3N+1)/2$ grid points in case of triangular truncation and more than $N_{\_Nlat} = (5N+1)/2$ grid points for rhomboidal truncation.

S.No.	Wave number truncation	No. of Gaussion latitudes (latitude circles) over 0-180^{O}	Grid size in Latitudinal direction in degree	No. of points per latitude circle 0-360^{O}	Grid size in Longitudinal direction in degree	Total no. of grid points.	Total no. of spectral coefficients
Rhomboidal Truncation							
1	**R 7**	20	9	24	15	480	98
2	**R 12**	32	5.625	48	7.5	1536	288
3	**R 15**	40	4.5	64 (48)	5.5 (7.5)	2560 (1920)	512
4	**R 21**	54	3.3	64	5.5	3456	882
5	**R 24**	62	2.9	80	4.5	4960	1152
6	**R 30**	80	2.25	96	3.75	7680	1922
7	**R 40**	100	1.8	128	2.8	12800	3200
Triangular Truncation							
8	**T 15**	24	7.5	48	7.5	1152	272
9	**T 30**	48	3.75	96	3.75	4608	992
10	**T 40**	64	2.8	128	2.8	8192	1722
11	**T42**	64	2.8	128	2.8	8192	1892
12	**T62**	94	1.9	192	2.5	18048	4032
13	**T 63**	96	1.875	192	1.875	18432	4095
14	**T 80**	128	1.4	256	1.4	32768	6642
15	**T 95**	144	1.25	288	1.25	41472	9312
16	**T 126**	190	0.9	384	0.9	73960	16256

Truncation for wave number J

Rhomboidal: No. of Gaussian latitudes $\geq (5J+1)/2$ and No. of points per latitude circles $> (3J+1)$

Total number of spectral coefficients $\leq 2(J+1)^2$

Triangular: No. of Gaussian latitudes $\geq (3J+1)/2$ and No. of points per latitude circles $> (3J+1)$

Total number of spectral coefficients $\leq (J+1)(J+2)$

CLIMATE AND THE OCEAN CIRCULATION[1]

I. THE ATMOSPHERIC CIRCULATION AND THE HYDROLOGY OF THE EARTH'S SURFACE

SYUKURO MANABE

Geophysical Fluid Dynamics Laboratory, ESSA, Princeton, N.J.

Mon. Wea. Rev., 1969, Vol 97

ABSTRACT

The effect of the hydrology of the earth's surface is incorporated into a numerical model of the general circulation of the atmosphere developed at the Geophysical Fluid Dynamics Laboratory of the Environmental Science Services Administration (ESSA). The primitive equation of motion is used for this study. The nine levels of the model are distributed so as to resolve the surface boundary layer and stratosphere. The depletion of solar radiation and the transfer of the terrestrial radiation are computed taking into consideration cloud and atmospheric absorbers such as water vapor, carbon dioxide, and ozone. The scheme treating the hydrology of our model involves the prediction of water vapor in the atmosphere and the prediction of soil moisture and snow cover. In order to represent the mositure-holding capacity of soil, the continent is assumed to be covered by boxes, which can store limited amounts of water. The ocean surface is idealized to be a completely wet surface without any heat capacity. The temperature of the earth's surface is determined in such a way that it satisfies the condition of heat balance. To facilitate the analysis and the interpretation of the results, a simple and idealized distribution of the ocean and the continental region is chosen for this study. The numerical integrations are performed for the annual mean distribution of solar insolation.

In general, the qualitative features of hydrologic and thermodynamic regimes at the earth's surface are successfully simulated. Particularly, the horizontal distribution of rainfall is in excellent qualitative agreement with the observations. For example, the typical subtropical desert, the break of the subtropical dry belt along the east coast of the continent, and the equatorial rain belt emerged as the result of numerical time integration. Some features of the spatial distributions of heat and water balance components at the earth's surface also agree well with those obtained by Budyko for the actual atmosphere.

Owing to the lack of seasonal variation of solar insolation and lack of poleward transport of heat by ocean currents in the model, excessive snow cover develops at higher latitudes. Accordingly, the temperature in the polar region is much lower than the annual mean temperature observed in the actual atmosphere.

This investigation constitutes a preliminary study preceding the numerical integration of the general circulation model of joint ocean-atmosphere interaction, in which the transport of heat by ocean currents plays an important role.

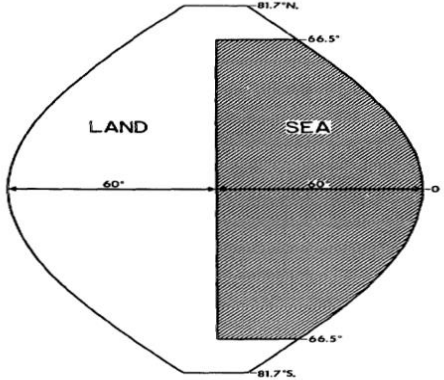

FIGURE 2.—Diagram depicting the distribution of ocean and continent. Cyclic continuity is assumed at the eastern and western ends of the domain. The distribution in the Southern Hemisphere is symmetric to the distribution in the Northern Hemisphere.

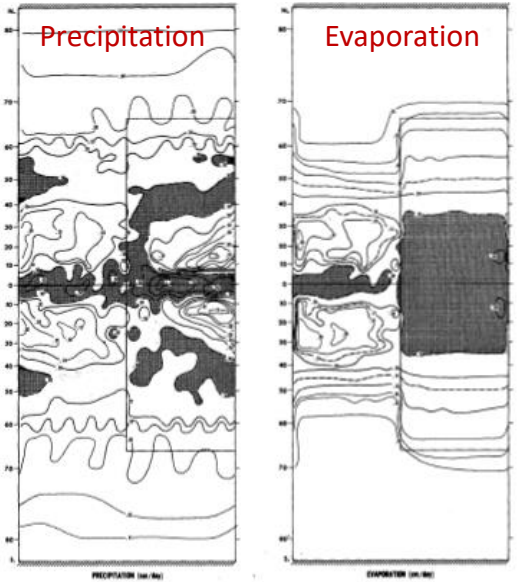

FIGURE 20.—Horizontal distribution of precipitation and evaporation of the model.

Climate Calculations with a Combined Ocean-Atmosphere Model

SYUKURO MANABE AND KIRK BRYAN

Geophysical Fluid Dynamics Laboratory, ESSA, Princeton University, Princeton, N. J.

13 March 1969 and 6 May 1969 **J.Atmos.Sci., 1969**

Empirical evidence indicates that the poleward heat transport by ocean currents is of the same order of magnitude as the poleward transport of energy in the atmosphere (Sverdrup, 1957). A significant contribution to the heat exchange across latitude circles is also associated with polar pack ice. Thus, any serious attempt to calculate climate must take into account the entire fluid envelope of the earth, consisting of the atmosphere and the hydrosphere. Although the cryosphere, consisting of ice packs over the oceans and continental ice, is not a fluid in the usual sense, it must be included in a general climatic model because of its large reflectivity to the solar insolation and its ability to store and transport heat.

The object of this note is to report the completion of a calculation based on a combined numerical model of the atmosphere and the ocean carried out at the Geophysical Fluid Dynamics Laboratory, ESSA. The extended numerical integration of this model is successful in producing many realistic features of climate starting with quite arbitrary initial conditions. Only a brief description will be given here. For the full details the reader is referred to Manabe (1969) and Bryan (1969).

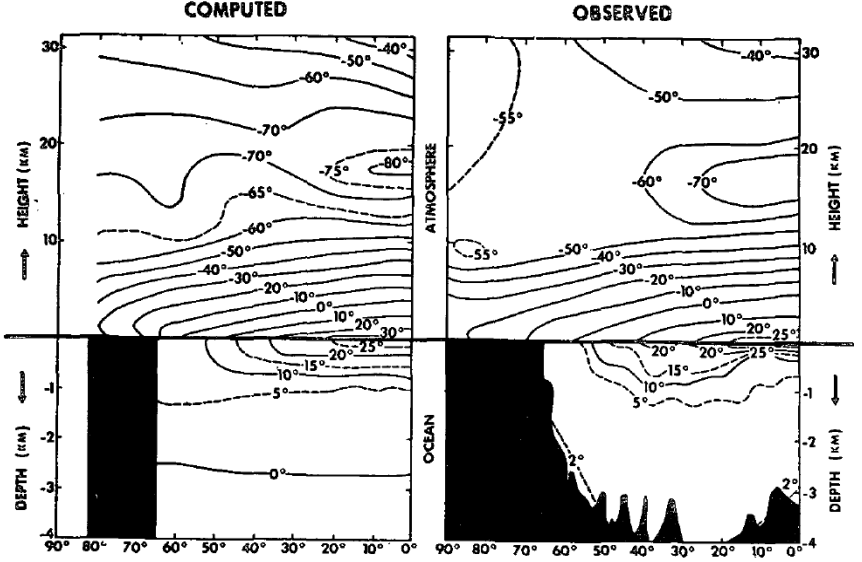

FIG. 2. Zonal mean temperature of the joint ocean-atmosphere system, left-hand side. This distribution, which is the average of two hemispheres, represents the time mean over two-sevenths of the period of the final stage of the time integration. The right-hand side shows the observed distribution in the Northern Hemisphere. The atmospheric part represents the zonally averaged, annual mean temperature. The oceanic part is based on a cross section for the western North Atlantic from Sverdrup *et al.* (1942).

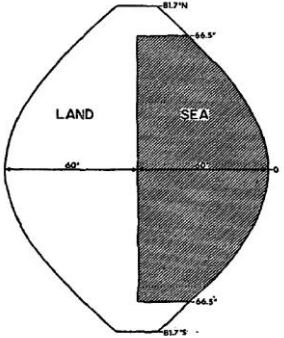

FIG. 1. Ocean-continent configuration of the model.

The most interesting result[1] of the calculation is the quantitative demonstration of the effect of ocean currents on the distribution of temperature, relative humidity, and precipitation patterns. This is done by comparing the state, which is obtained from the time integration of the atmospheric model (the first stage) with the state, which is obtained from that of the joint ocean-atmosphere model (the final stage). For example,

The Effects of Doubling the CO_2 Concentration on the Climate of a General Circulation Model[1]

SYUKURO MANABE AND RICHARD T. WETHERALD

1975

Geophysical Fluid Dynamics Laboratory/NOAA, Princeton University, Princeton, N.J. 08540

(Manuscript received 6 June 1974, in revised form 8 August 1974)

ABSTRACT

An attempt is made to estimate the temperature changes resulting from doubling the present CO_2 concentration by the use of a simplified three-dimensional general circulation model. This model contains the following simplifications: a limited computational domain, an idealized topography, no heat transport by ocean currents, and fixed cloudiness. Despite these limitations, the results from this computation yield some indication of how the increase of CO_2 concentration may affect the distribution of temperature in the atmosphere. It is shown that the CO_2 increase raises the temperature of the model troposphere, whereas it lowers that of the model stratosphere. The tropospheric warming is somewhat larger than that expected from a radiative-convective equilibrium model. In particular, the increase of surface temperature in higher latitudes is magnified due to the recession of the snow boundary and the thermal stability of the lower troposphere which limits convective heating to the lowest layer. It is also shown that the doubling of carbon dioxide significantly increases the intensity of the hydrologic cycle of the model.

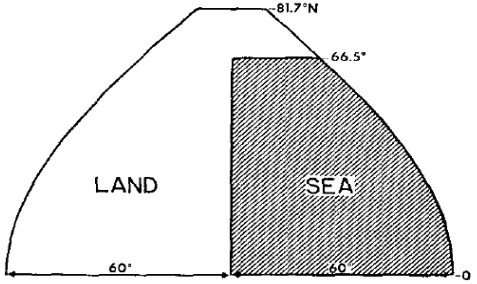

FIG. 1. Diagram illustrating the distribution of continent and "ocean." Cyclic continuity is assumed at the eastern and western ends of the domain.

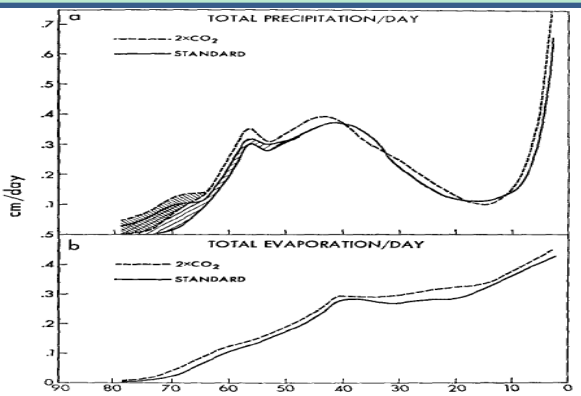

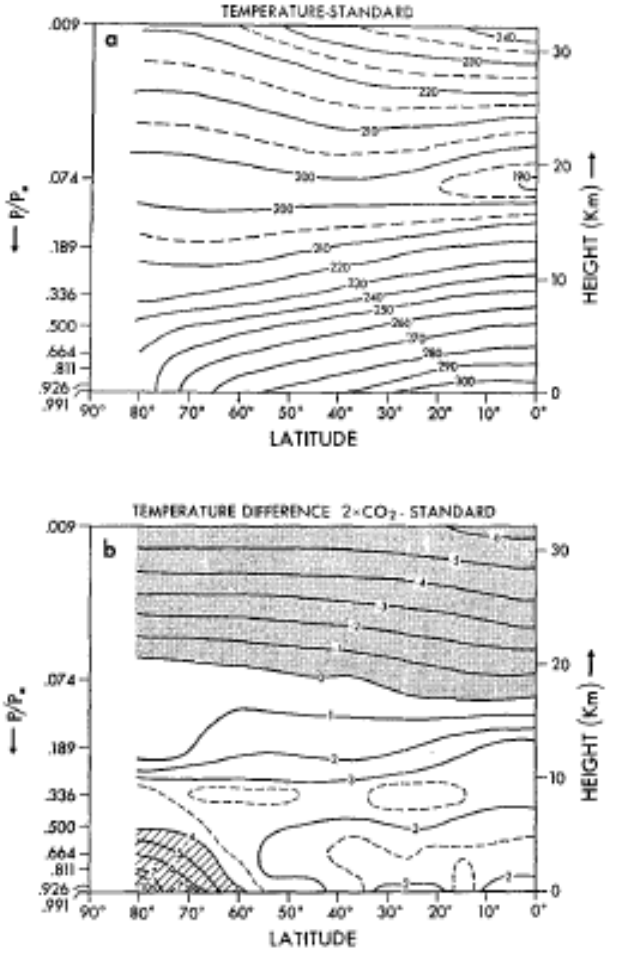

FIG. 4. Latitude-height distribution of the zonal mean temperature (K) for the standard case (a) and of the increase in zonal mean temperature (K) resulting from the doubling of CO_2 concentration (b). Stippling indicates a decrease in temperature.

Prof. Syukuro Manabe, GFDL, Princeton - Pioneer of coupled climate modelling

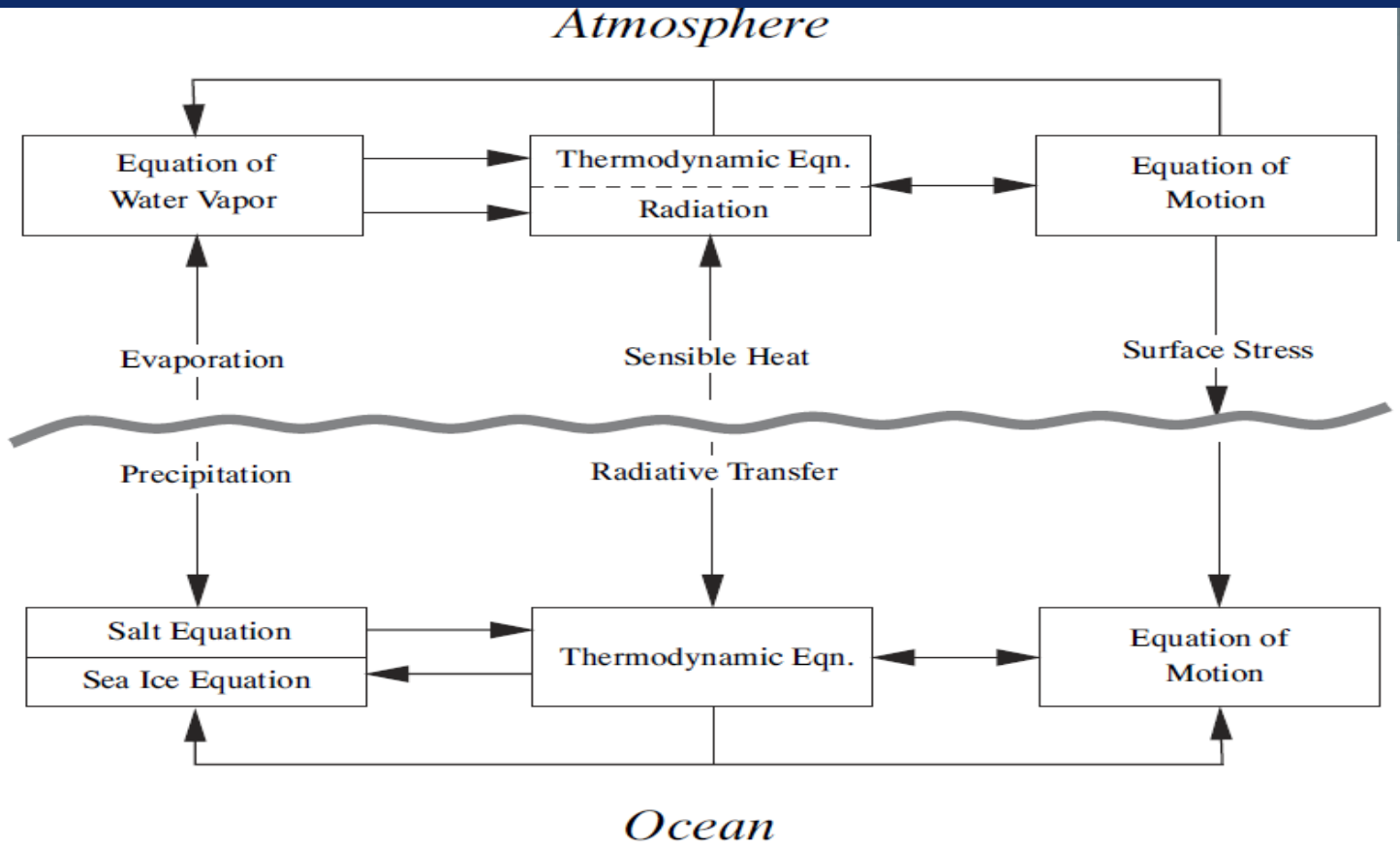

Figure 8.1: Diagram of the different model parts and fluxes of water, heat and momentum. Redrawn from Fig. 1 in Manabe and Stouffer (1988).

Earth System models – Fundamental for understanding climate change and dealing with their impacts. Powerful tools for representing and quantifying processes within and between the atmosphere, ocean, cryosphere and the biosphere (terrestrial & marine). ESMs provide information about physical, chemical and biological mechanisms governing the rates of change of elements of the Earth system.

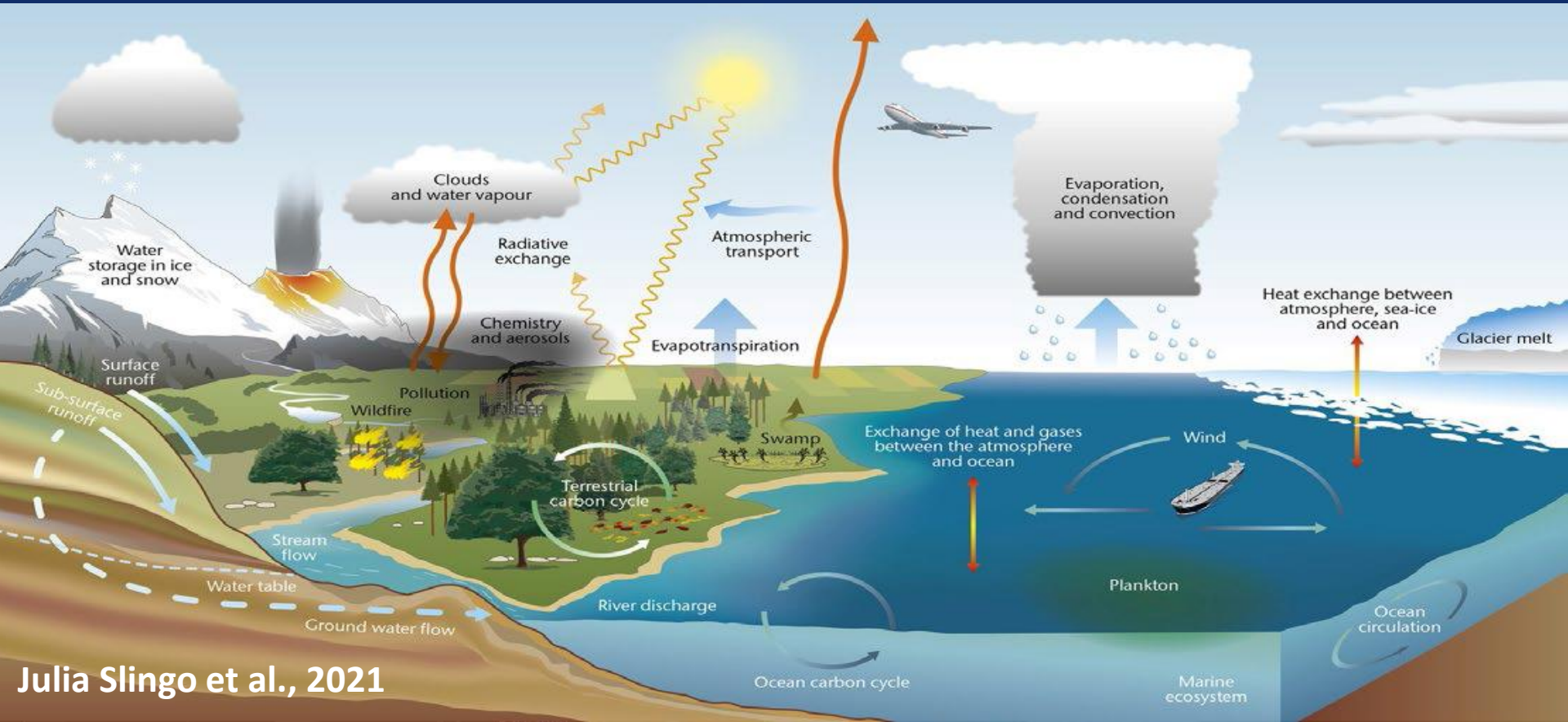

Julia Slingo et al., 2021

How it all started at CCCR-IITM …

- Develop an Earth System Model (ESM) from India for long-term climate studies
- Participate in the CMIP6 experiments
- Contribute to the Intergovernmental Panel on Climate Change (IPCC) Sixth Assessment Report (AR6)

Coupled Model Intercomparison Project – Phase 6 (CMIP6)

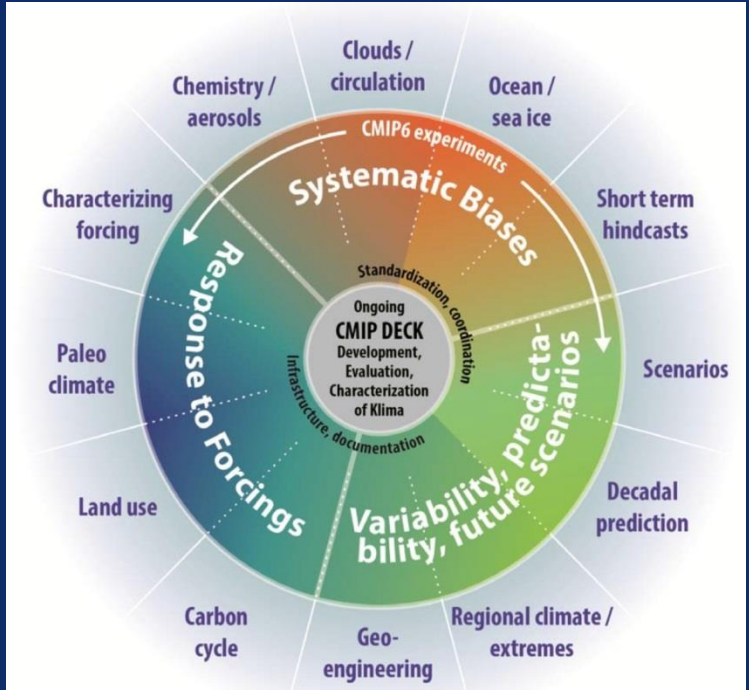

Human influence has warmed the climate at a rate that is unprecedented in at least the last 2000 years

Figure SPM.1

Changes in global surface temperature relative to 1850-1900

a) Change in global surface temperature (decadal average) as reconstructed (1-2000) and **observed** (1850-2020)

b) Change in global surface temperature (annual average) as **observed** and simulated using human & natural and only natural factors (both 1850-2020)

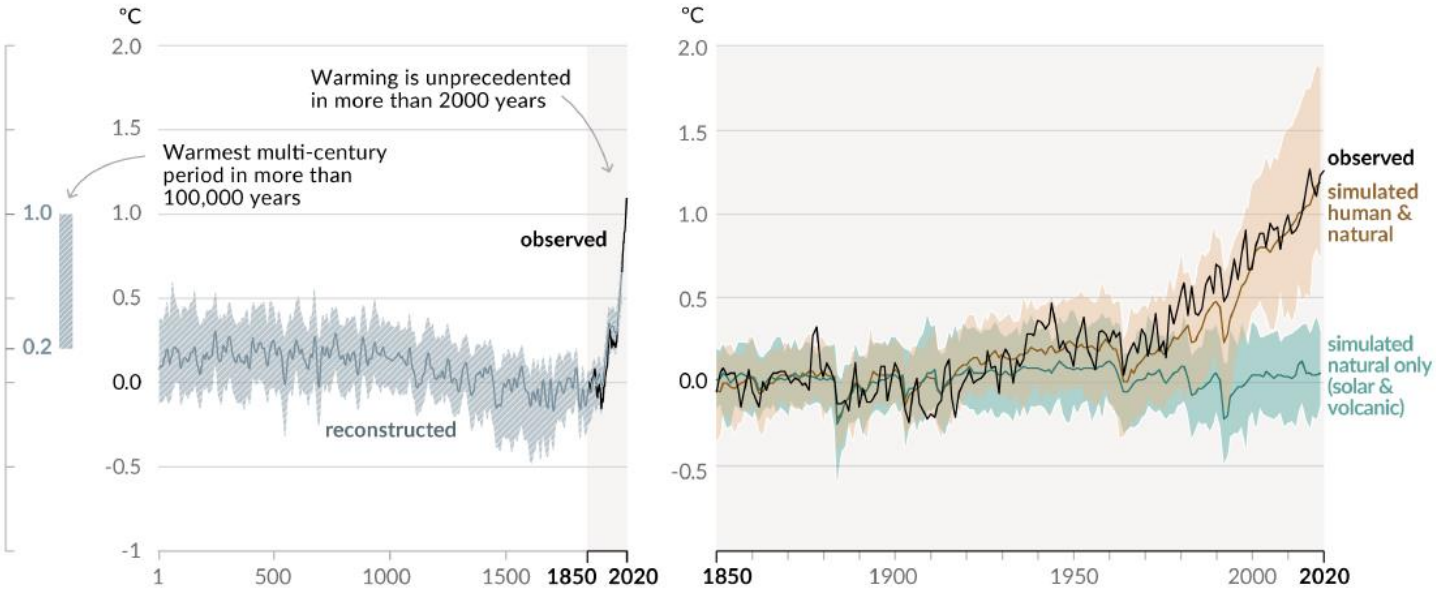

B.1 **Global surface temperature will continue to increase until at least the mid-century under all emissions scenarios considered. Global warming of 1.5°C and 2°C will be exceeded during the 21st century unless deep reductions in CO_2 and other greenhouse gas emissions occur in the coming decades.**

Warming projections

a) Global surface temperature change relative to 1850-1900

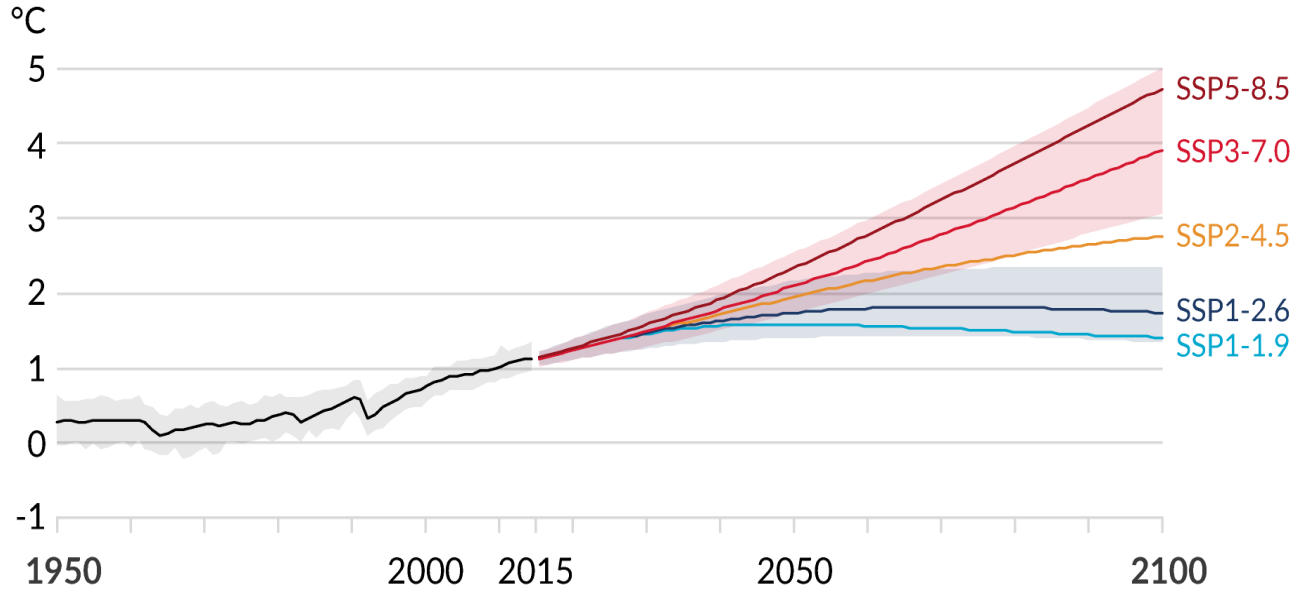

Figure SPM.8

Simulated and observed changes compared to the 1995–2014 average in key large-scale indicators of climate change across the climate system, for continents, ocean basins and globally up to 2014.

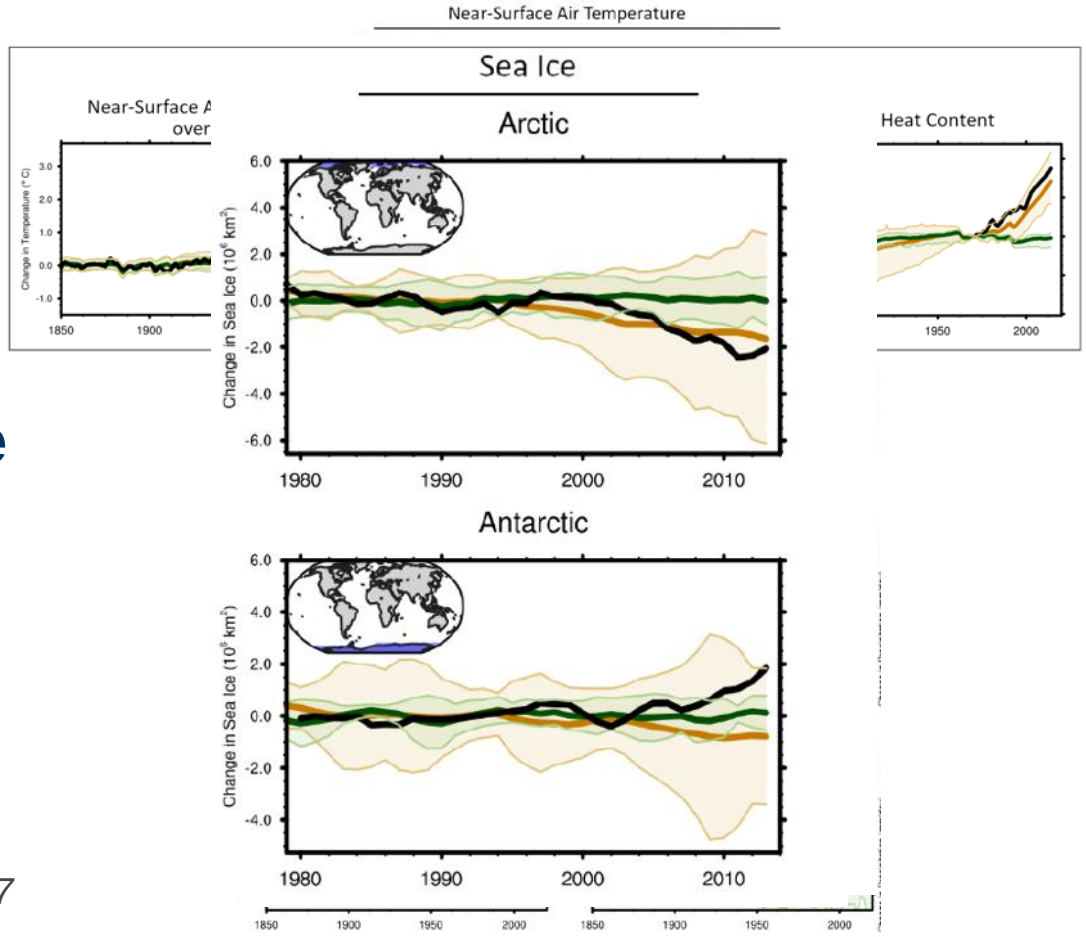

Figure TS.7

Ocean warming dominates the energy inventory change, accounting for 91% of the observed energy increase for the period 1971-2018

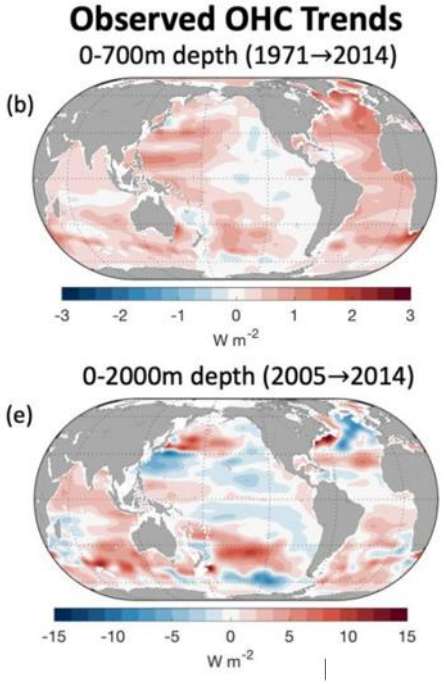

Figure 9.6

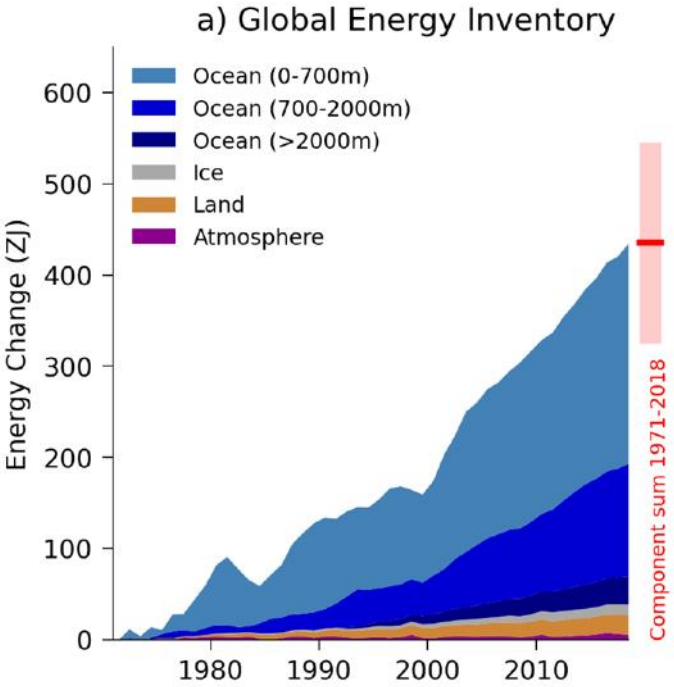

Cross Chapter Box 9.1 Figure 1

Combining the attributable contributions from glaciers, ice sheet surface mass balance and thermal expansion, it is *very likely* that human influence was the main driver of the observed global mean sea level rise since at least 1970.

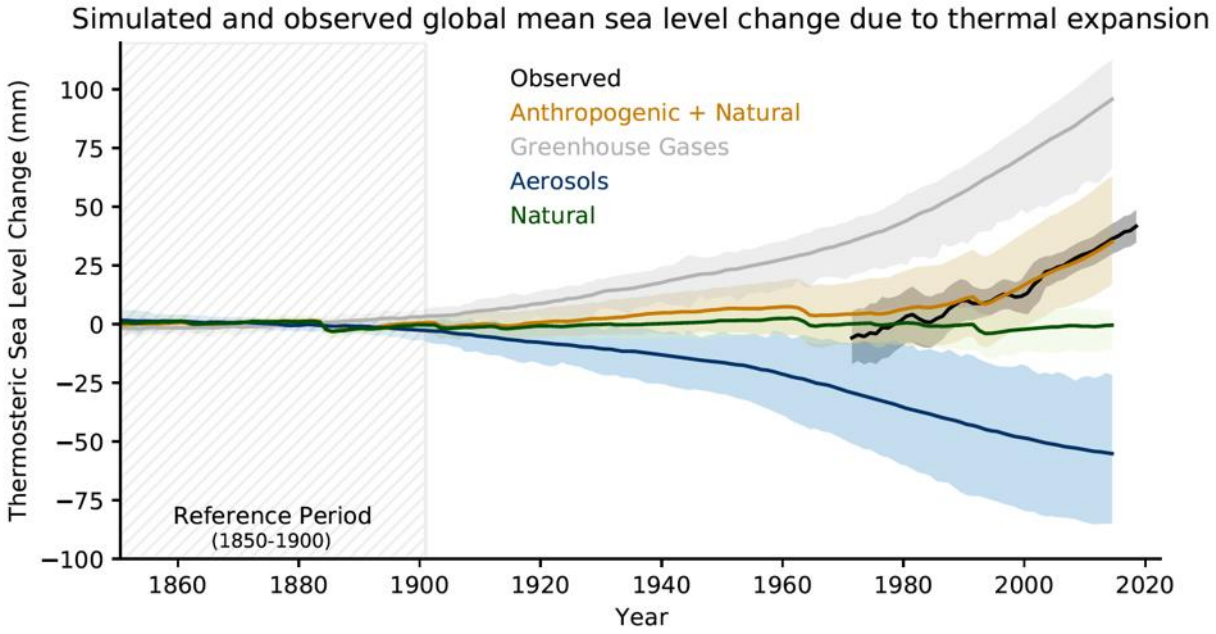

Figure 3.29

With every increment of global warming, changes get larger in regional mean temperature, precipitation and soil moisture

Figure SPM.5

a) Annual mean temperature change (°C) at 1 °C global warming

Warming at 1 °C affects all continents and is generally larger over land than over the oceans in both observations and models. Across most regions, observed and simulated patterns are consistent.

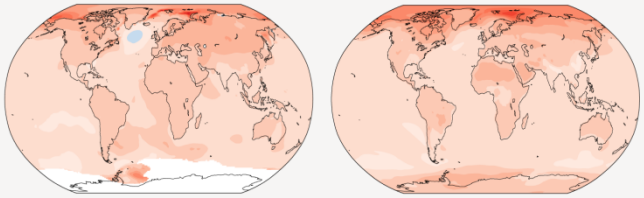

b) Annual mean temperature change (°C) relative to 1850-1900

Across warming levels, land areas warm more than oceans, and the Arctic and Antarctica warm more than the tropics.

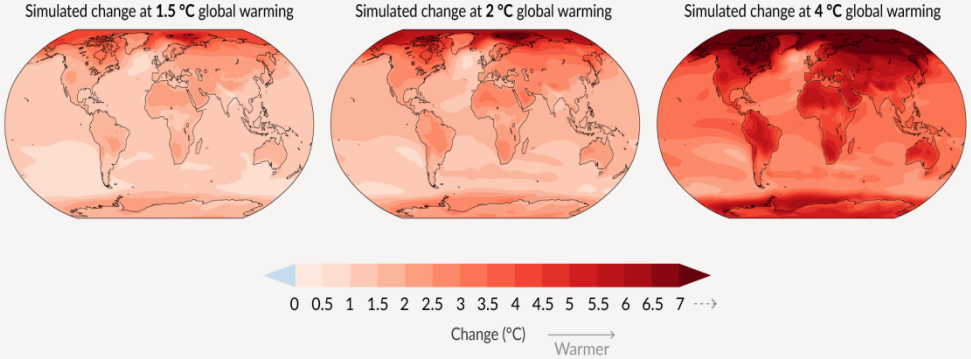

c) Annual mean precipitation change (%) relative to 1850-1900

Precipitation is projected to increase over high latitudes, the equatorial Pacific and parts of the monsoon regions, but decrease over parts of the subtropics and in limited areas of the tropics.

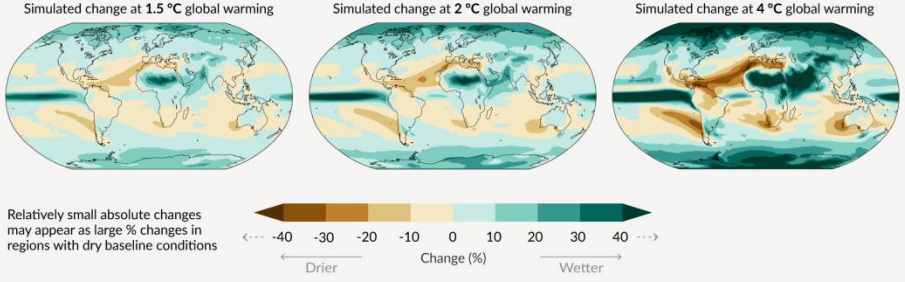

d) Annual mean total column soil moisture change (standard deviation)

Across warming levels, changes in soil moisture largely follow changes in precipitation but also show some differences due to the influence of evapotranspiration.

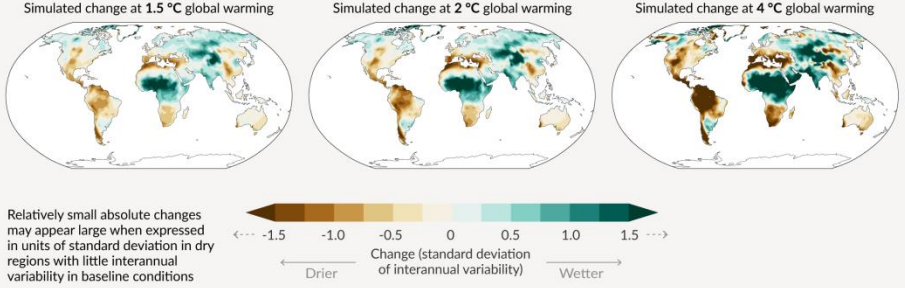

Observed warming is driven by emissions from human activities, with greenhouse gas warming partly masked by aerosol cooling

Figure SPM.2

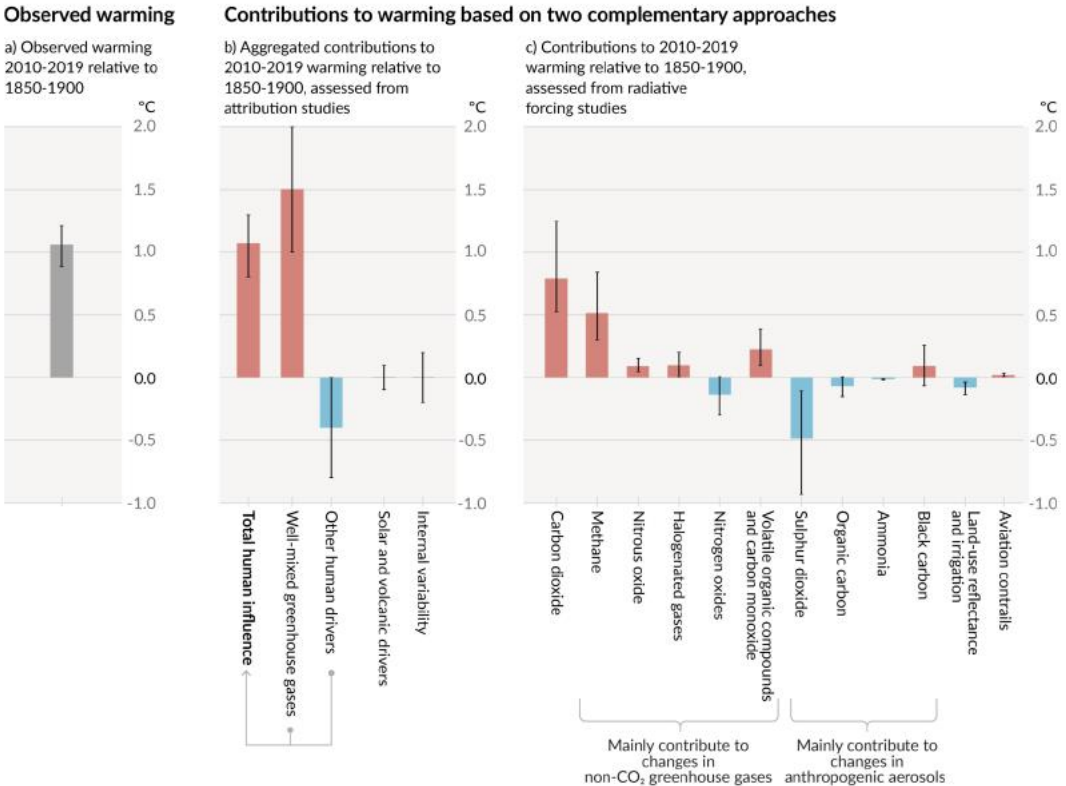

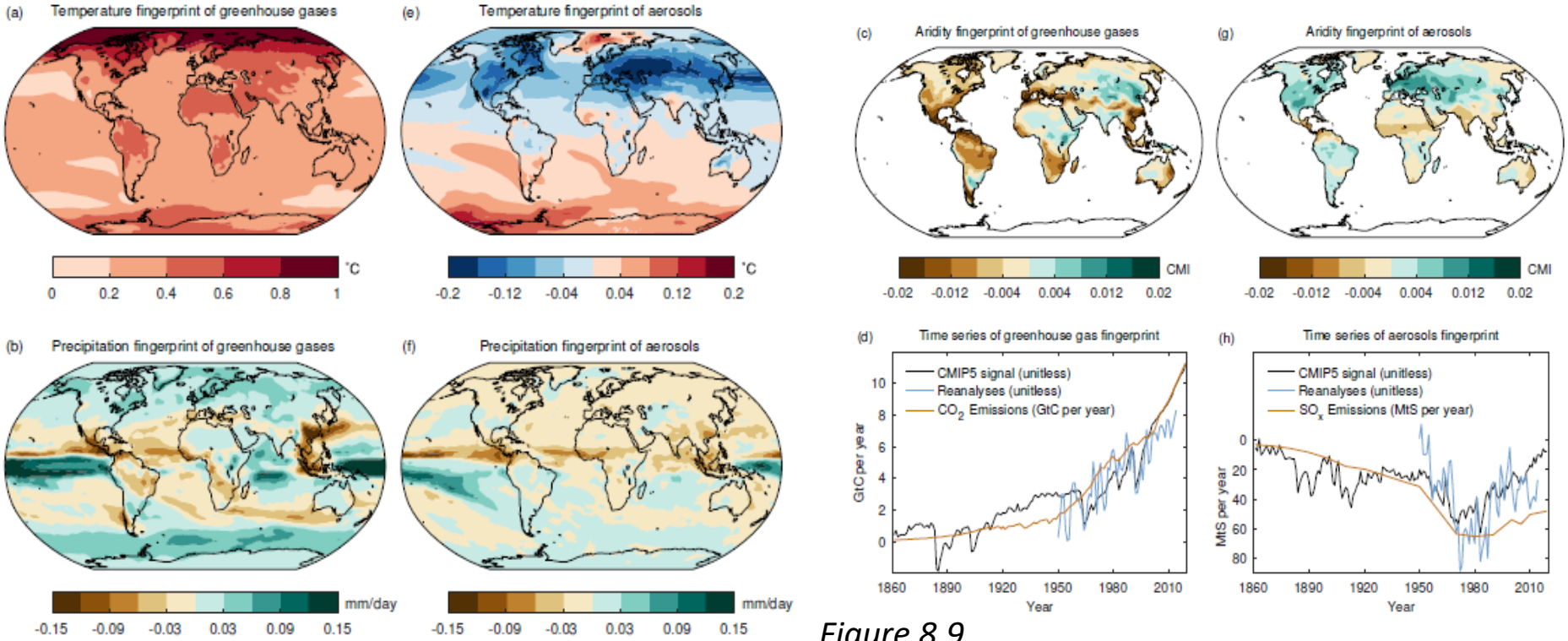

Figure 8.9

Figure 8.9: Spatial expressions (a-c; e-g) of the leading multivariate fingerprints of temperature (˚C), precipitation (mm/day), and aridity (CMI; the Climate Moisture Index) in CMIP5 historical simulations and the corresponding temporal evolution in both CMIP5 and reanalysis products (d, h). The first leading fingerprint is associated with greenhouse gas forcing (a-d) and the second leading fingerprint is associated with aerosol forcing (e-h). CMI is a dimensionless aridity indicator that combines precipitation and atmospheric evaporative demand. Figure after (Bonfils et al., 2020). Further details on data sources and processing are available in the chapter data table (Table 8.SM.1).

Science of Climate Change

Detection, attribution & projection of global climate and regional monsoons, variability and change

Roadmap for Earth System Model (ESM) development

- Start with an atmosphere-ocean coupled model with realistic mean climate
  - Fidelity in capturing the global and monsoon climate
  - Realistic representation of monsoon interannual variability
  - Features of ocean-atmosphere coupled interactions
  - …
- Include components / modules of the ESM
  - Biogeochemistry
  - Interactive Sea-ice
  - Aerosol and Chemistry Transport
  - …

Formal agreement for collaboration: The Ministry of Earth Sciences, Govt. of India and NOAA, USA in **2011.** Implement the NCEP CFS-2 model at IITM, Pune for seasonal prediction of the Indian monsoon.

Basic modeling framework: Coupled Forecast System (CFS-2) T126L64

- The **NCEP CFS** Components
- Atmospheric **GFS (Global Forecast System) model**
  - – T126 ~ 110 km; vertical: 64 sigma – pressure hybrid levels
  - – Model top 0.2 mb
  - – Simplified Arakawa-Schubert convection (Pan)
  - – Non-local PBL (Pan & Hong)
  - – SW radiation (Chou, modifications by Y. Hou)
  - – Prognostic cloud water (Moorthi, Hou & Zhao)
  - – LW radiation (GFDL, AER in operational wx model)
  - - Land surface processes (Noah land model)
- Interactive Ocean: **GFDL MOM4** (Modular Ocean Model, ver.4) Griffies et al. 2003
  - – 0.5 deg poleward of 10^{o}N and 10^{o}S; and 0.25 deg near equator (10^{o}S – 10^{o}N)
  - – 40 levels
  - – Interactive sea-ice

THE IITM EARTH SYSTEM MODEL

Transformation of a Seasonal Prediction Model to a Long-Term Climate Model

2014

BY P. SWAPNA, M. K. ROXY, K. APARNA, K. KULKARNI, A. G. PRAJEESH, K. ASHOK, R. KRISHNAN, S. MOORTHI, A. KUMAR, AND B. N. GOSWAMI

This work documents the fidelity of the newly developed Indian Institute of Tropical Meteorology climate model simulations and demonstrates its suitability to address the climate variability and change issues relevant to the South Asian monsoon.

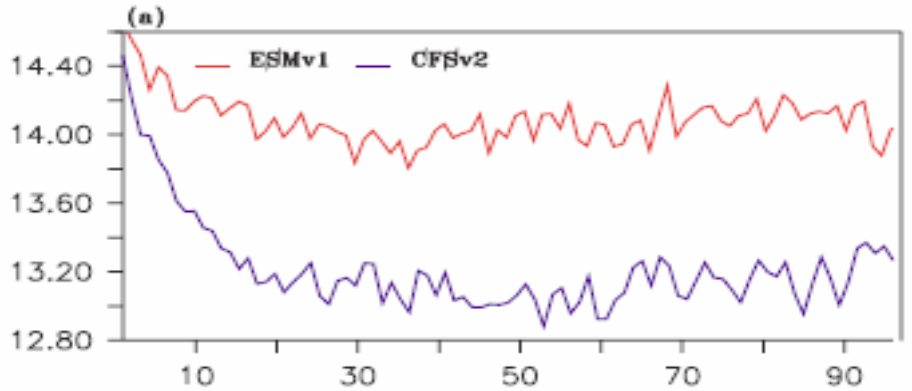

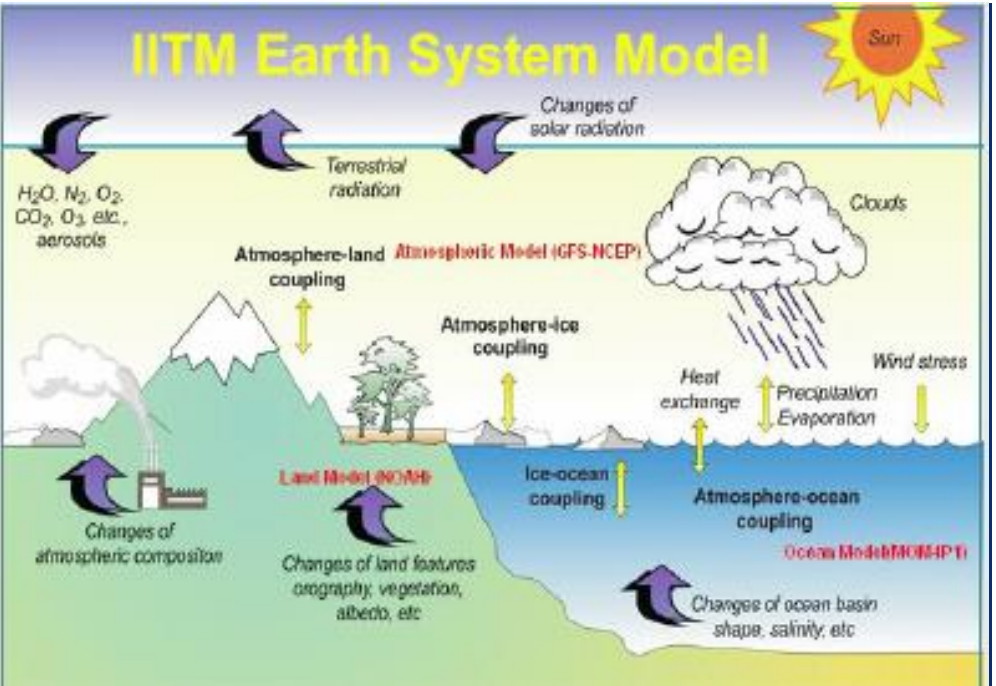

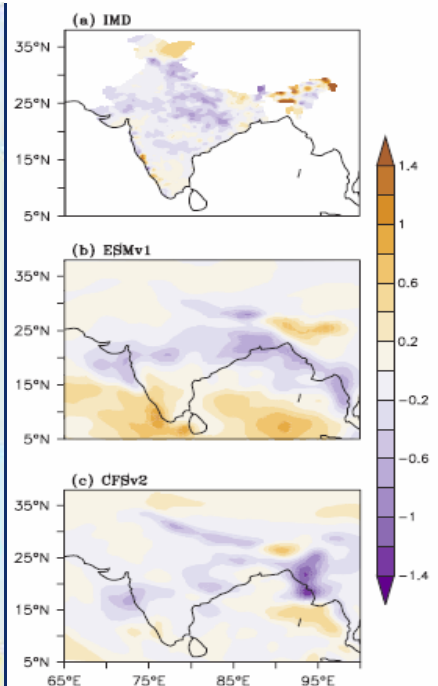

Atmosphere: T126 spectral (~ 190 km), 64 vertical levels – ESMv1

Ocean : 0.5 deg grid, ~ 0.25 deg between 10N-10S, 40 vertical levels

Annual mean temperature

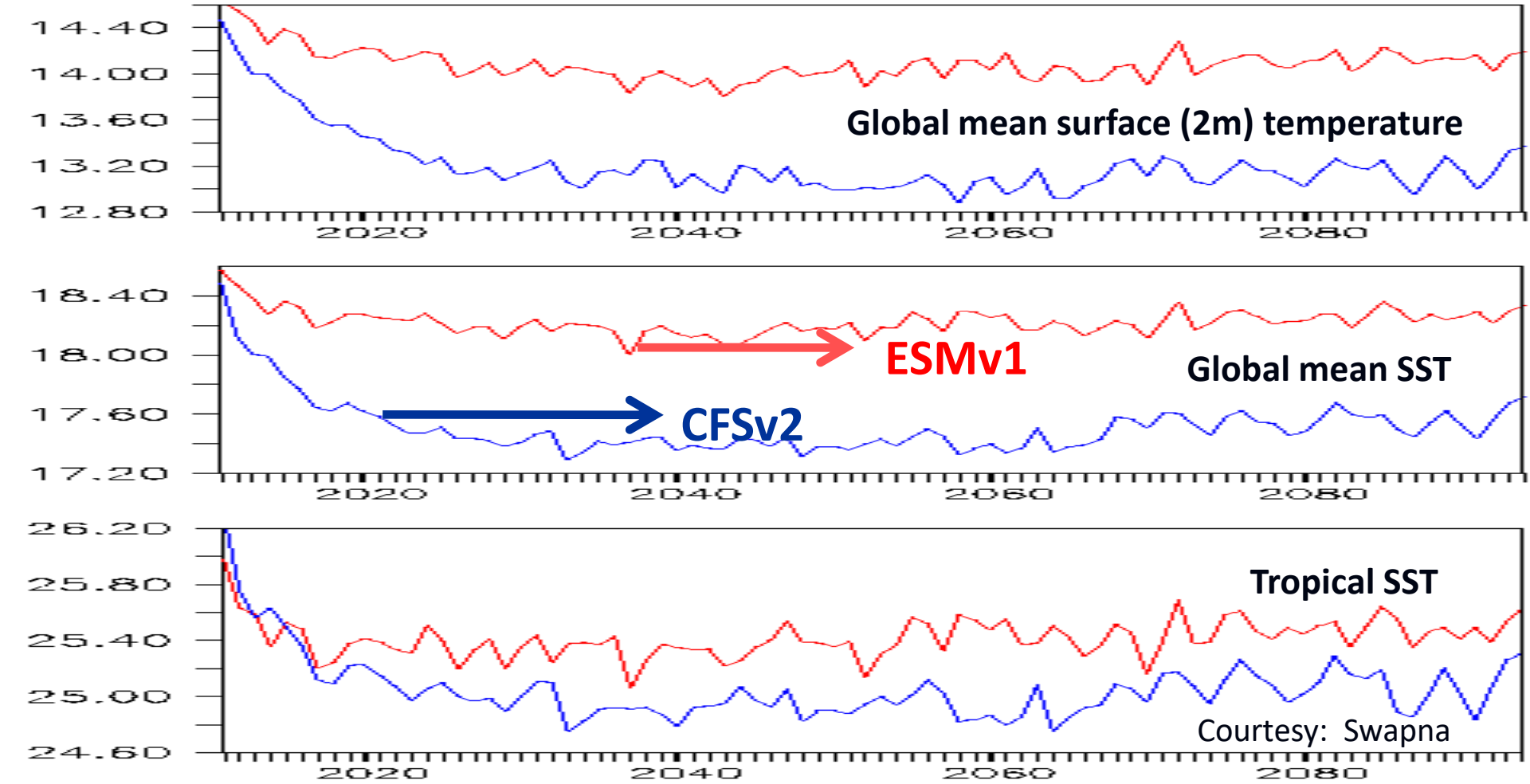

Coupled models drift towards a more equilibrated state. Initial rapid cooling of SST followed by warming trend. Significant subsurface drifts seen through multiple centuries of simulation. Vertical redistribution of heat with tendency of cooling in upper layers and warming in the sub-surface – Delworth et al. 2006

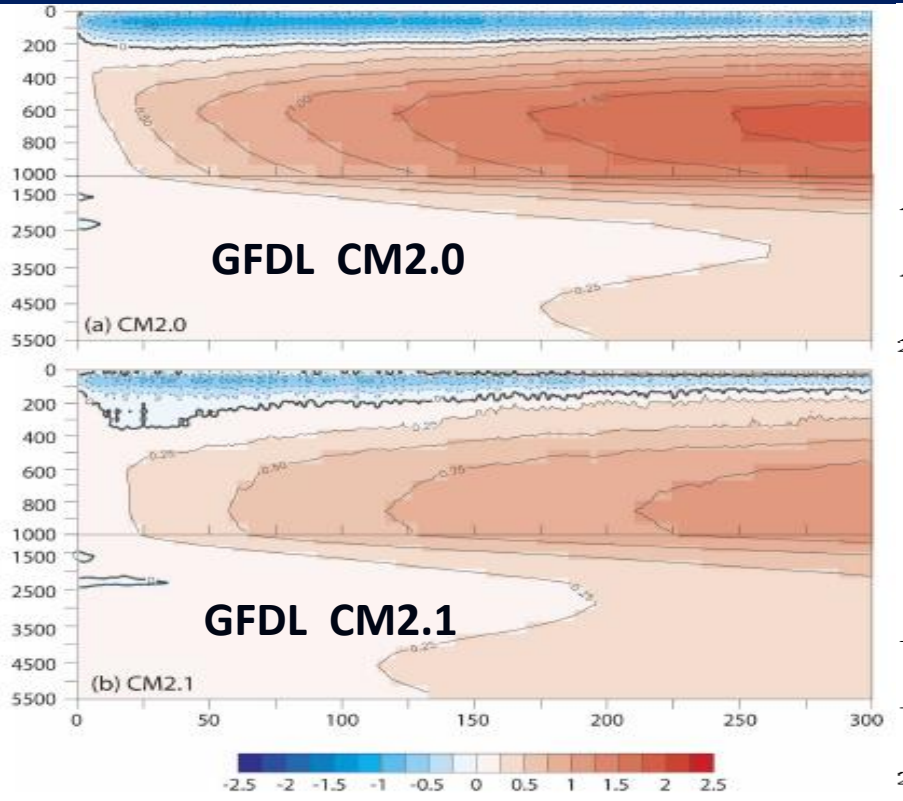

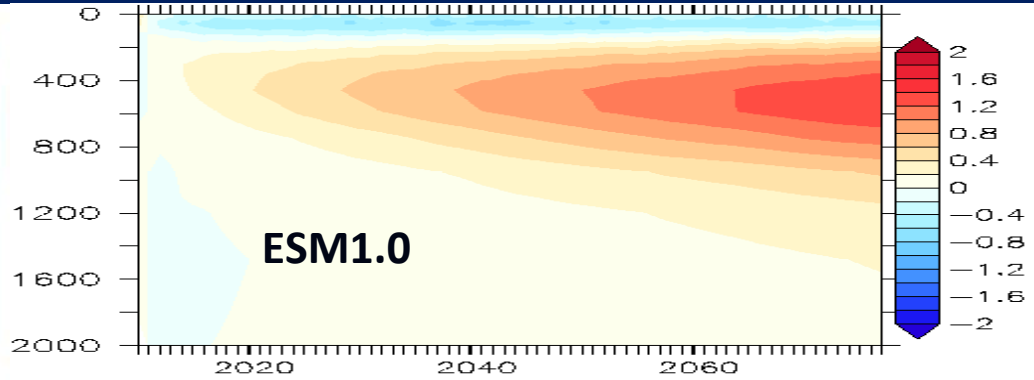

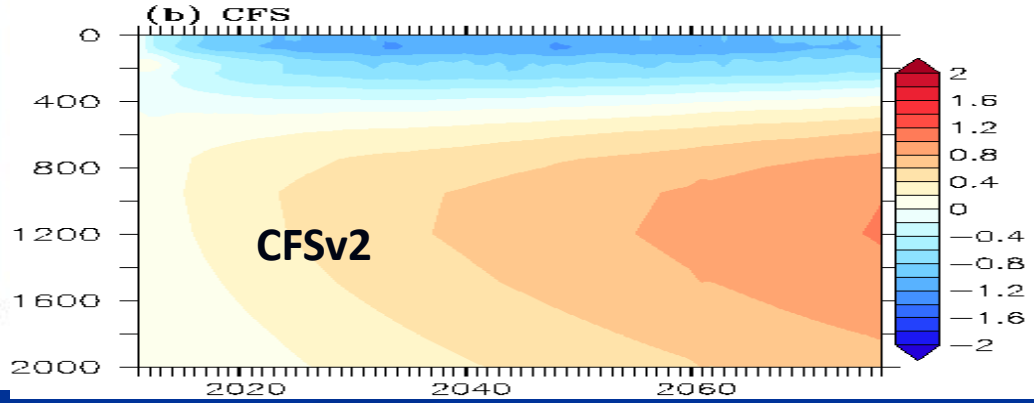

Differences between simulated and observed long-term global-mean ocean temperature as a function of depth and time.

Interannual variability: Standard deviation of SST

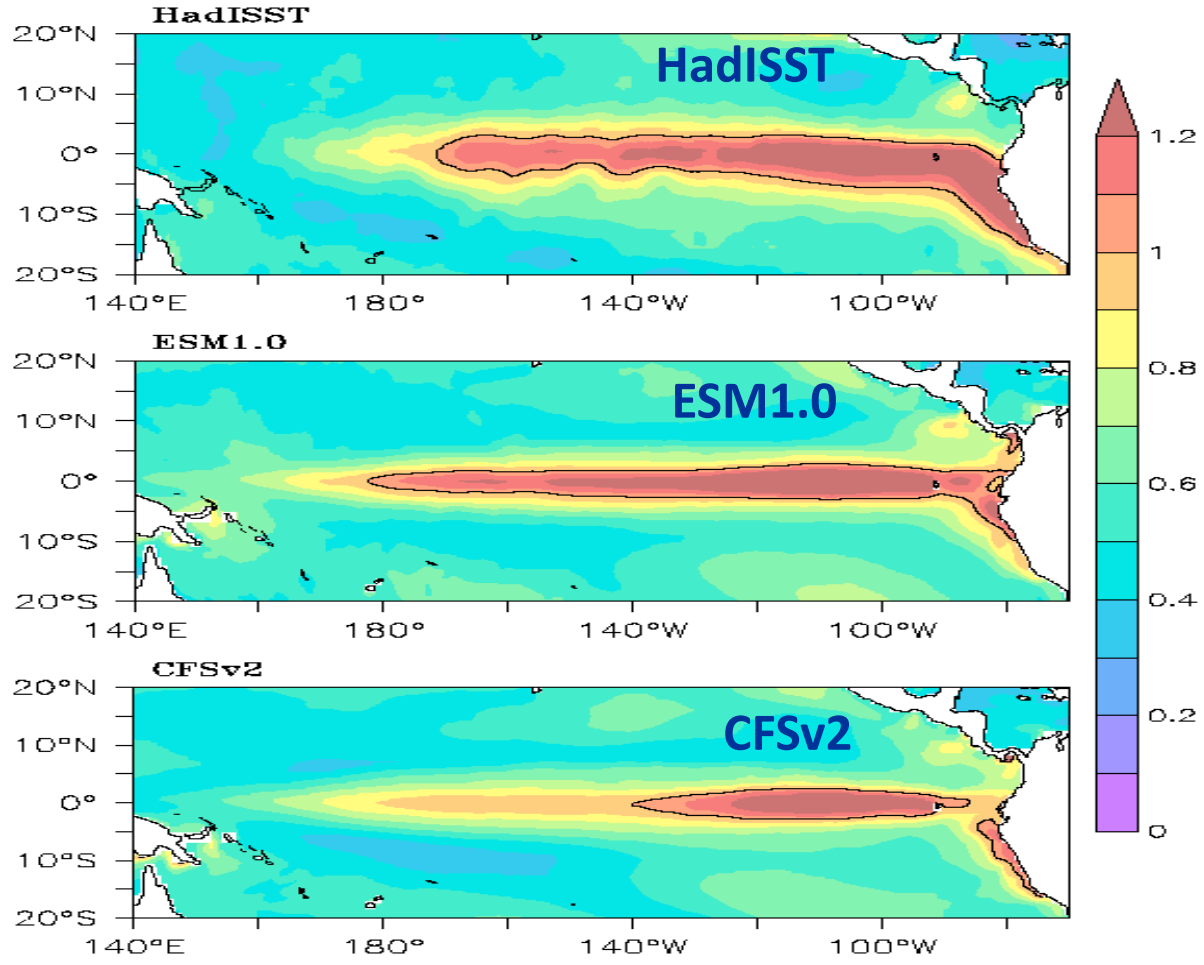

Interannual variability of Pacific SST in CFSv2 is mostly confined to the eastern equatorial Pacific; more realistic in ESM1.0

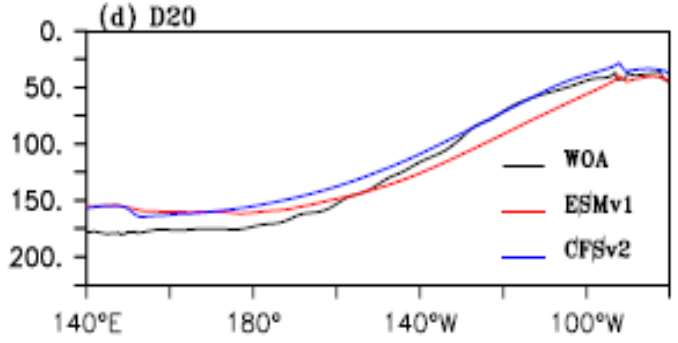

Courtesy: Swapna

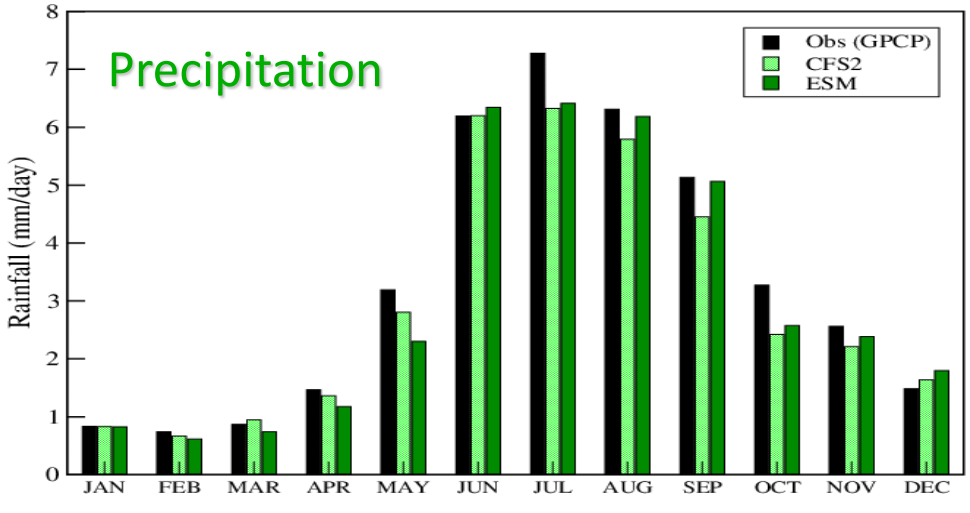

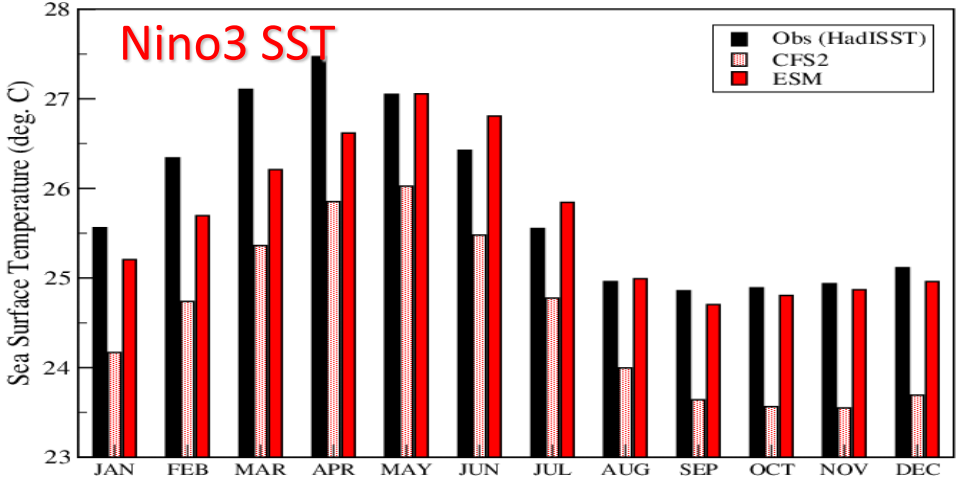

Precipitation

(5N-35N; 65E-95E)

Indian (land + ocean)

ENSO-Monsoon relationship

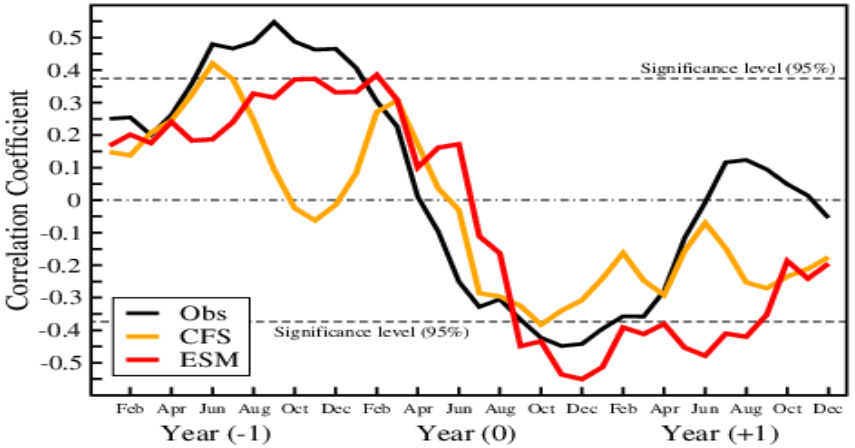

Lagged correlation between ISMR and Nino3 SST in the preceding/following months

CFS2 : 30 years (yr17-yr46)

ESM : 30 years (yr17-yr46)

Wavelet Power Spectrum of PC1 time-series. Power $(C)^2$ as a function of period and time

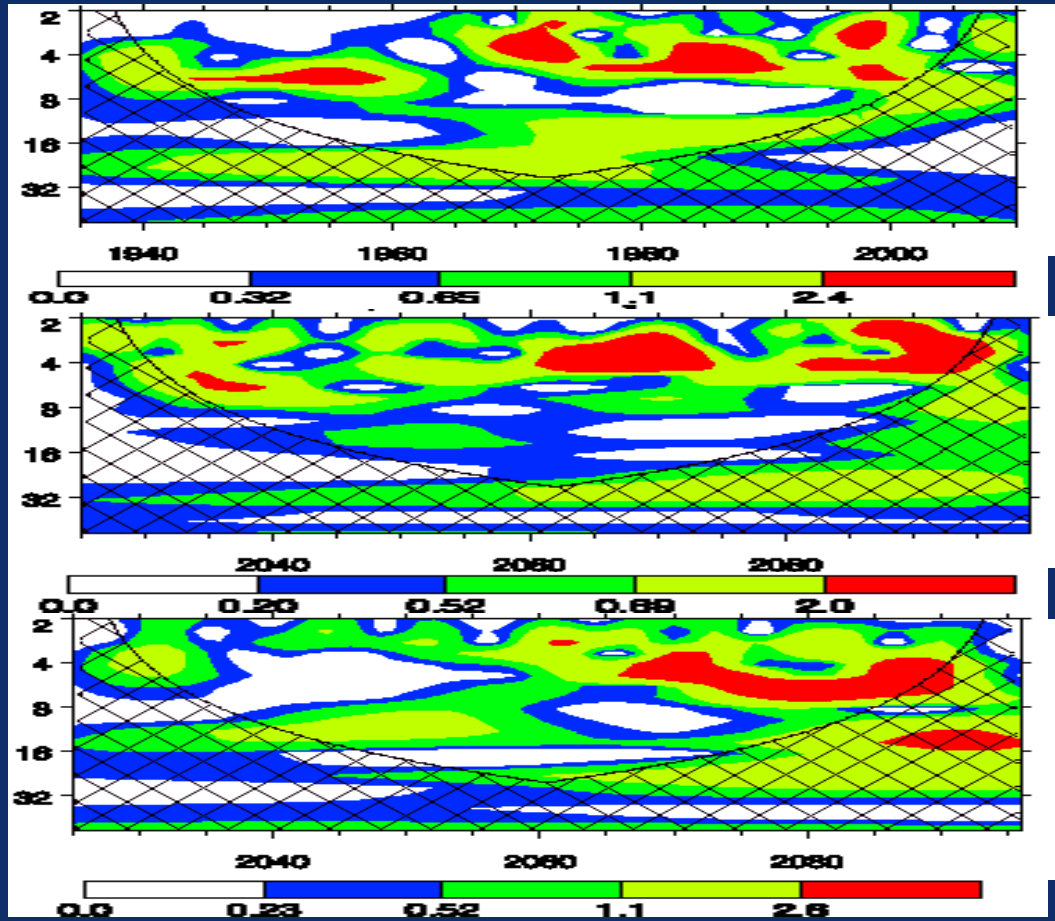

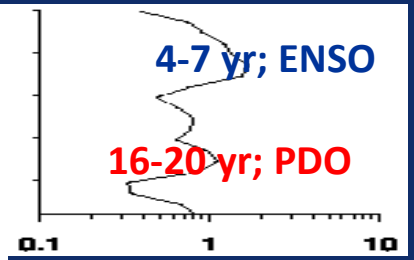

HadISST

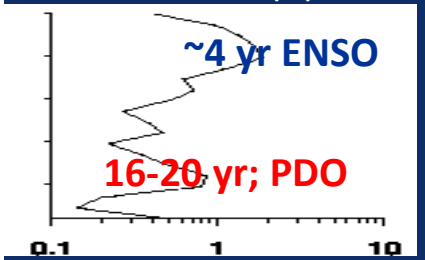

ESM1.0

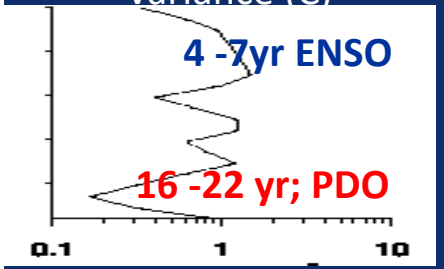

CFSv2

Courtesy: Swapna

IITM Earth System Model for long term climate studies – the first from India

Journal of Advances in Modeling Earth Systems

RESEARCH ARTICLE
10.1029/2017MS001262

Long-Term Climate Simulations Using the IITM Earth System Model (IITM-ESMv2) with Focus on the South Asian Monsoon

P. Swapna[1], R. Krishnan[1], N. Sandeep[1], A. G. Prajeesh[1], D. C. Ayantika[1], S. Manmeet[1], and R. Vellore[1]

Key Points:
- IITM-ESMv2 simulations show fidelity in capturing large-scale circulation

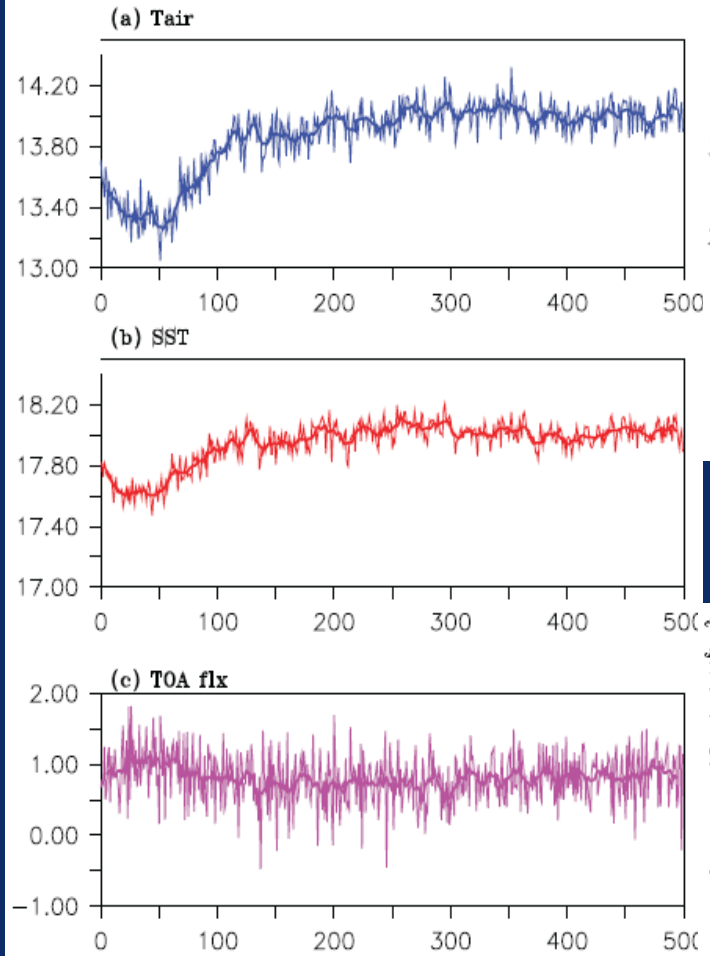

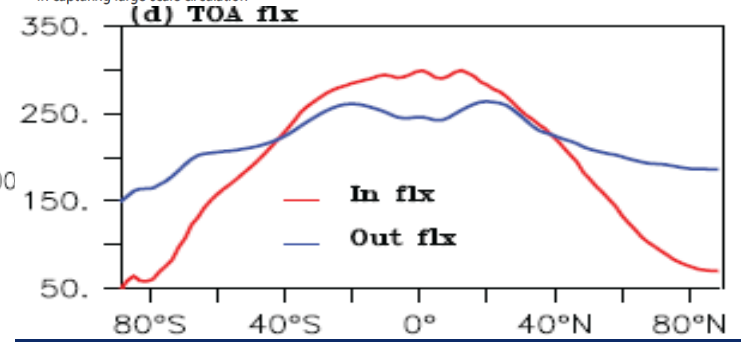

Improved simulation of sea-ice

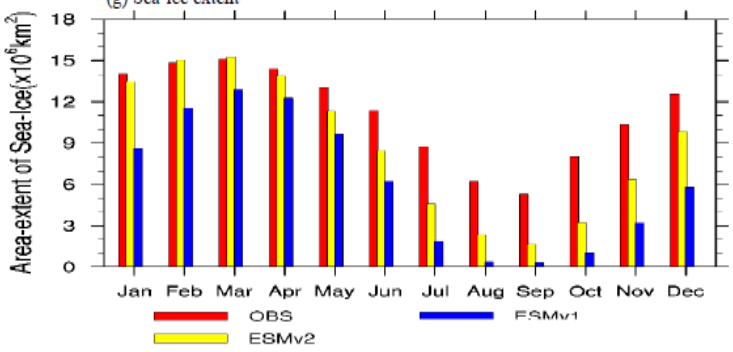

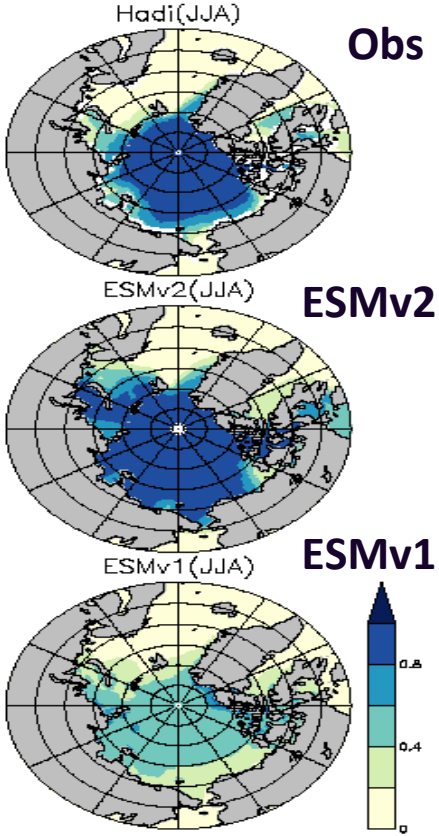

IITM-ESM for long-term climate change studies

Centre for Climate Change Research, Indian Institute of Tropical Meteorology, Pune

Atmosphere : GFS (Global Forecast System)

- **T62 ; vertical: 64 sigma – pressure hybrid levels**
- **Resolution ~200 km**
- **Model top 0.2 mb**
- **Prescribed MAC-v2 aerosols**

Land surface : Noah LSM

Ocean: Modular Ocean Model v4p1 (MOM4p1)

- **Tripolar; 360x200 ; 1 deg poleward ; 0.33 deg near equator**
- **50 levels ; Top grid cell 5m**
- **Ocean Biogeochemistry : TOPAZ**
- **Ice Model : Sea Ice Simulator**

Energy Balance in IITM ESM

Energy Balance in IITM ESM

	Net flux TOA ($W\ m^{-2}$)	Net Flux Surface ($W\ m^{-2}$)	Difference ($W\ m^{-2}$)
ESMv1 (T126)	6.6	1.2	5.4
ESMv2 (T62)	0.80	0.75	0.05

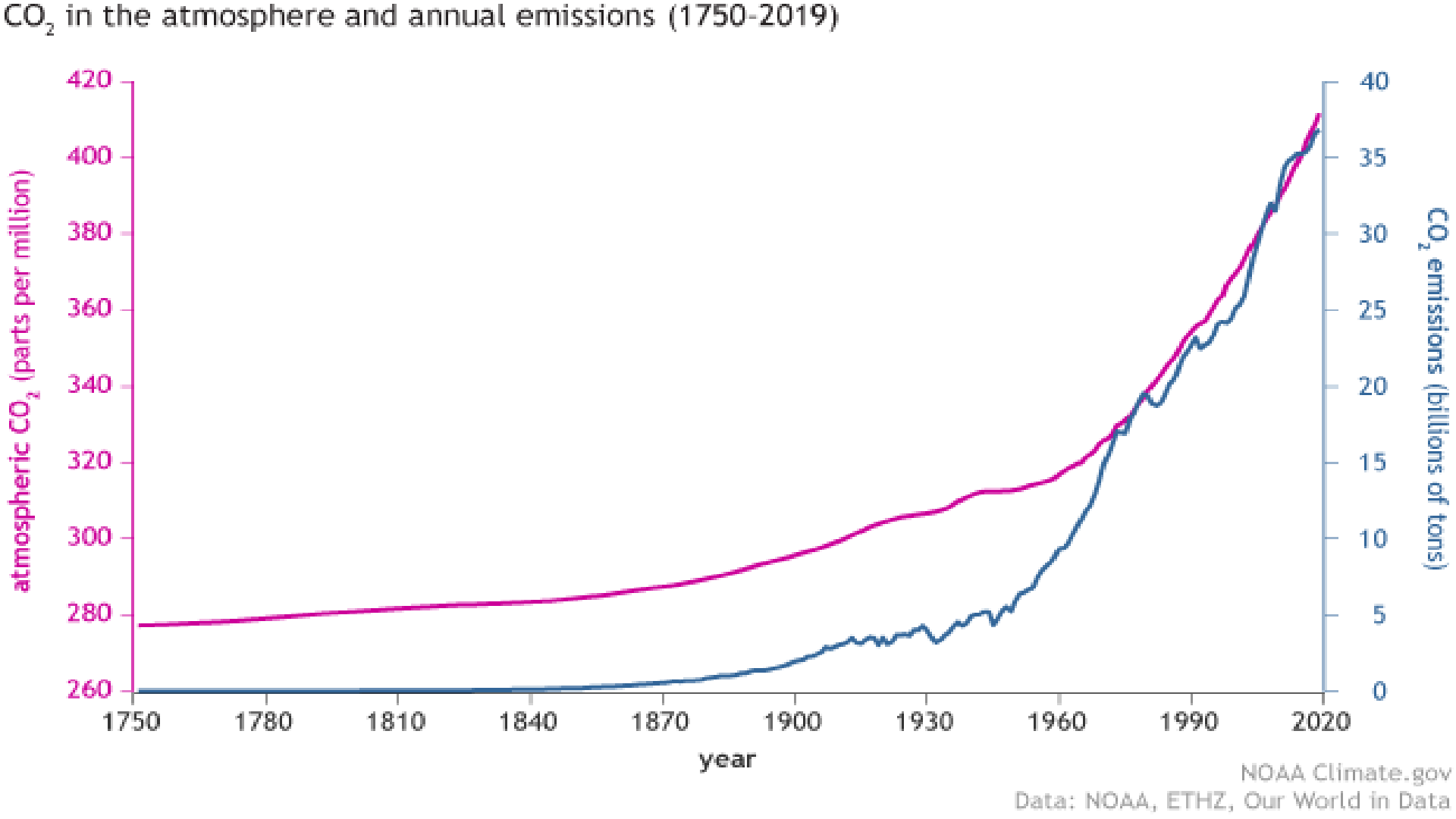
CO_2 in the atmosphere and annual emissions (1750-2019)
atmospheric CO_2 (parts per million)
420
400
380
360
340
320
300
280
260
CO_2 emissions (billions of tons)
40
35
30
25
20
15
10
5
0
1750
1780
1810
1840
1870
1900
1930
1960
1990
2020
year
NOAA Climate.gov
Data: NOAA, ETHZ, Our World in Data

COMBINED HEATING INFLUENCE OF GREENHOUSE GASES

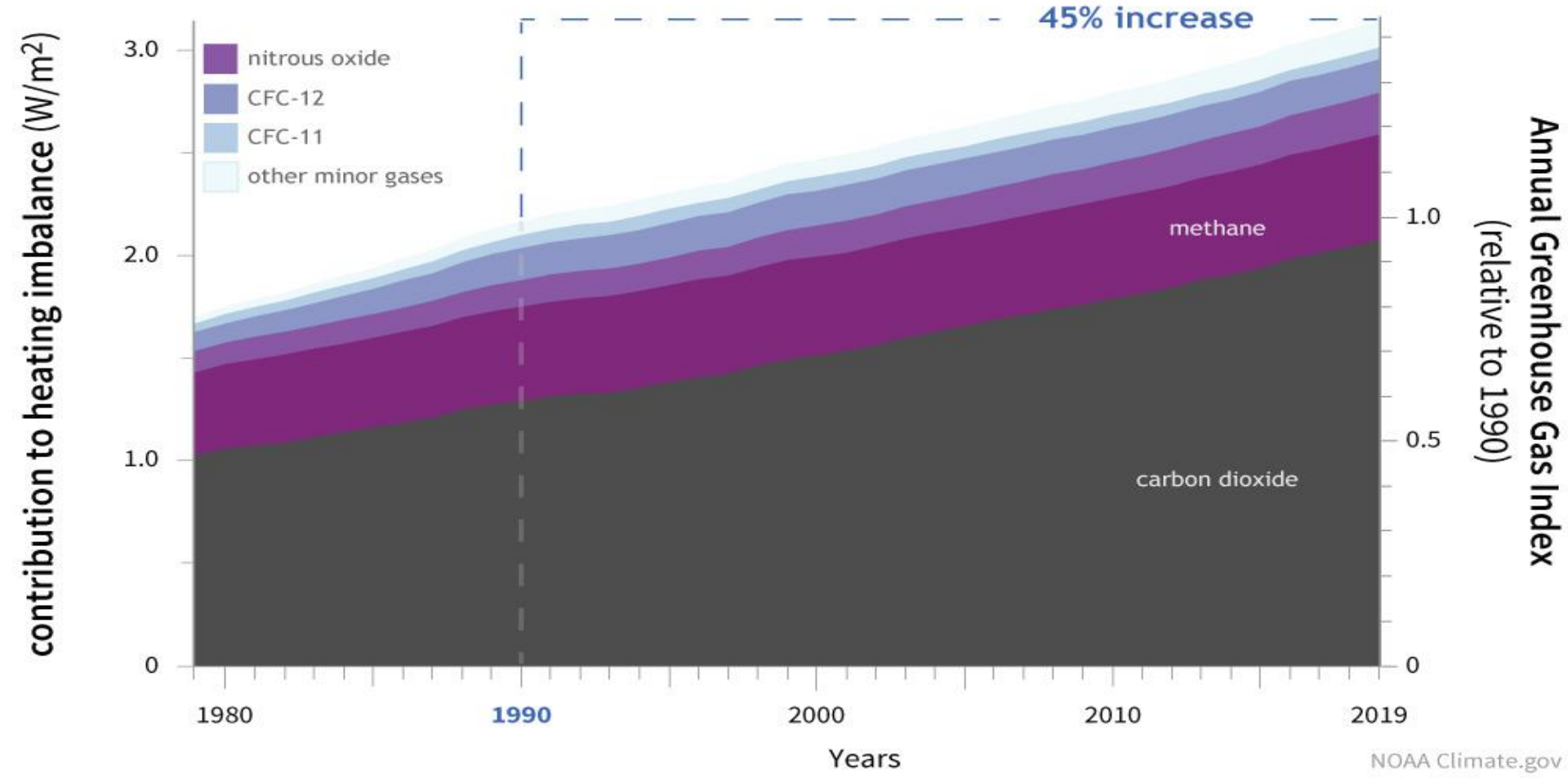

NOAA Climate.gov
Data: ESRL

TOA Energy Imbalance (CMIP5 Models)

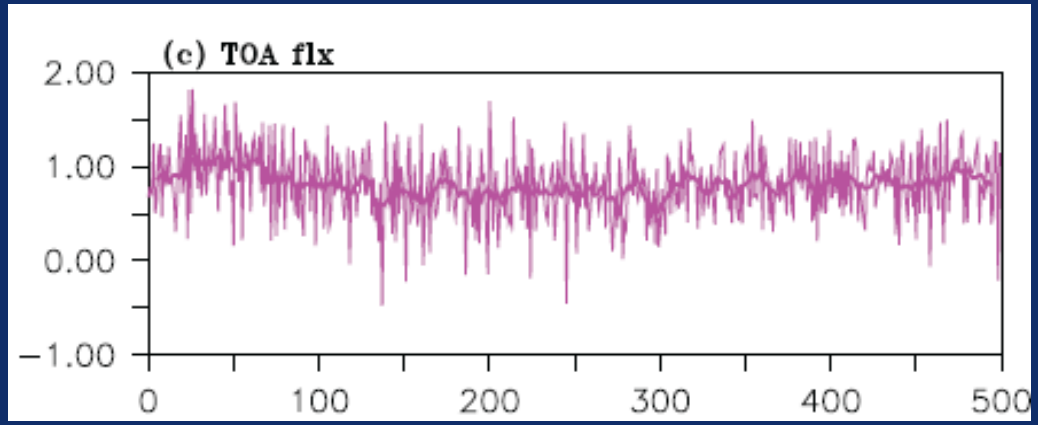

Energy Balance in IIITM ESMv2

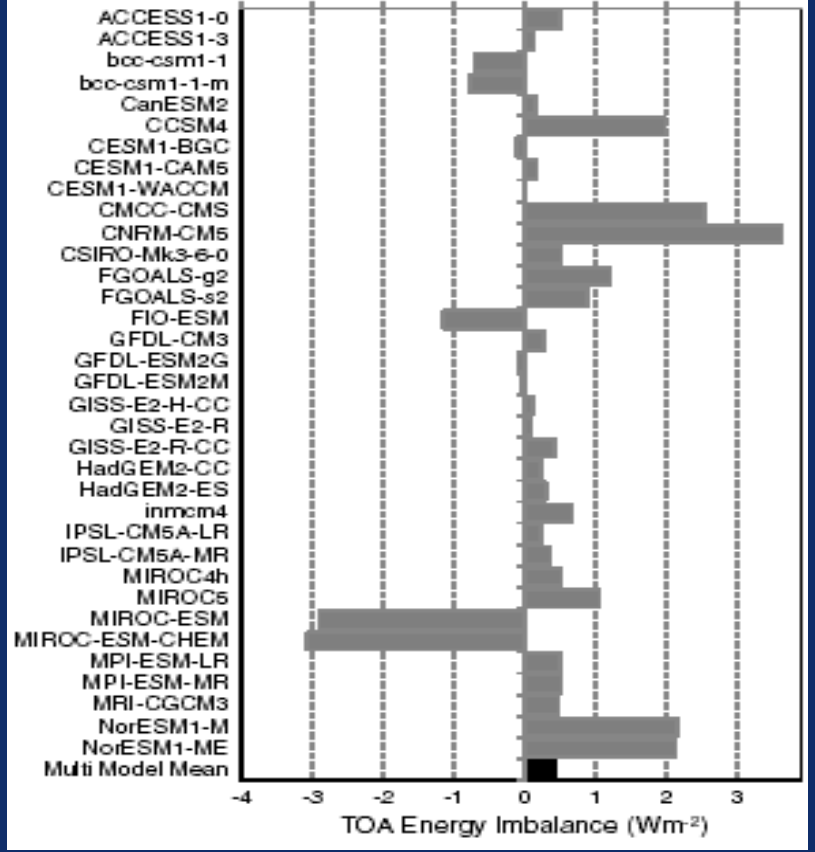

Preindustrial TOA (Wm^{-2}) energy imbalance for CMIP5 models (Forster et al., 2013)

Net Radiation (W m^{-2}) at TOA

Obs (CERES)

IITM-ESMv2

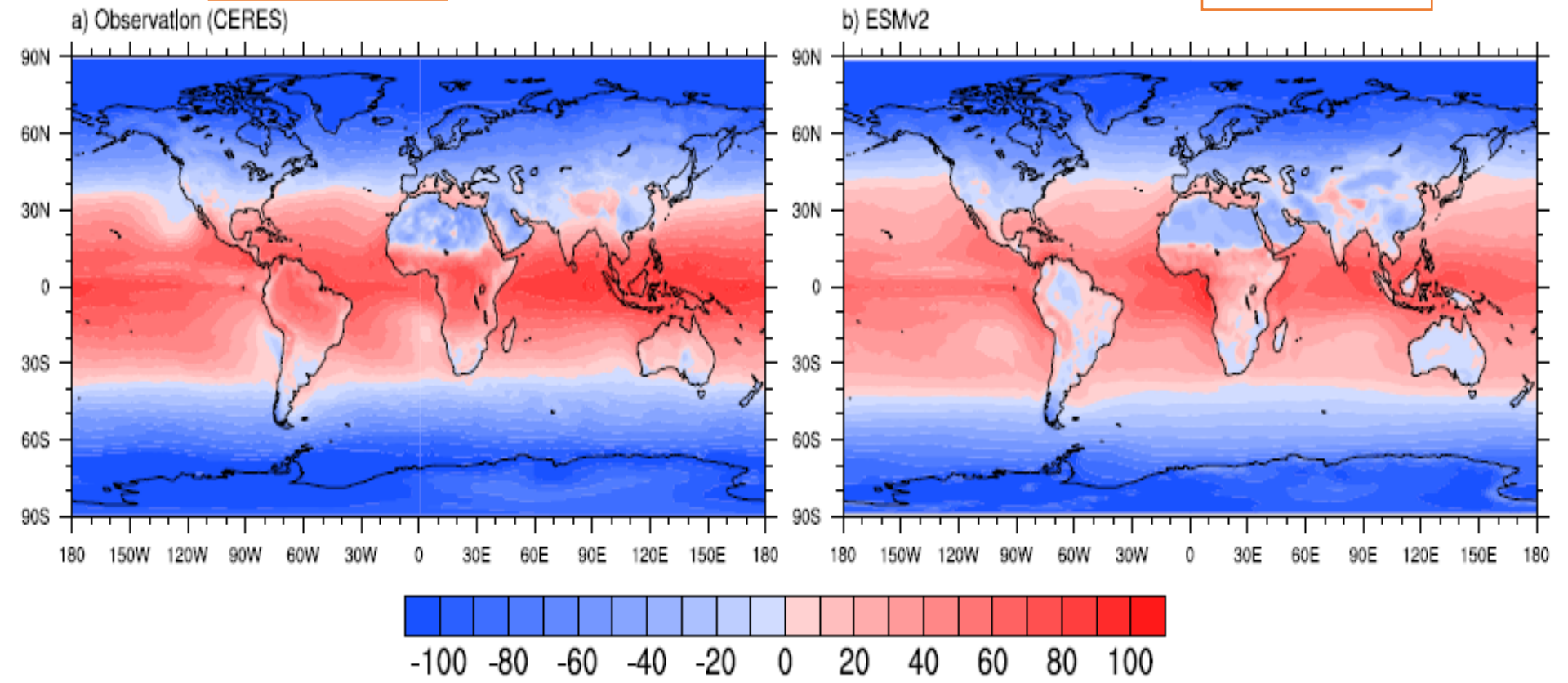

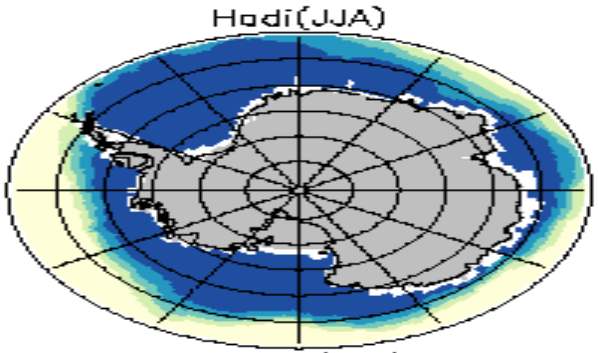

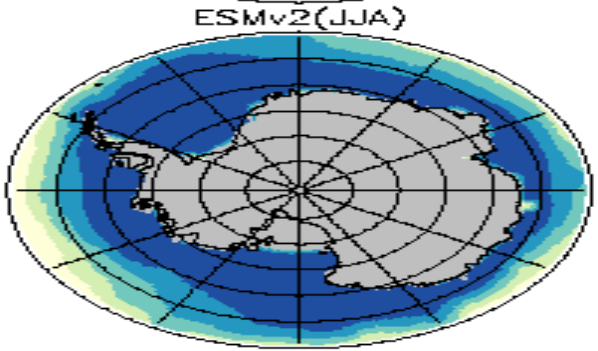

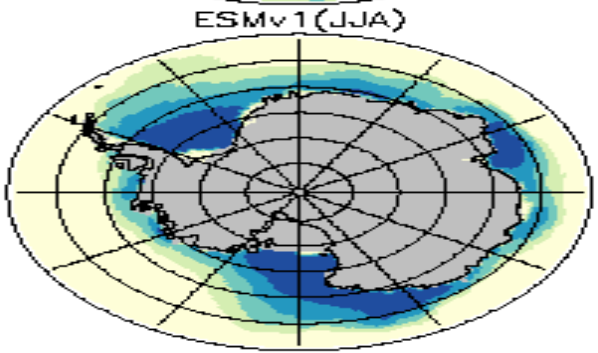

Obs

ESMv2

Improved simulation of sea-ice during JJA

ESMv1

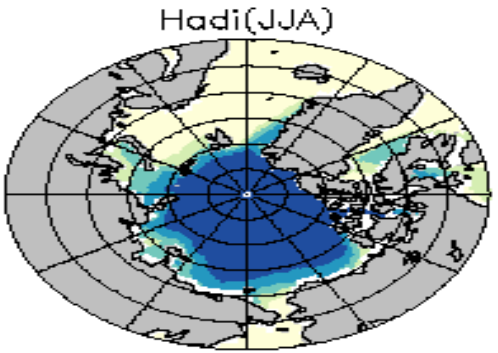

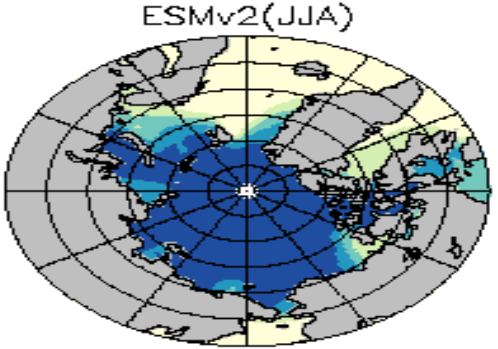

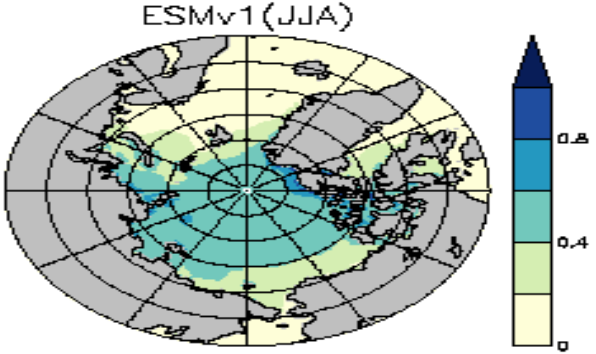

Thermohaline Circulation (THC)
Global Conveyor Belt

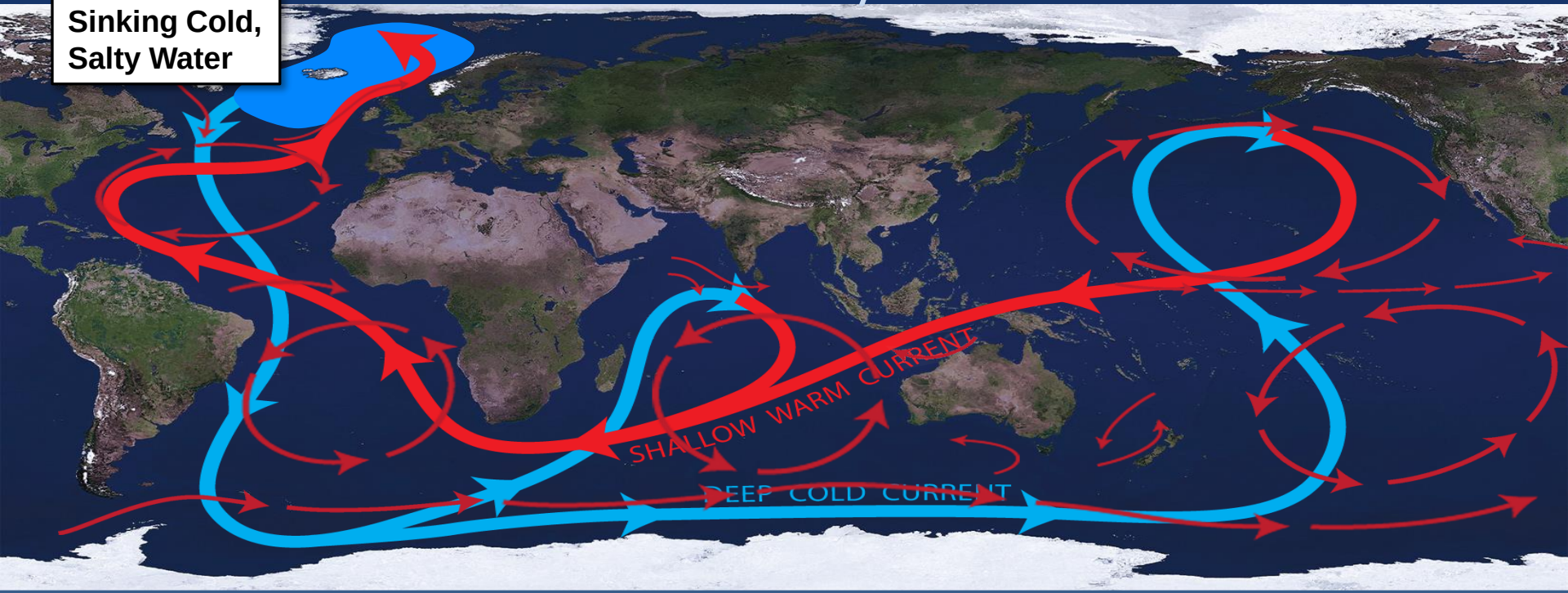

Improved simulation of AMOC in IITM-ESMV2

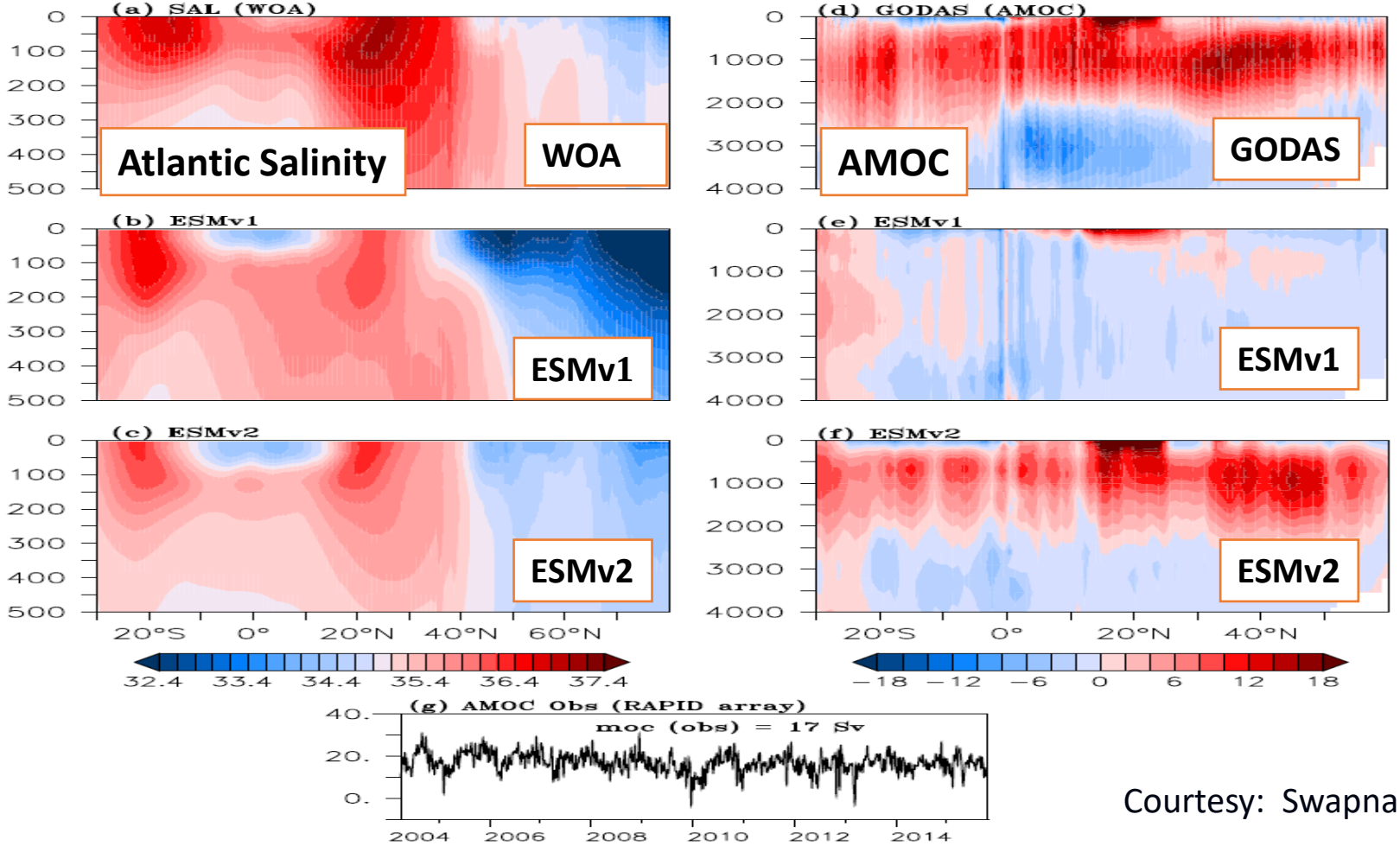

Courtesy: Swapna

Ocean-Atmosphere coupled feedbacks in IITM-ESM

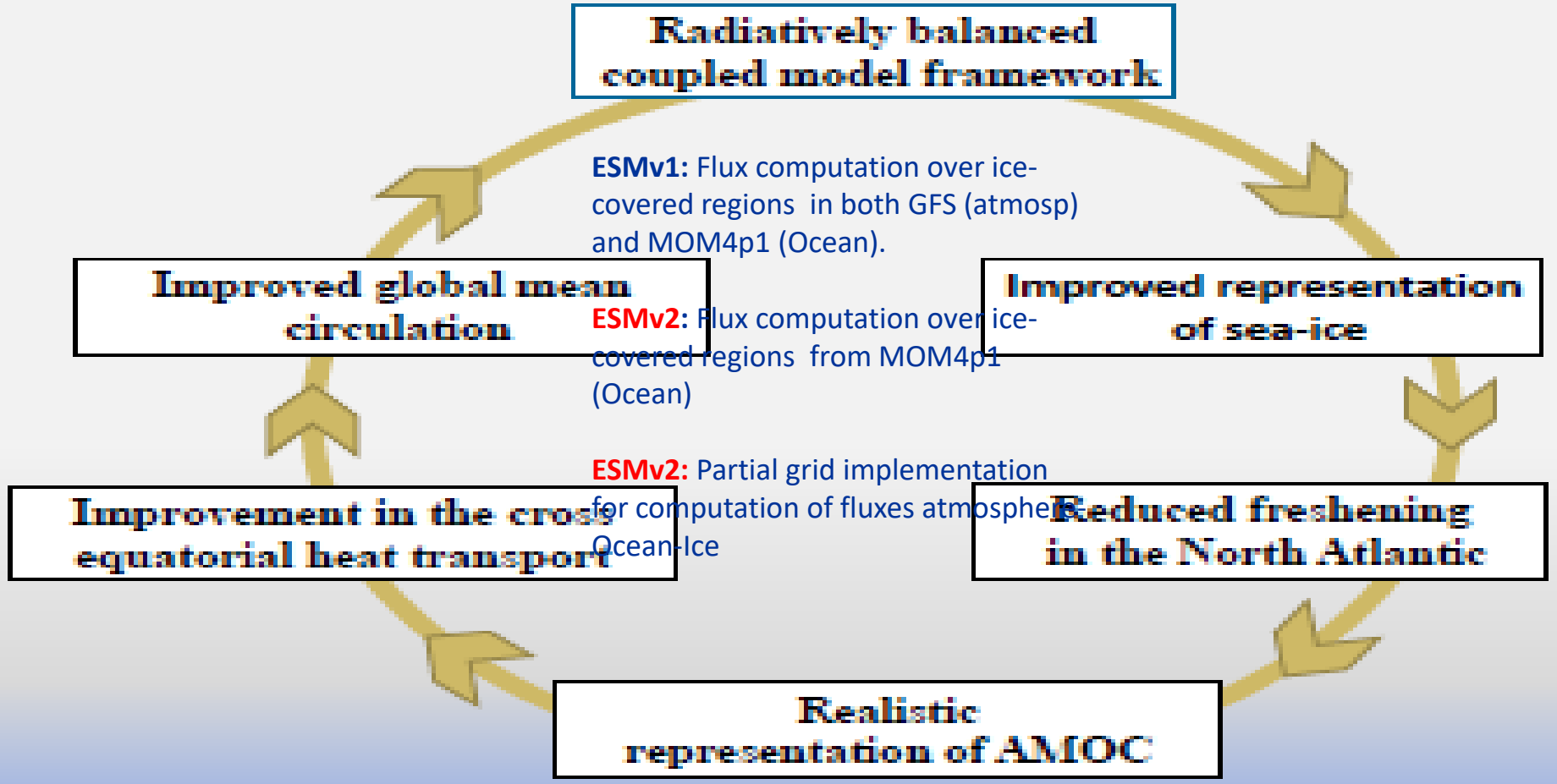

ESMv1: Flux computation over ice-covered regions in both GFS (atmosp) and MOM4p1 (Ocean).

ESMv2: Flux computation over ice-covered regions from MOM4p1 (Ocean)

ESMv2: Partial grid implementation for computation of fluxes atmosphere-Ocean-Ice

Precipitation (June-Sept)

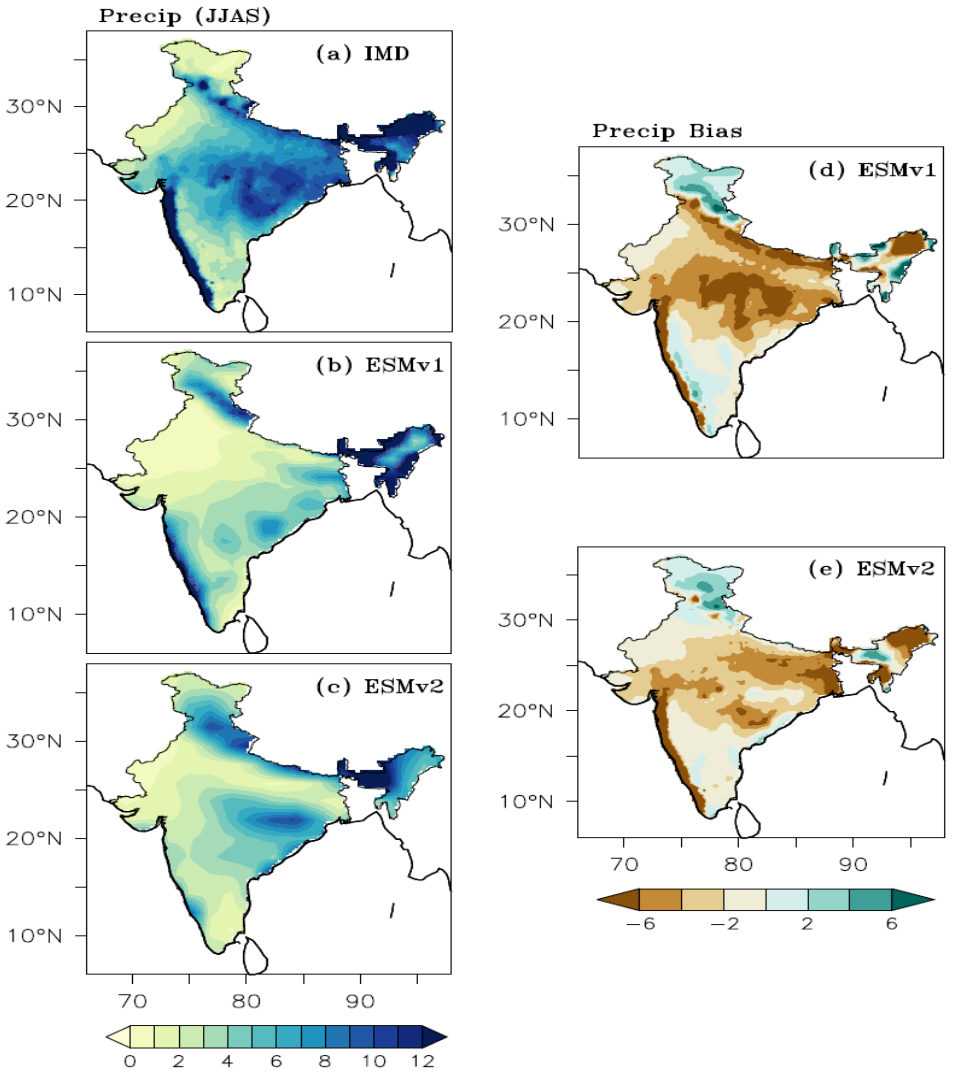

Impact of Revised SAS (Simplified Arakawa Schubert) convective parameterization on monsoon rainfall simulation in CFSv2 - Malay, G, Phani, R.M, P. Mukhopadhyay

Climate Dynamics (2014)

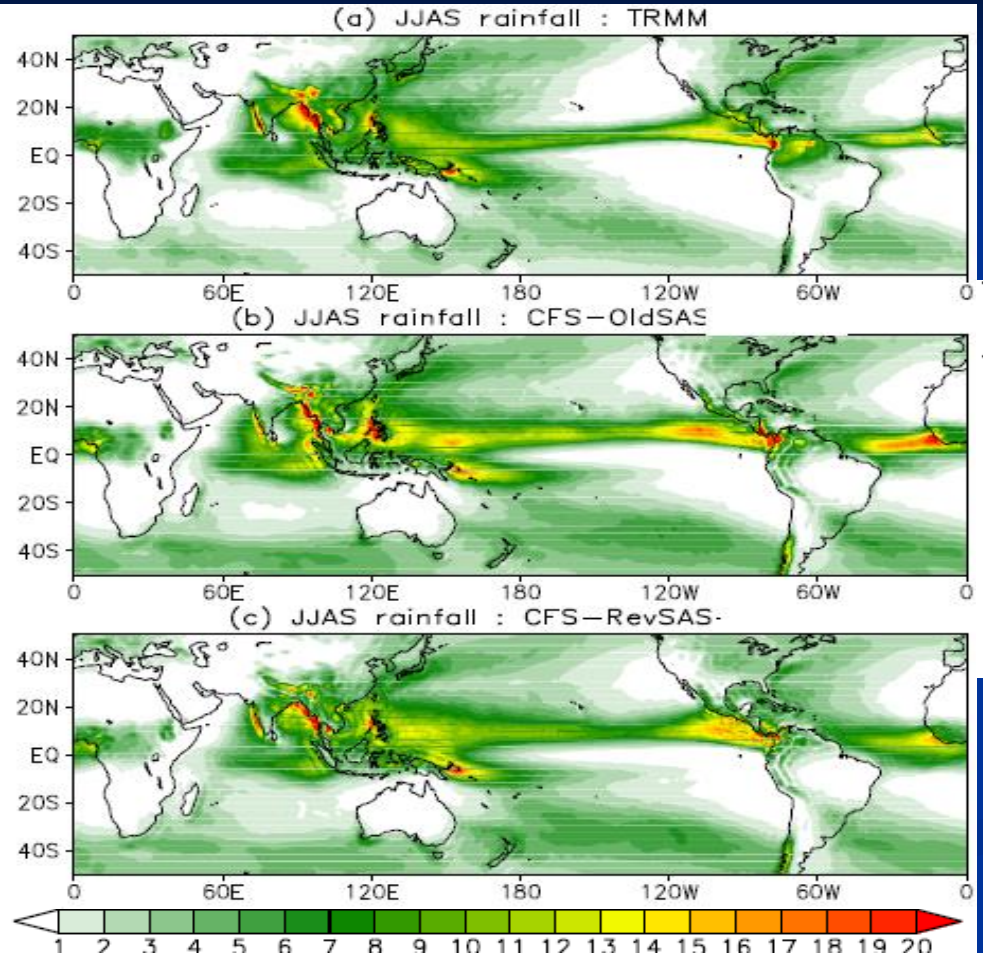

Annual cycle of rainfall over Indian region

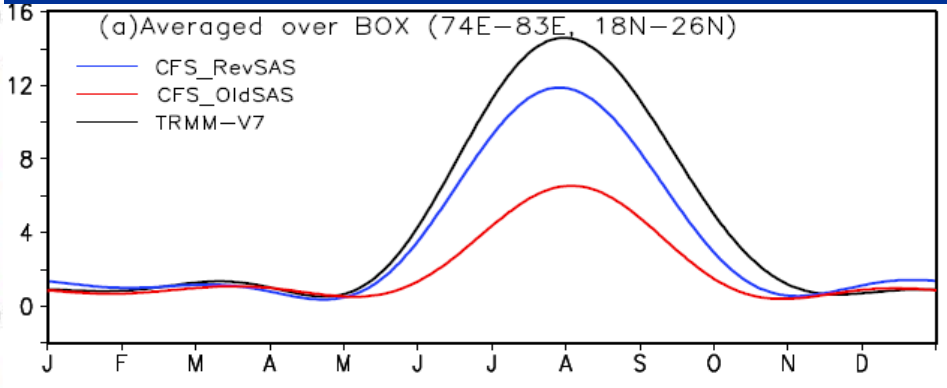

CFSv2 T126 free run: 15 years - Courtesy: P. Mukhopadhyay, IITM

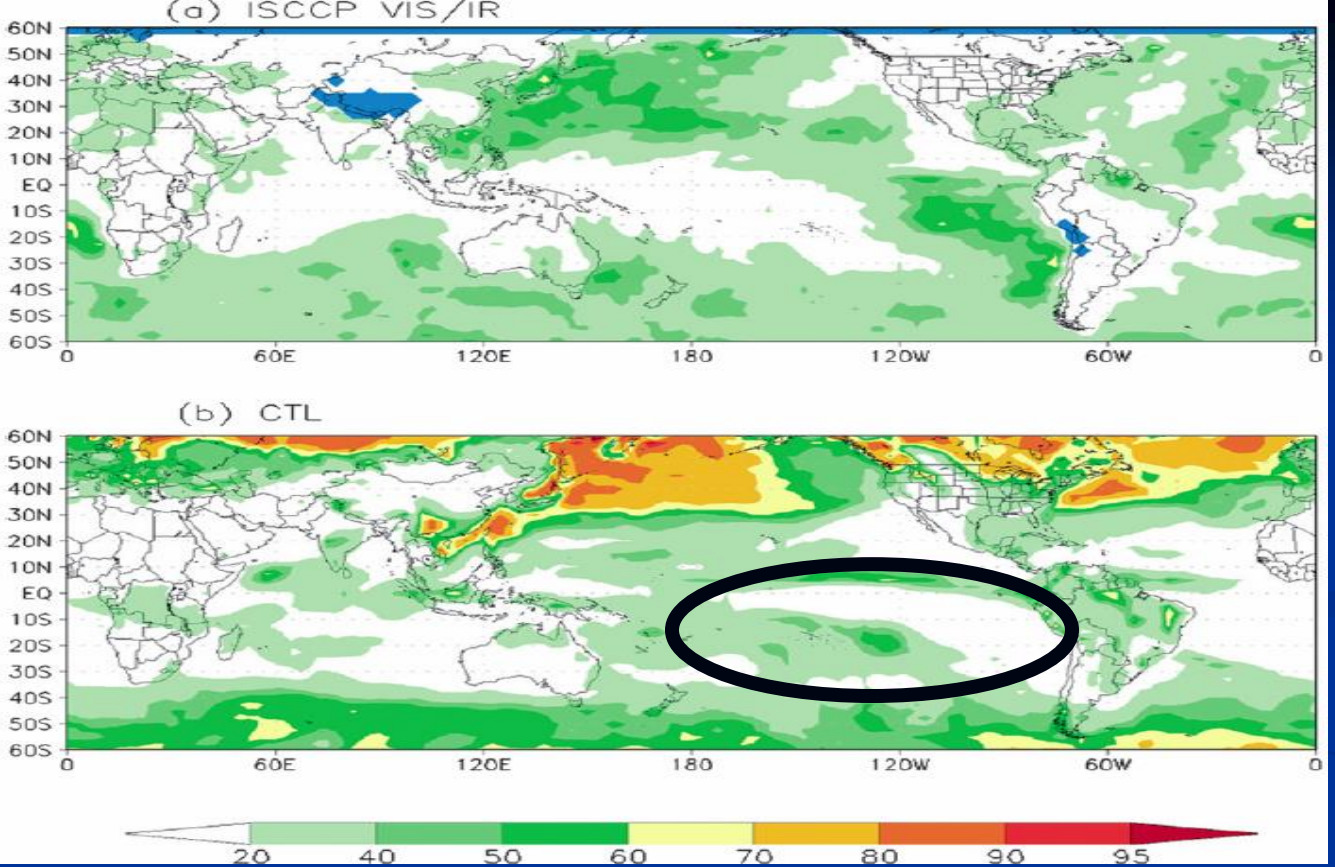

Monthly mean low cloud cover (%) for January 2003 from ISCCP (Rossow and Schiffer, 1991) VIS/IR satellite observations (blue color indicates 'no data' available).

Control simulation using the old shallow convection Scheme of NCEP GFS

Han and Pan, 2011

Long-standing problems in NCEP GFS: Systematic underestimation of stratocumulus clouds in the eastern Pacific and Atlantic Oceans; and the frequent occurrence of unrealistic excessive heavy precipitation, the so-called grid-point storms

Revision of Convection and Vertical Diffusion Schemes in the NCEP Global Forecast System

Han and Pan (2011): Weather and Forecasting

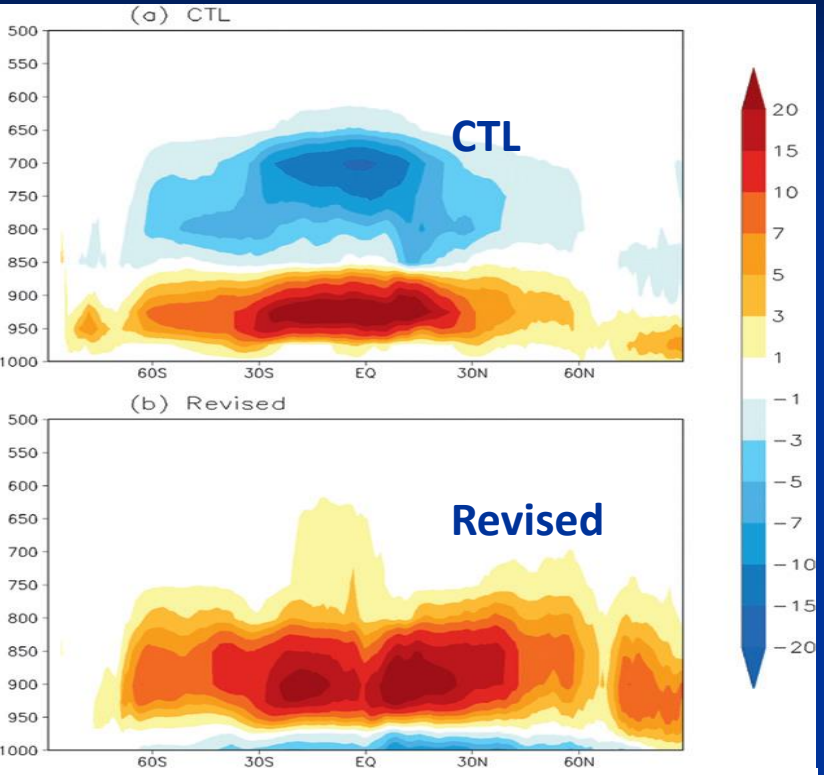

FIG. 4. Zonally averaged heating rates (10^{-6} K s^{-1}) due to the shallow convection for January 2003 from the (a) control and (b) revised model simulations.

Revised convection and planetary boundary layer (PBL) schemes in the NCEP's GFS.

The shallow convection scheme in the revision employs a mass flux parameterization replacing the old turbulent diffusion-based approach. For deep convection, the scheme is revised to make cumulus convection stronger and deeper to deplete more instability in the atmospheric column and result in suppression of the excessive grid-scale precipitation.

The PBL model was revised to enhance turbulence diffusion in stratocumulus regions. A remarkable difference between the new and old SC schemes is seen in the heating or cooling behavior in lower-atmospheric layers above the PBL. While the old SC scheme produces a pair of layers in the lower atmosphere with cooling above and heating below, the new SC scheme using the mass-flux approach produces heating throughout the convection layers.

In particular, the new SC scheme does not destroy stratocumulus clouds off the west coasts of South America and Africa as the old scheme does. On the other hand, the revised deep convection scheme, having a larger cloud-base mass flux and higher cloud tops, appears to effectively eliminate the remaining instability in the atmospheric column that is responsible for the excessive grid-scale precipitation in the old scheme.

Mean summer rainfall (June-Sept)

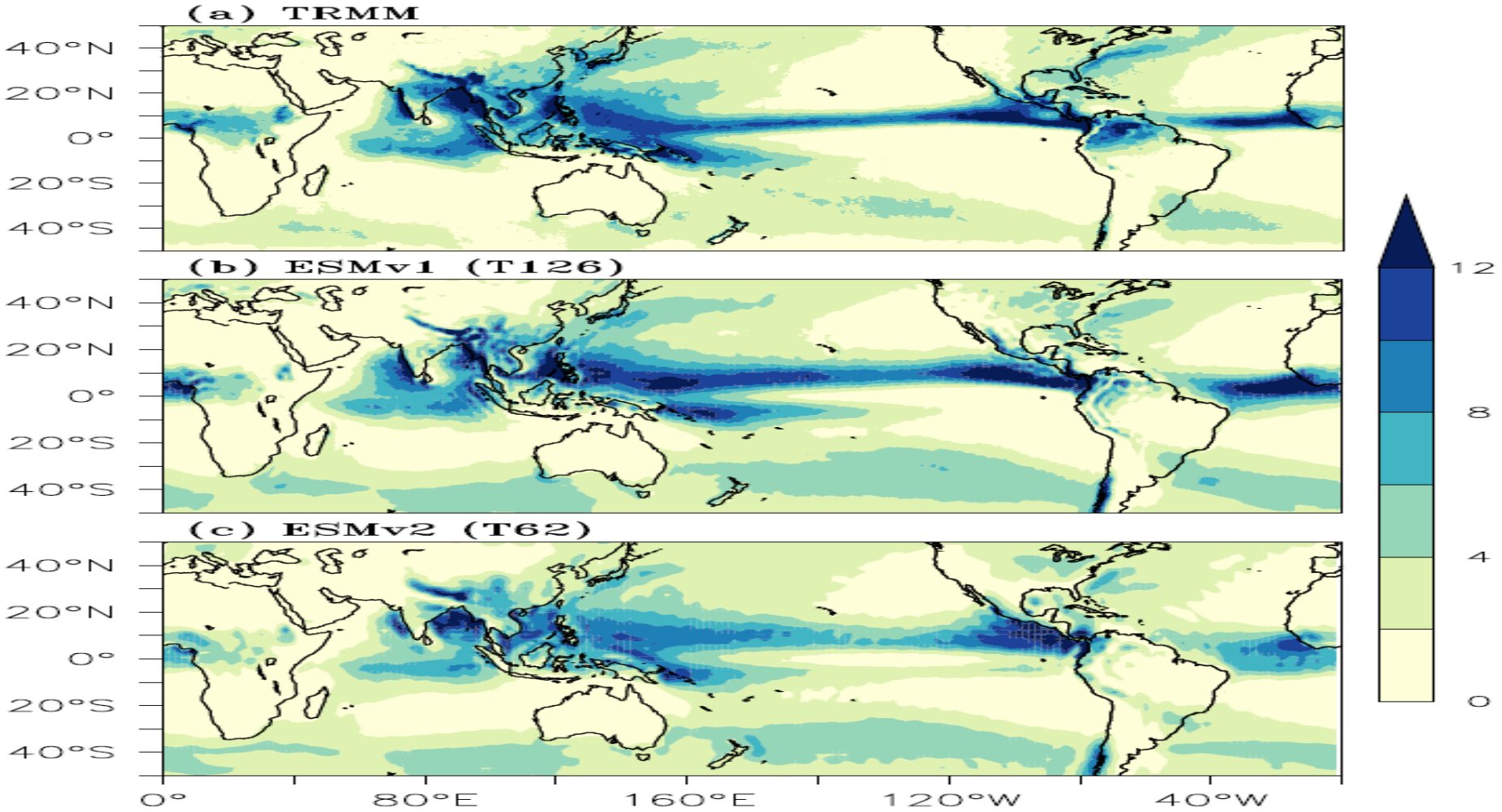

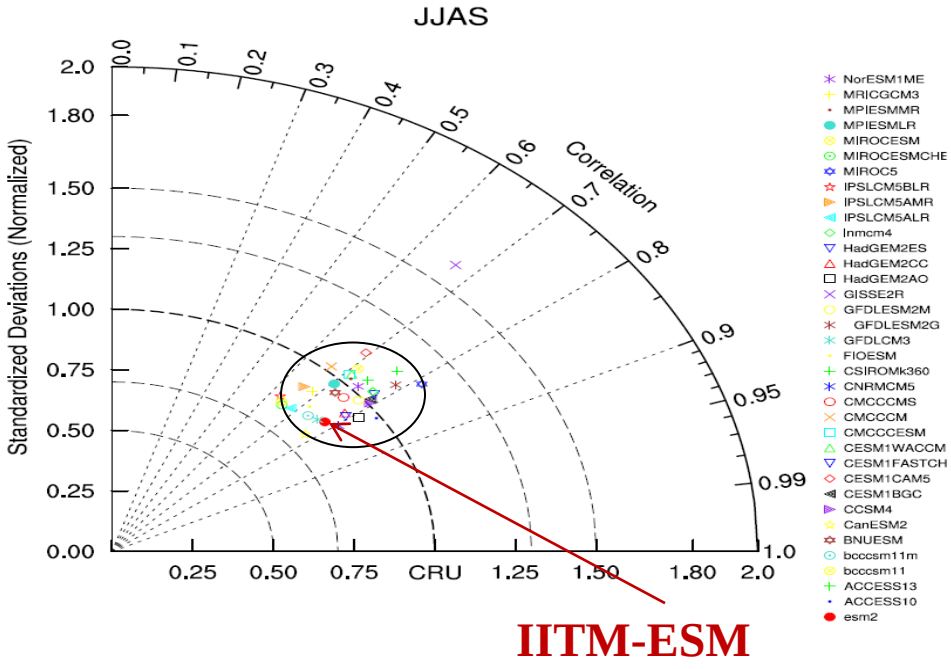

IITM-ESM

Asian region (JJAS precipitation)

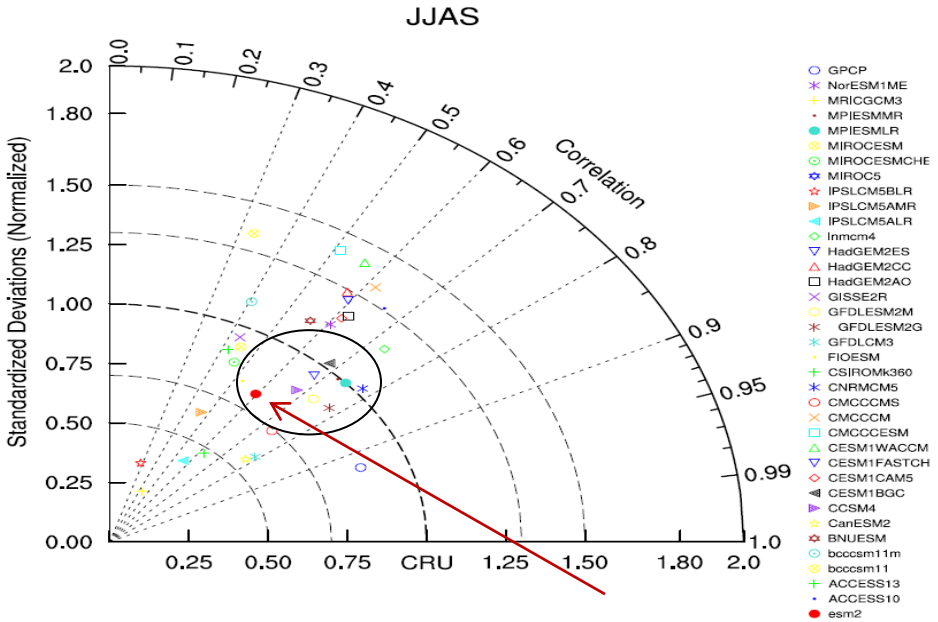

Indian region (JJAS precipitation)

IITM-ESM

Courtesy: Swapna

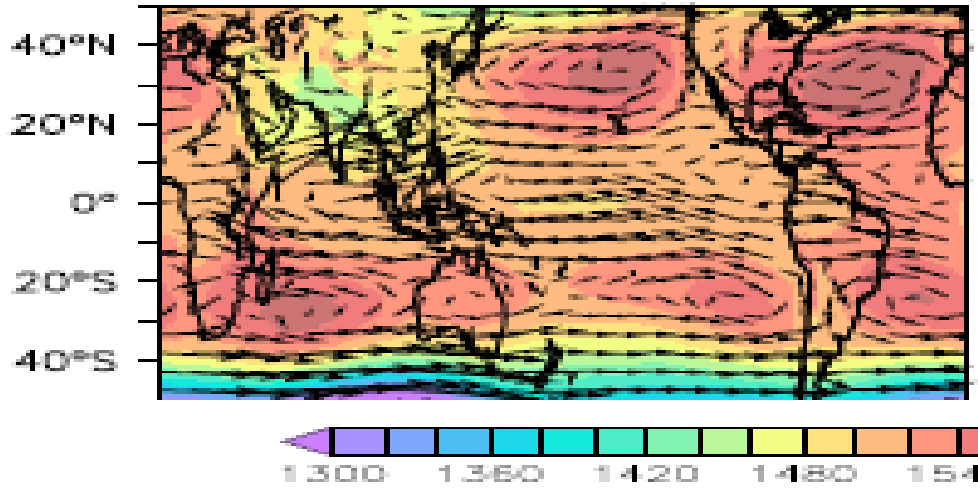

Winds & Geopotential Height: 850 hPa

JJAS

ERA-Interim

- Pacific sub-tropical anticyclone
- Easterly trade winds over Pacific

ESM-v1

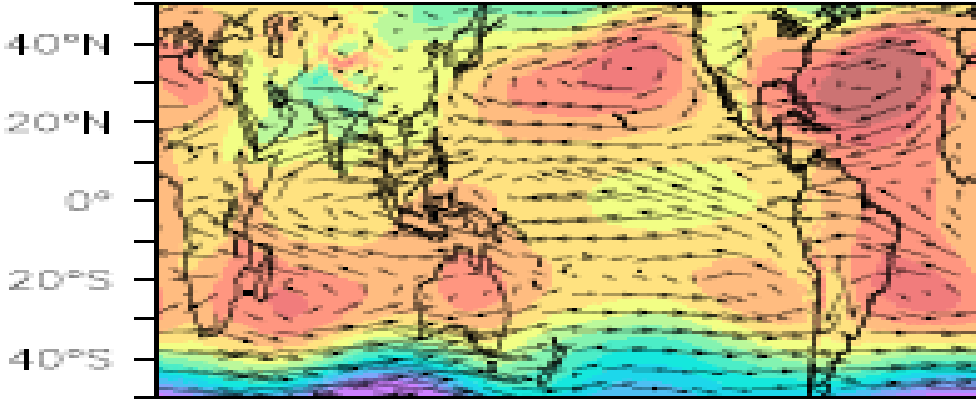

ESM-v2

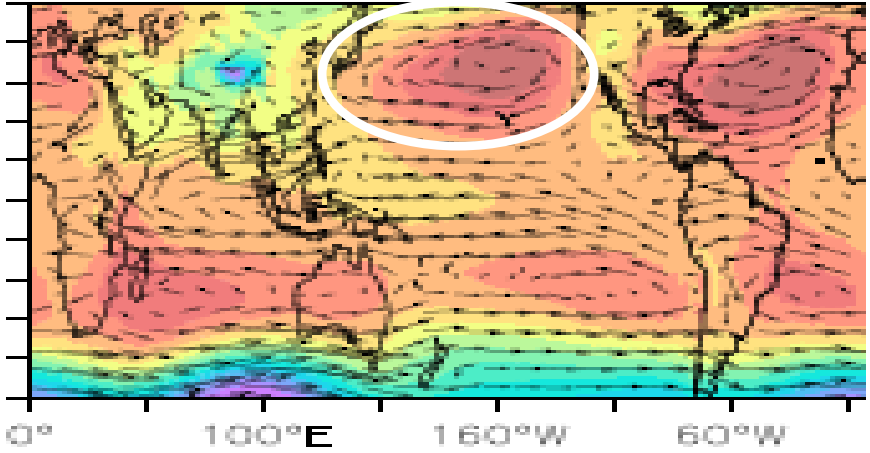

Winds & Geopotential Height: 850 hPa

DJF

ERA-Interim

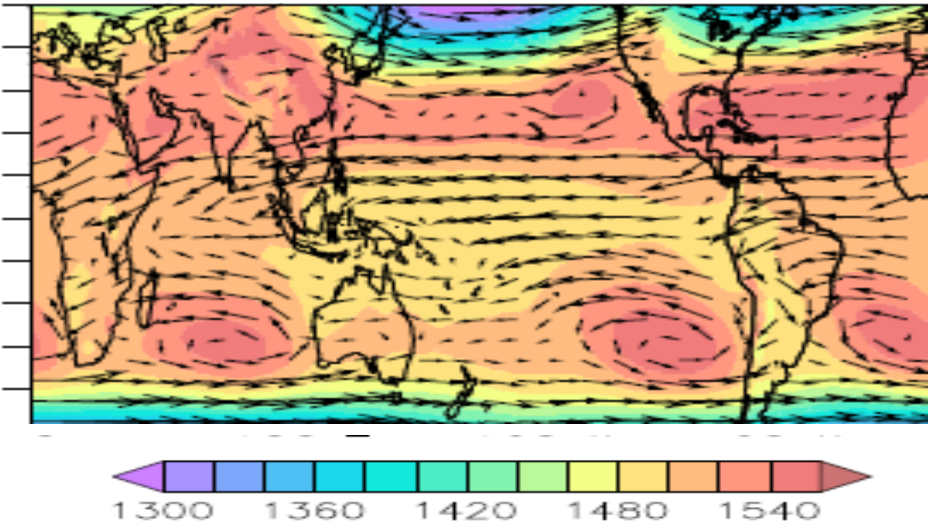

ESM-v1

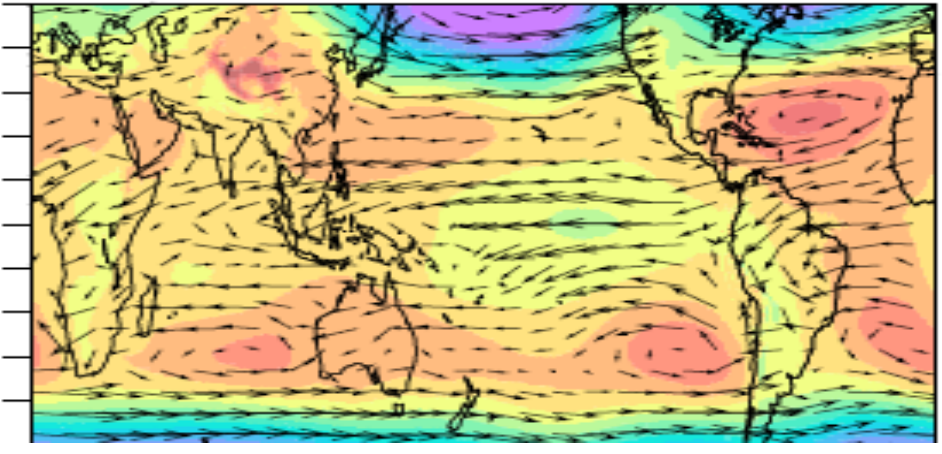

ESM-v2

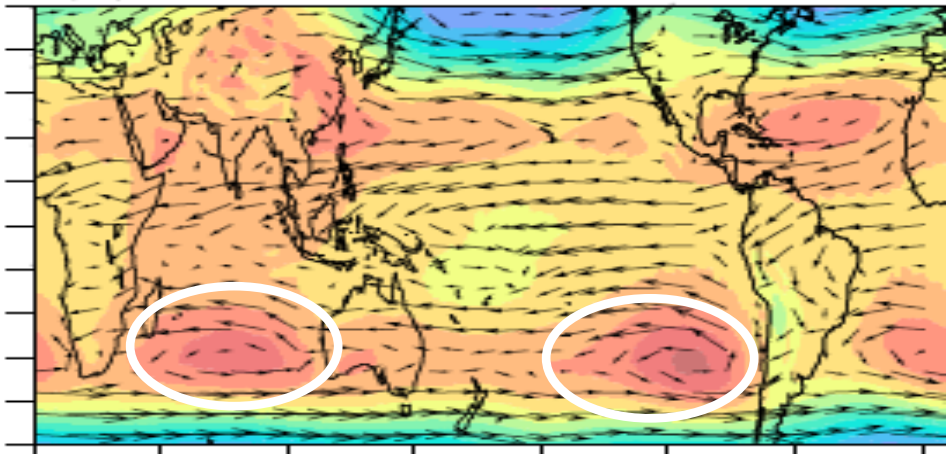

Seasonal variability of NINO3.4

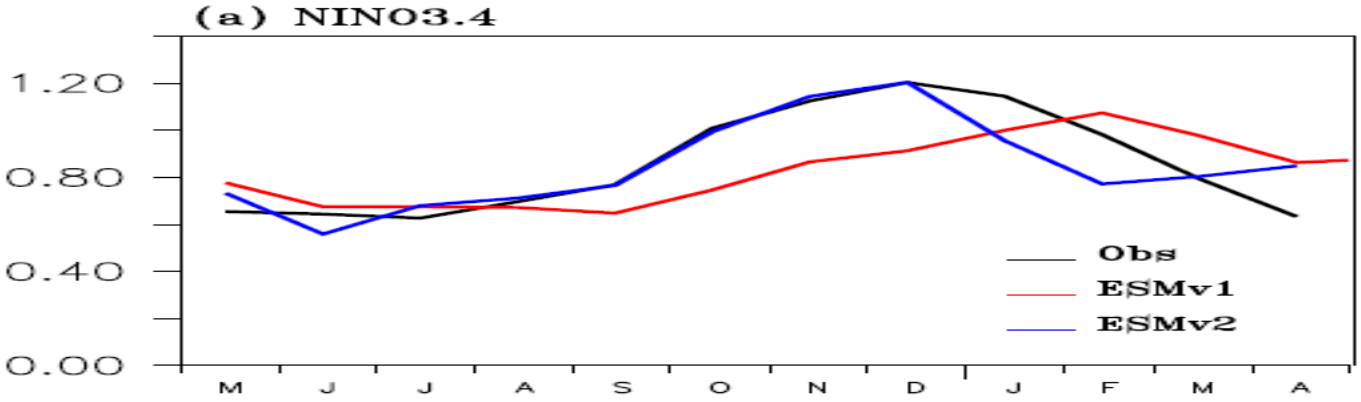

ENSO-Monsoon teleconnection

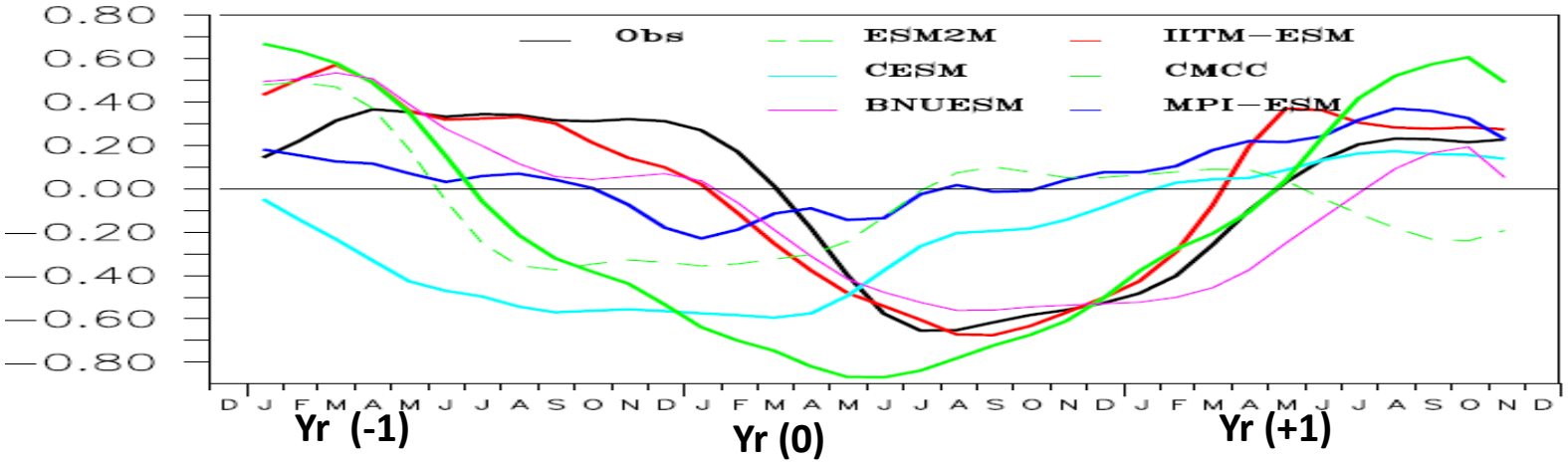

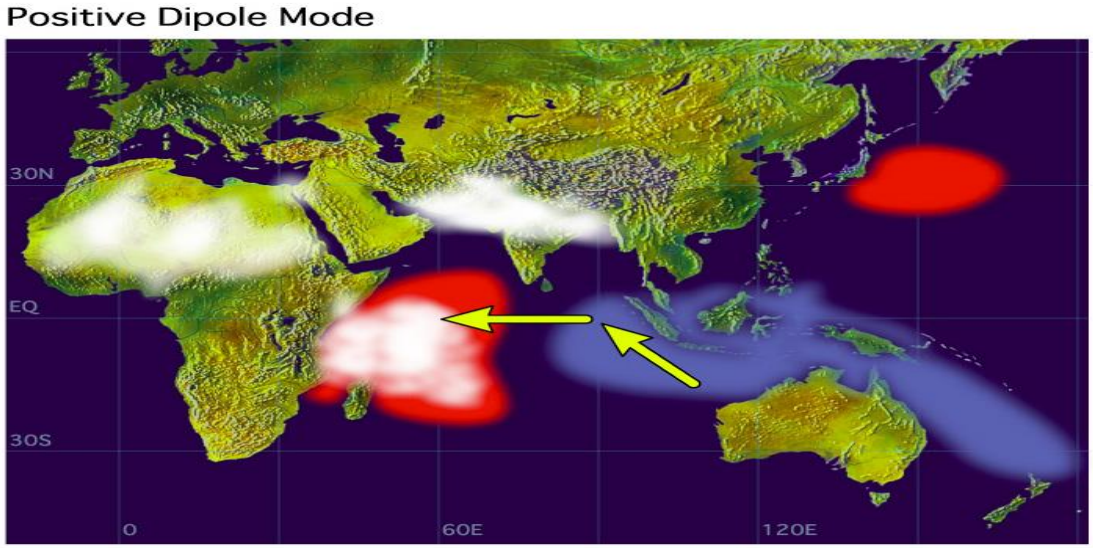

Indian Ocean Dipole - Saji et al., 1999

Schematic: SST anomalies (red - warming; blue - cooling) during positive IOD. White patches - increased convective activity.

- Enhanced monsoon precipitation over India during positive IOD events - **e.g., 1994, 1961, 2019**
- Intensified **cross-equatorial transport of moisture** from the Southeastern equatorial Indian Ocean (SETIO)

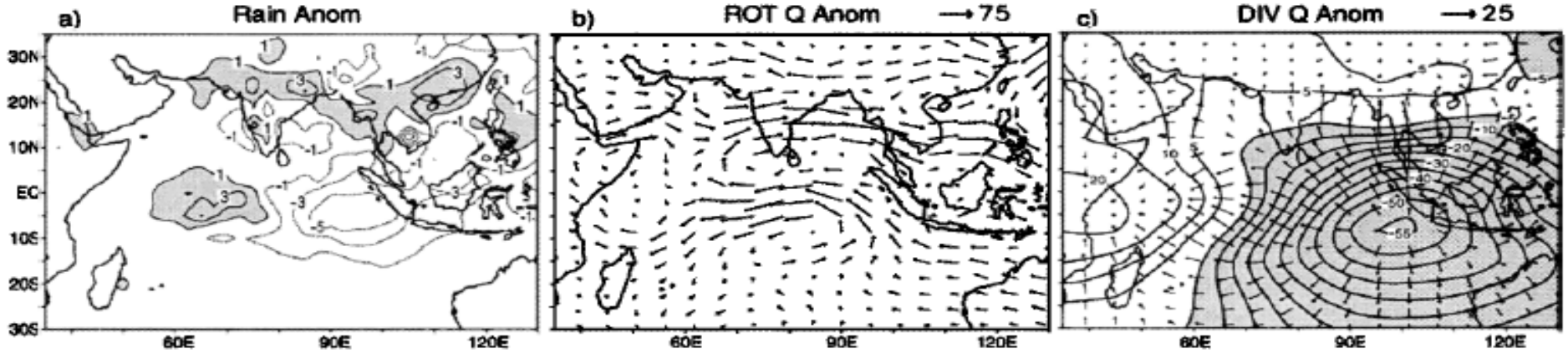

Behera, Krishnan and Yamagata, 1999 GRL

JJAS mean rainfall (mm/day) & moisture transport (kg/m2/s)

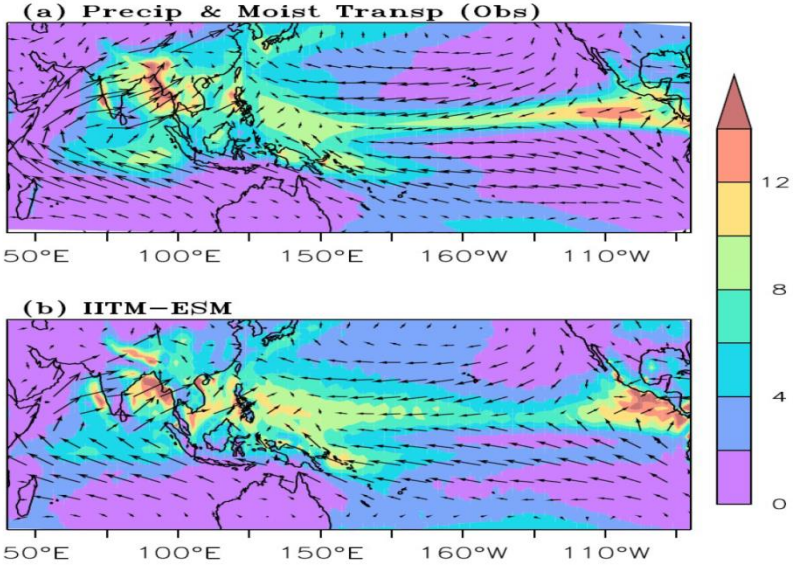

Anomaly composite of JJAS rainfall (mm/day) during positive IOD years from observation and IITM-ESM

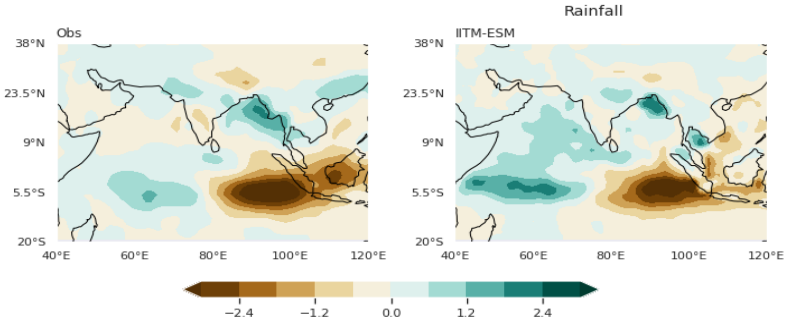

Spatial pattern of leading modes of Indian Ocean SST variability for observation [left]. [a,c] 1st EOF and [b,d] 2nd EOF of monthly SST anomaly. EOFs are computed during 1950-2014 from HadiSST & historical run of IITM-ESM.

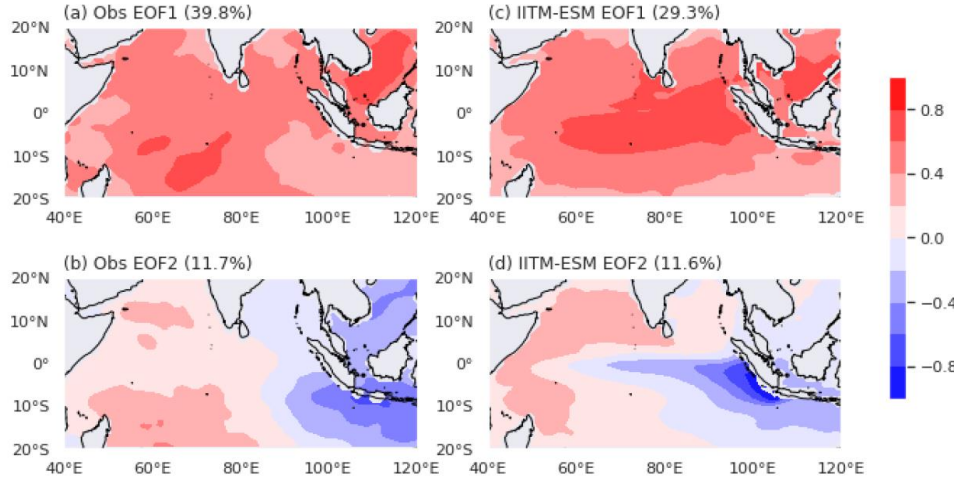

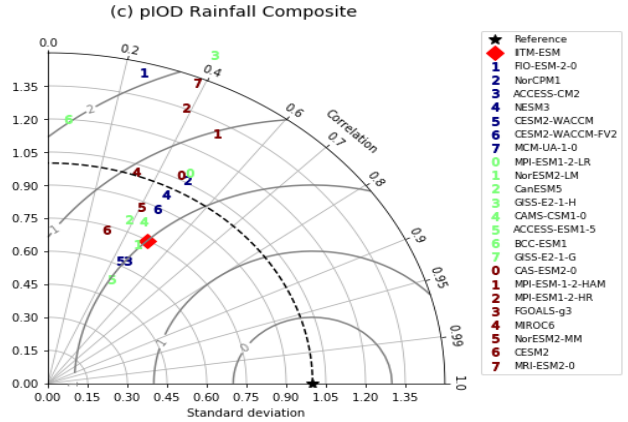

Taylor diagram showing the skill of IITM-ESM and other CMIP6 models in reproducing the rainfall anomaly over Indian land mass during pIOD years. Pattern correlation and stddev are computed from the pIOD composite anomalies of rainfall.

Prajeesh et al. 2021

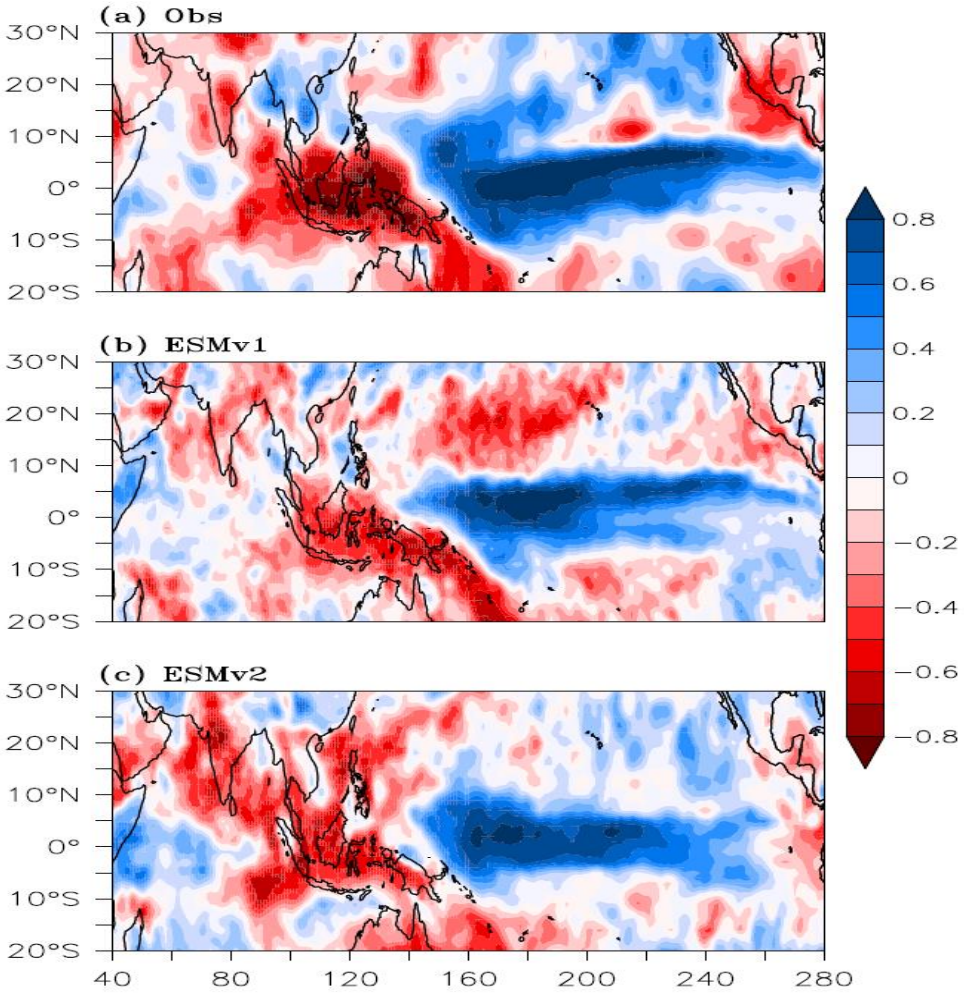

ENSO – Monsoon teleconnection

Precipitation anomalies during El Nino events from observations and IITM-ESMv1 and IITM-ESMv2.

MOM4p1 forced ocean simulation – 130 year spin up

Physical and Biogeochemical Parameters for Tropical Indian Ocean

SST and currents)

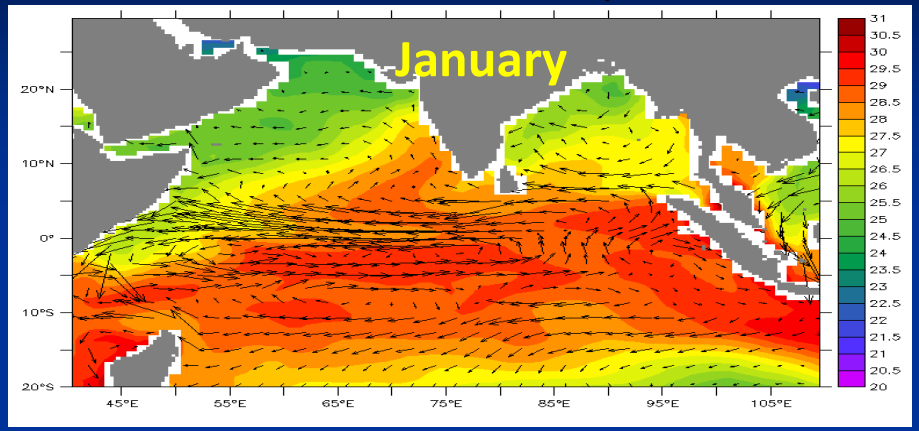

SST and currents)

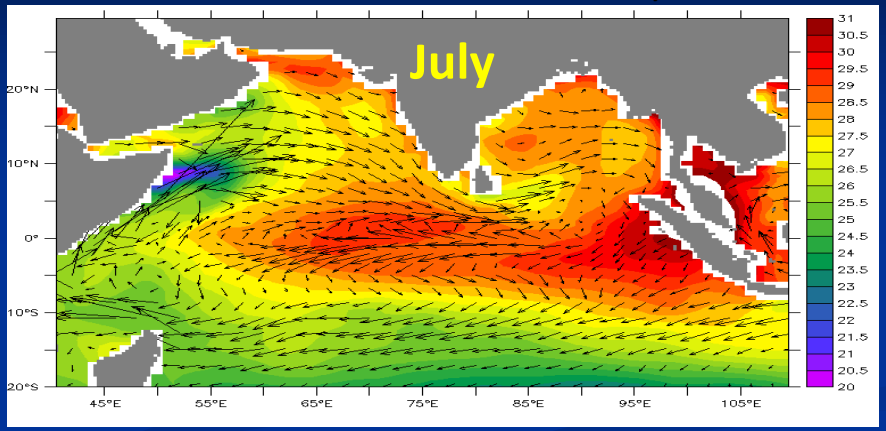

Chlorophyll

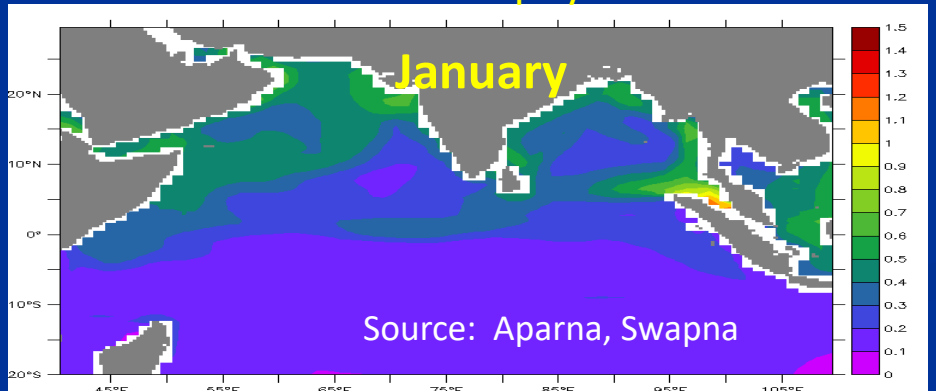

Source: Aparna, Swapna

Chlorophyll

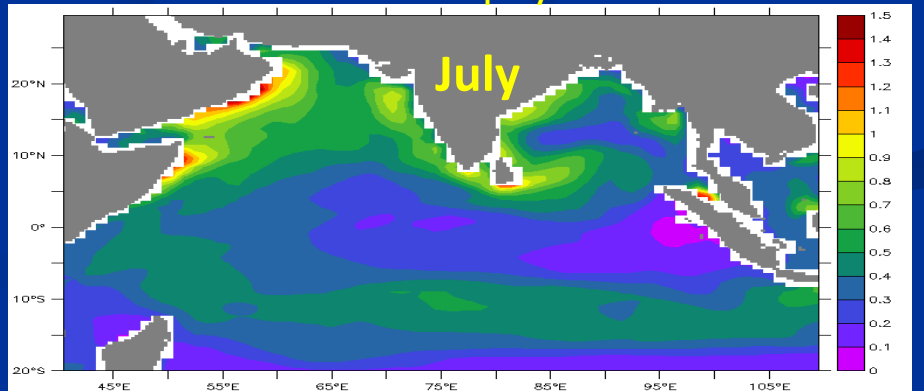

1997-98: Strongest El Niño ever recorded!

Sea Surface Temperature

Dec 1997 minus Dec 1998

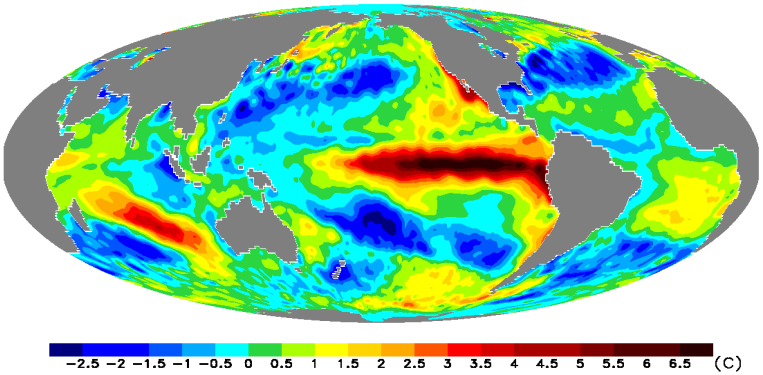

In January 1998 (top right) the 1997-1998 El Nino event was at its height. Because of the weakness of the trade winds at this time, the upwelling of nutrient-rich water was suppressed in the equatorial Pacific. The absence of a green band along the equator in this image is indicative of relatively low chlorophyll concentrations there.

By July 1998 (bottom right) the trade winds had strengthened and equatorial upwelling had resumed giving rise to widespread phytoplankton blooms in the equatorial belt

(Ref: Wallace and Hobbs, 2006)

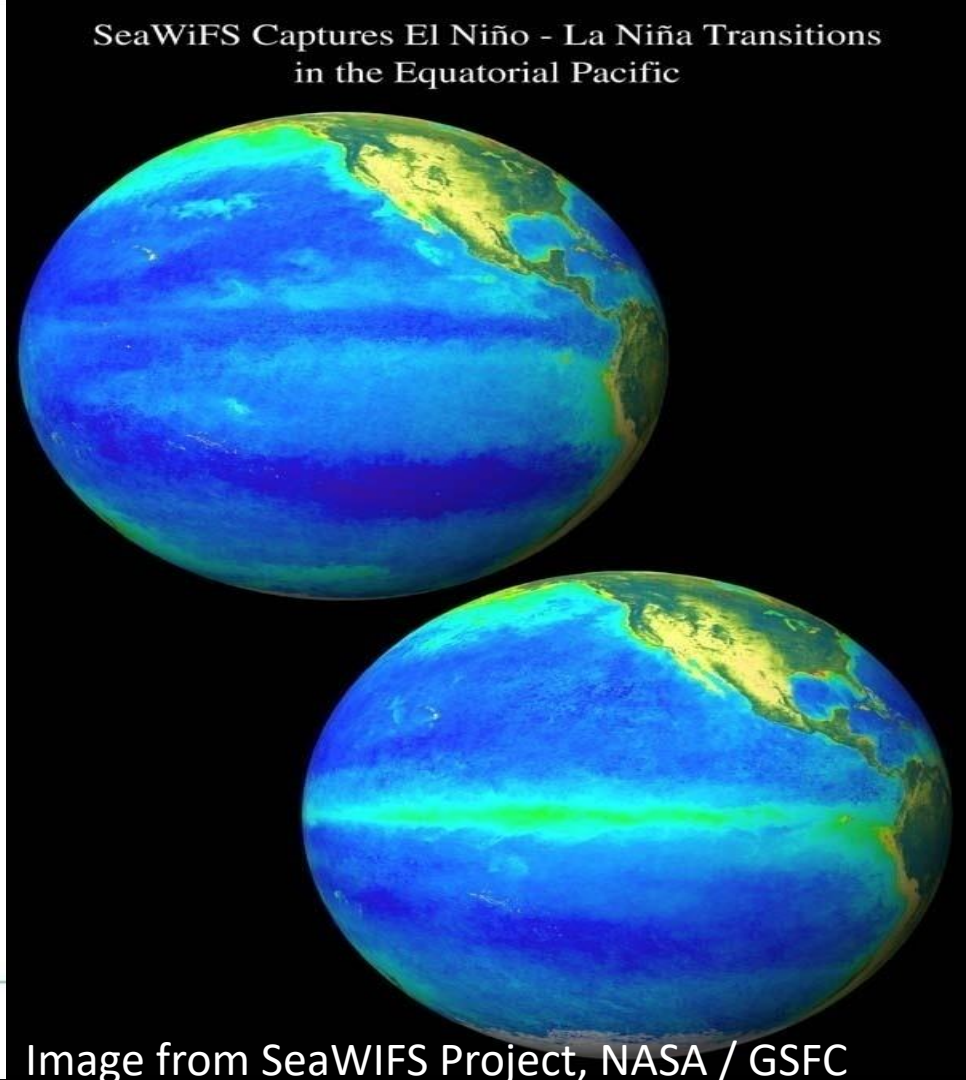

Image from SeaWIFS Project, NASA / GSFC

Chlorophyll Concentration (Mg m^{-3})

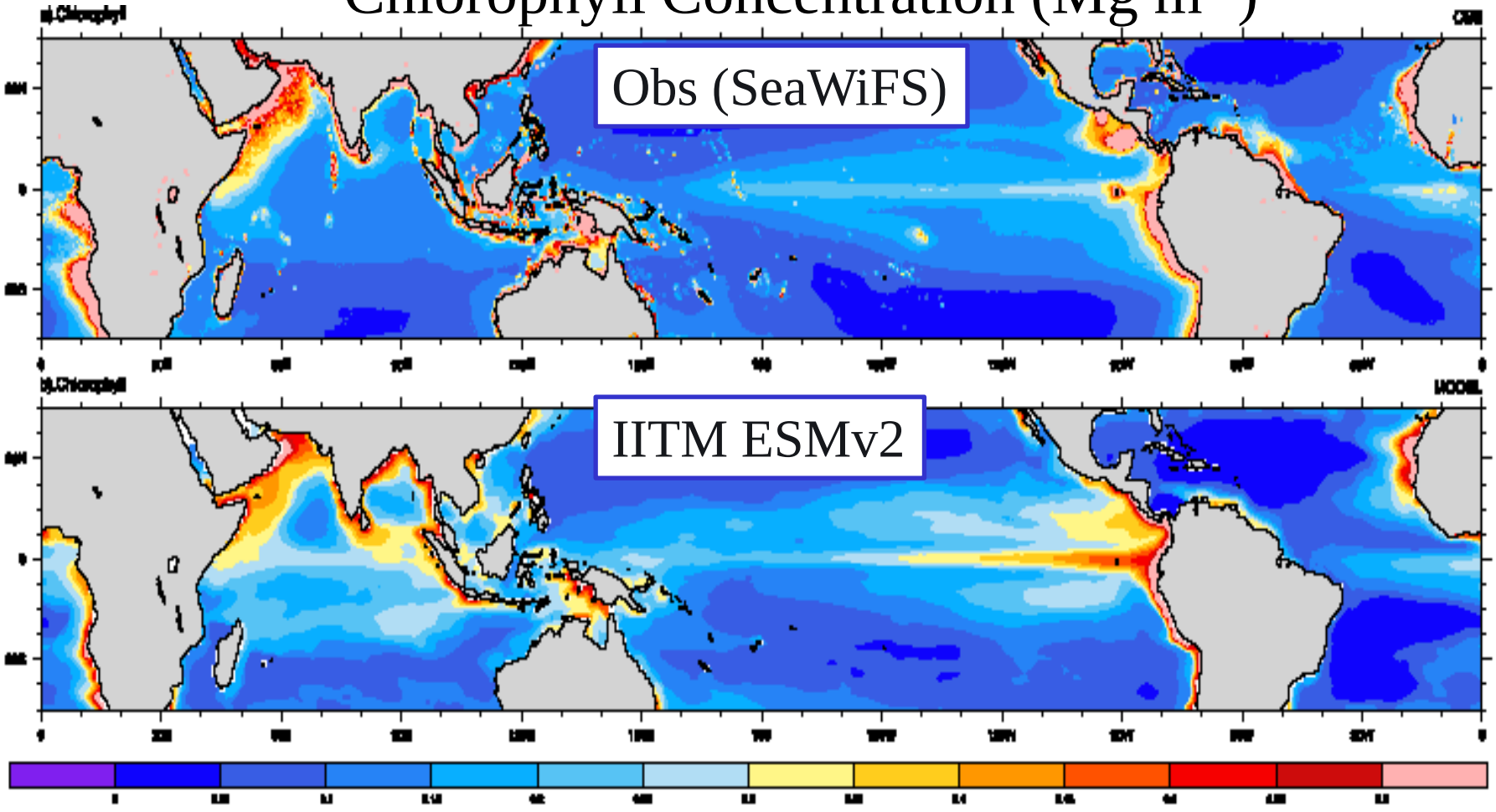

Courtesy: Sandeep, CCCR

MACv2-SP: a parameterization of anthropogenic aerosol optical properties and an associated Twomey effect for use in CMIP6

Bjorn Stevens[1], Stephanie Fiedler[1], Stefan Kinne[1], Karsten Peters[1], Sebastian Rast[1], Jobst Müsse[1], Steven J. Smith[2], and Thorsten Mauritsen[1]

[1]Max Planck Institute for Meteorology, Hamburg, Germany
[2]Joint Global Change Research Institute, Pacific Northwest National Laboratory, College Park, MD, USA

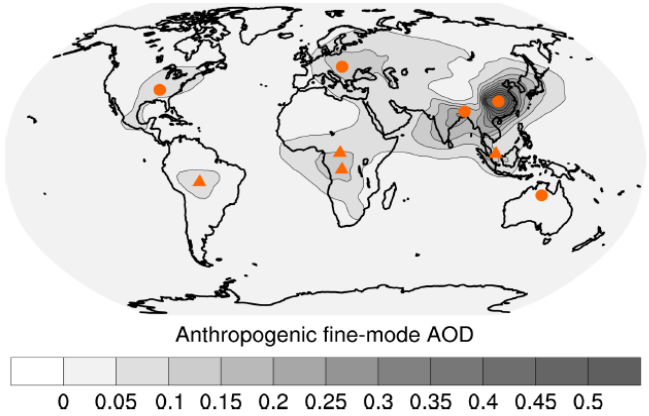

Figure 1. Global distribution of annually averaged anthropogenic aerosol optical depth τ_a at 550 nm. Also indicated are the locations of MACv2-SP plume centers. Industrial and biomass plumes are distinguished by the choice of symbol: circles for industrial plumes and triangles for biomass plumes.

Ayantika et al., 2020

No.	Source region	Lat.	Long.	Type	Main features of annual cycle
1	Europe	49.4	20.6	Industrial	Amplitude 25 %, May max
2	North America	40.1	277.5	Industrial	Amplitude 30 %, July max
3	East Asia	30.0	114.0	Industrial	Amplitude 15 %, biharmonic, Oct and Apr max
4	South Asia	23.3	88.0	Industrial	Amplitude 10 %, maximum in mid-July
5	North Africa	3.5	22.5	Biomass	Non-harmonic, Dec max, Mar–Oct min
6	South America	−10.3	298.0	Biomass	Non-harmonic, Sep max, Jan–Jun min
7	Maritime Continent	−1.0	106.0	Biomass	Non-harmonic, Sep max, Jan–Jun min
8	South central Africa	−3.5	16.0	Biomass	Non-harmonic, Aug max, Jan–Dec min
9	Australia	−20.0	135.0	Industrial	Amplitude 60 %, Sep max

Sensitivity experiments using IITM-ESM

Expt	CO2	Aerosols
PICTL (1850 cond)	284.2 ppmv	Natural
GHG	367.5 ppmv	Natural
AER	284.2 ppmv	Natural + Anthropogenic
COMB	367.5 ppmv	Natural + Anthropogenic

Changes in JJAS mean precipitation (mm / day) relative to PICTL

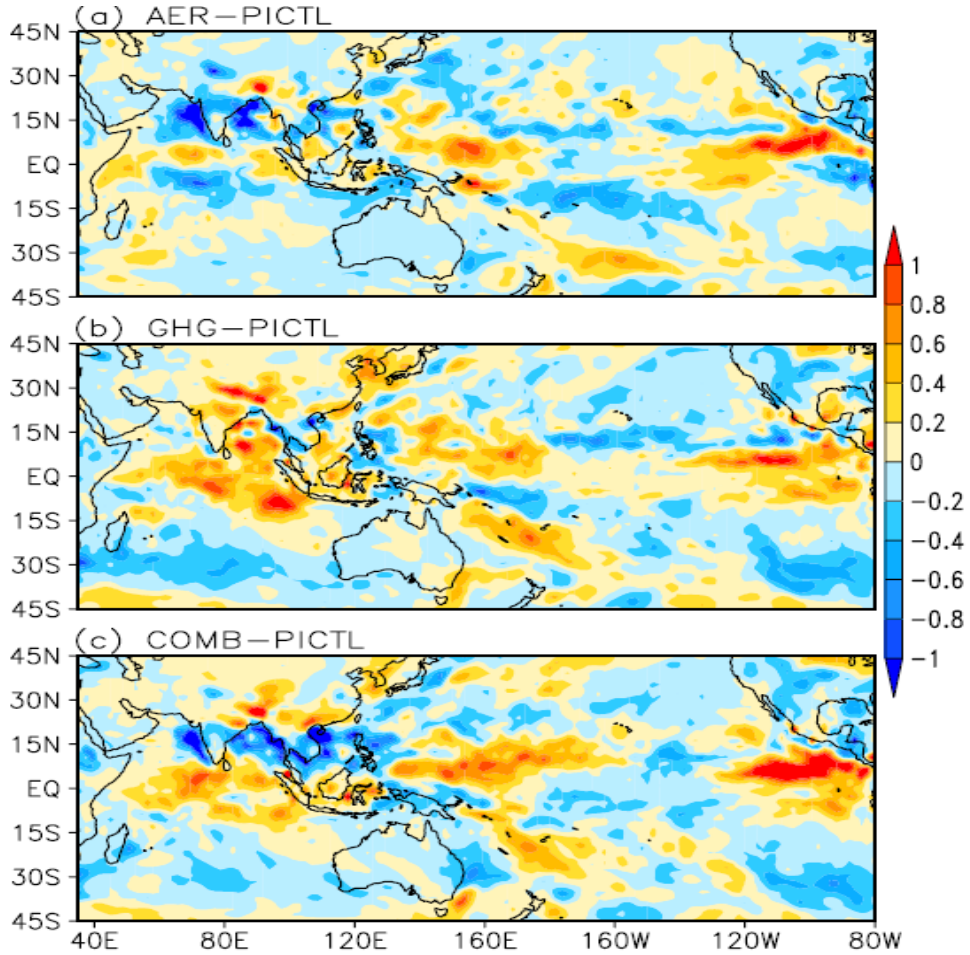

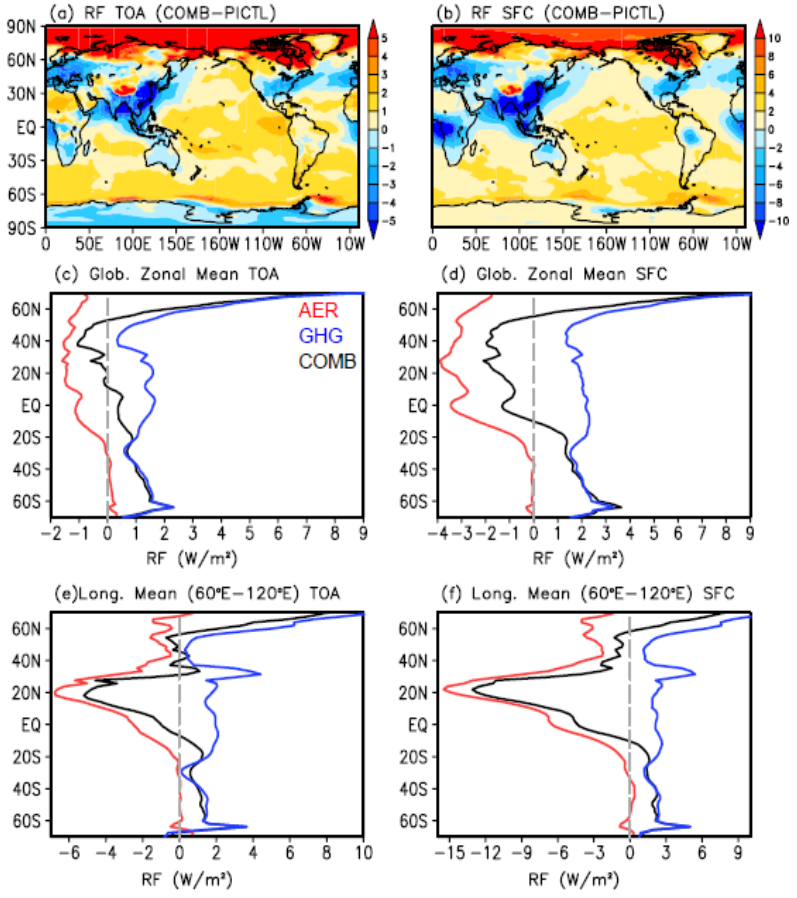

Ayantika et al., 2020

Large volcanic eruptions can trigger El Ninos

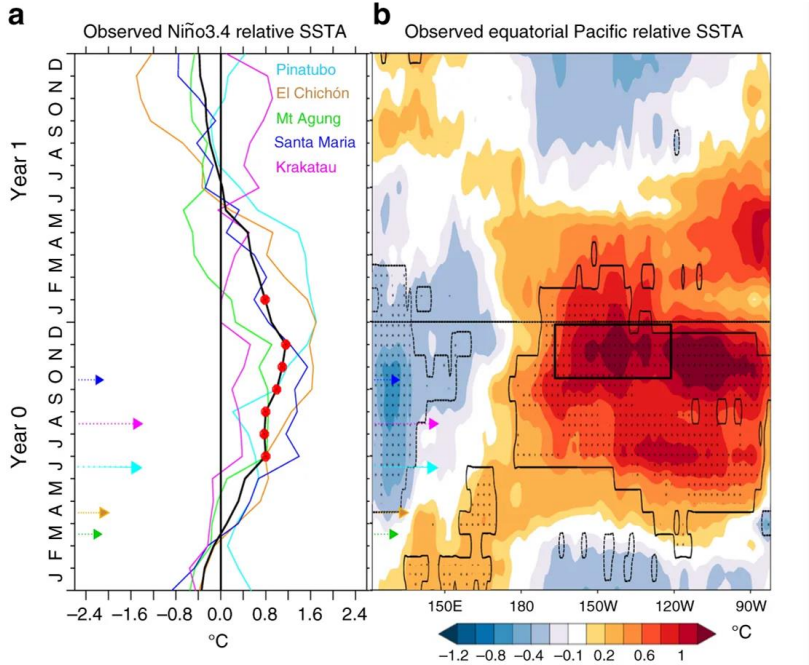

Khodri, M., Izumo, T., Vialard, J., Janicot, S., Cassou, C., Lengaigne, M., Mignot, J., Gastineau, G., Guilyardi, E., Lebas, N. and Robock, A., 2017. Tropical explosive volcanic eruptions can trigger El Niño by cooling tropical Africa. *Nature communications*, *8*(1), pp.1-13.

Agung eruption 1963-64, Bali, Indonesia. Photograph taken on 16 May 1963

Phase coherence analysis (PCA) observed ENSO-IM time series (Maraun and Kurths 2005)

Filtered ENSO and AIR

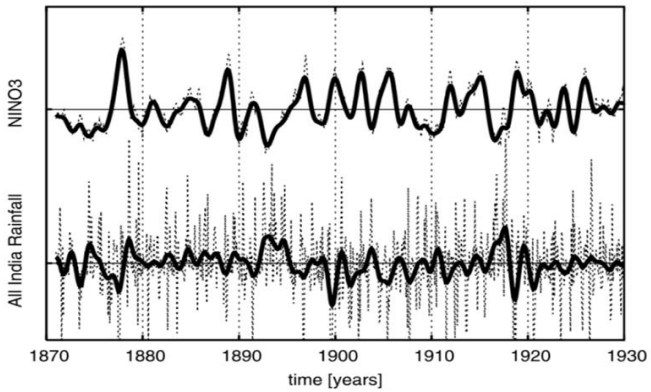

ENSO and IM phase difference and Volcanic Radiative Forcing (VRF)

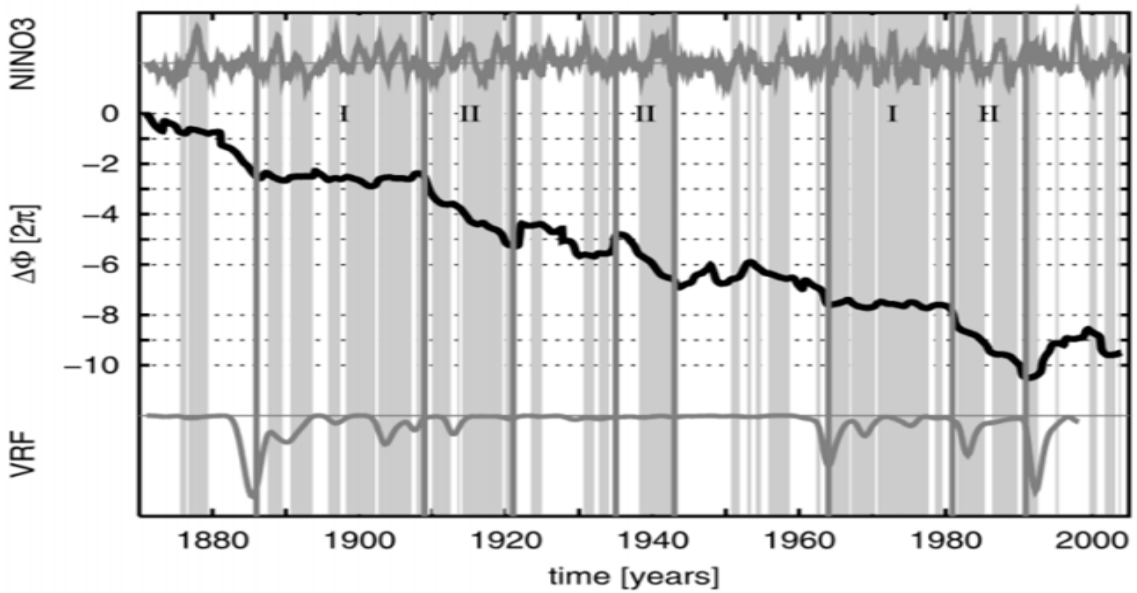

Maraun, D. and Kurths, J., 2005. Epochs of phase coherence between El Nino/Southern Oscillation and Indian monsoon. Geophysical Research Letters, 32(15).

IITM-ESM Large Ensemble Experiments: Volcanic forcing & ENSO-Indian monsoon Coupling

SCIENCE ADVANCES | RESEARCH ARTICLE

GEOLOGY

Fingerprint of volcanic forcing on the ENSO–Indian monsoon coupling

M. Singh[1,2], R. Krishnan[1]*, B. Goswami[3,4], A. D. Choudhury[1], P. Swapna[1], R. Vellore[1], A. G. Prajeesh[1], N. Sandeep[1], C. Venkataraman[2], R. V. Donner[3,5], N. Marwan[3], J. Kurths[3,6]

Coupling of the El Niño–Southern Oscillation (ENSO) and Indian monsoon (IM) is central to seasonal summer monsoon rainfall predictions over the Indian subcontinent, although a nonstationary relationship between the two nonlinear phenomena can limit seasonal predictability. Radiative effects of volcanic aerosols injected into the stratosphere during large volcanic eruptions (LVEs) tend to alter ENSO evolution; however, their impact on ENSO-IM coupling remains unclear. Here, we investigate how LVEs influence the nonlinear behavior of the ENSO and IM dynamical systems using historical data, 25 paleoclimate reconstructions, last-millennium climate simulations, large-ensemble targeted climate sensitivity experiments, and advanced analysis techniques. Our findings show that LVEs promote a significantly enhanced phase-synchronization of the ENSO and IM oscillations, due to an increase in the angular frequency of ENSO. The results also shed innovative insights into the physical mechanism underlying the LVE-induced enhancement of ENSO-IM coupling and strengthen the prospects for improved seasonal monsoon predictions.

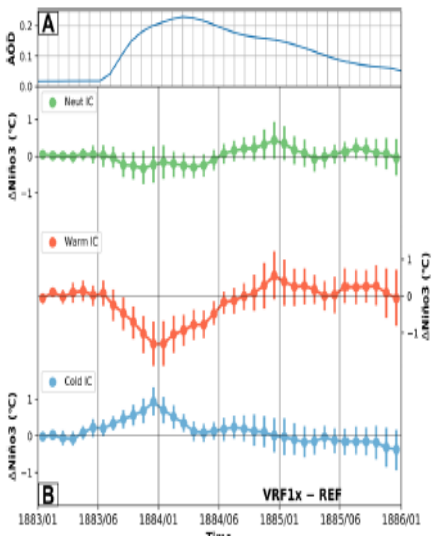

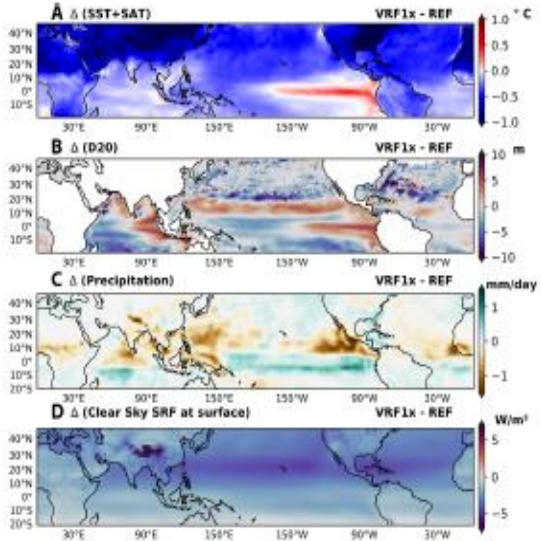

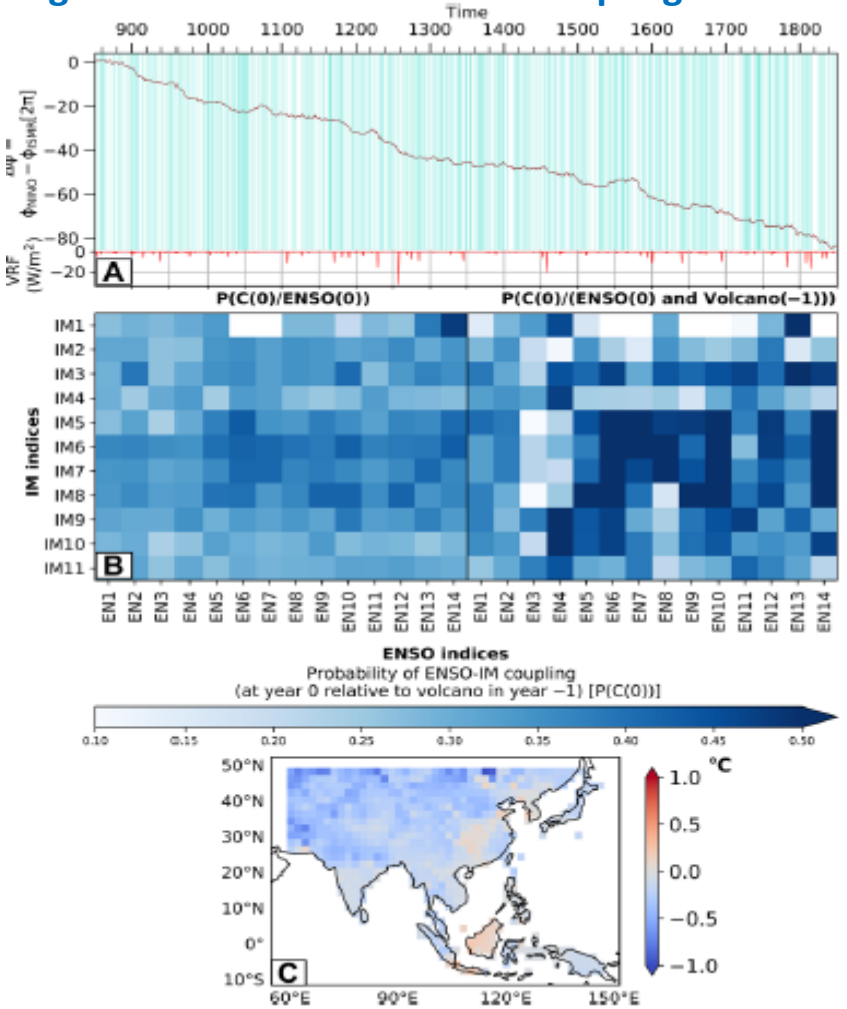

ARTICLE

https://doi.org/10.1038/s41467-021-24943-7 OPEN

Climate change modulates the stratospheric volcanic sulfate aerosol lifecycle and radiative forcing from tropical eruptions

Thomas J. Aubry[1,2✉], John Staunton-Sykes[3], Lauren R. Marshall[3], Jim Haywood[4,5], Nathan Luke Abraham[3,6] & Anja Schmidt[1,3]

Aubry et al., 2021

Explosive volcanic eruptions affect climate, but how climate change affects the stratospheric volcanic sulfate aerosol lifecycle and radiative forcing remains unexplored. We combine an eruptive column model with an aerosol-climate model to show that the stratospheric aerosol optical depth perturbation from frequent moderate-magnitude tropical eruptions (e.g. Nabro 2011) will be reduced by 75% in a high-end warming scenario compared to today, a consequence of future tropopause height rise and unchanged eruptive column height. In contrast, global-mean radiative forcing, stratospheric warming and surface cooling from infrequent large-magnitude tropical eruptions (e.g. Mt. Pinatubo 1991) will be exacerbated by 30%, 52 and 15% in the future, respectively. These changes are driven by an aerosol size decrease, mainly caused by the acceleration of the Brewer-Dobson circulation, and an increase in eruptive column height. Quantifying changes in both eruptive column dynamics and aerosol lifecycle is therefore key to assessing the climate response to future eruptions.

"What really matters is whether these [volcanic aerosols] are injected into the stratosphere—that is, above 16 kilometers in the tropics under current climate conditions and closer to 10 kilometers at high latitudes," explained Thomas Aubry (https://www.geog.cam.ac.uk/people/aubry/), a geophysicist at the University of Cambridge in the United Kingdom and lead author of the new study. "If [aerosols] are injected at these altitudes, they can stay in the atmosphere for a couple of years. If they are injected at lower altitudes, they are essentially going to be washed out by precipitation in the troposphere. The climatic effect will only last for a few weeks."

The power of a volcanic eruption influences the elevation at which gases enter the atmosphere, with stronger eruptions injecting more aerosols into the stratosphere. The buoyancy of the gases also contributes to the elevation at which they settle in the atmosphere. Climate change could affect this buoyancy: As the atmosphere warms, it becomes less dense, increasing the elevation at which aerosols reach neutral buoyancy.

Climate Change Will Alter Cooling Effects of Volcanic Eruptions

EOS, 2021

New research indicates the cooling effect of rare, large eruptions will increase, whereas the effects of more frequent, smaller eruptions will be reduced.

The eruption of Mount Pinatubo, Philippines, in June 1991 was one of the most powerful of the most powerful of the 20th century.

IITM-ESM CMIP6 simulations (Completed)

Experiments	Details of Simulation	No. of years of integration
PI-Control	Pre-industrial control simulation	500 yrs
Transient CO2 runs	1% /Yr increase in CO2 to quadrupling	140 yrs
	Abruptly Quadruple CO2 and fix	140 yrs
CMIP6	Historical	1850-2014 (165 yrs x 3 memb) = 495 years
GMMIP & AMIP	AMIP Simulation	1850-2014 (165 yrs)
DAMIP	GHG only, aerosol only and hist-nat	1850-2014 (165 yrs x 3 expts) = 495 years
FAFMIP	Heat & Freshwater exp	~70 yrs x 2 expts = 140 years
Future Projections	Future projections SSP1-2.6, SSP2-4.5, SSP3-7.0, SSP58.5	2015-2100 (86 yrs x 4 scenarios) = 344 years

Total = 2419 years

CMIP6 PROJECTED GLOBAL CHANGES OVER THE 21ST CENTURY

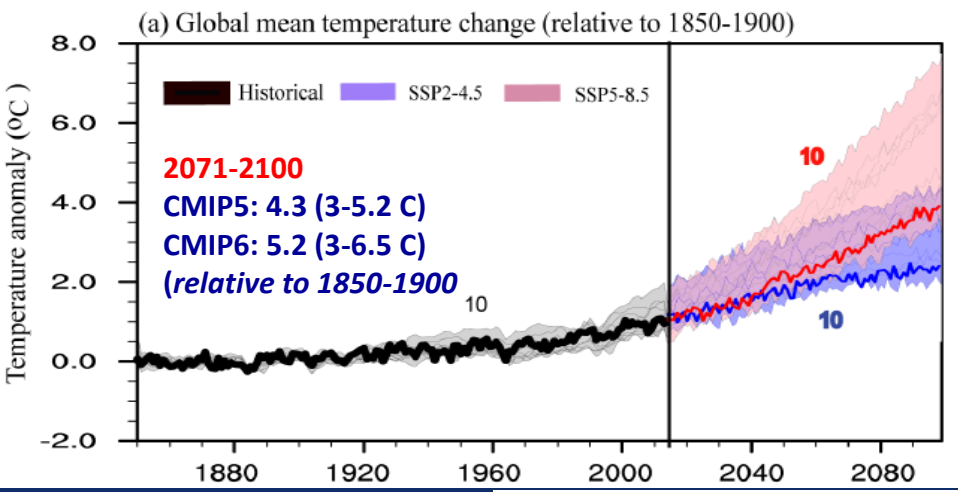

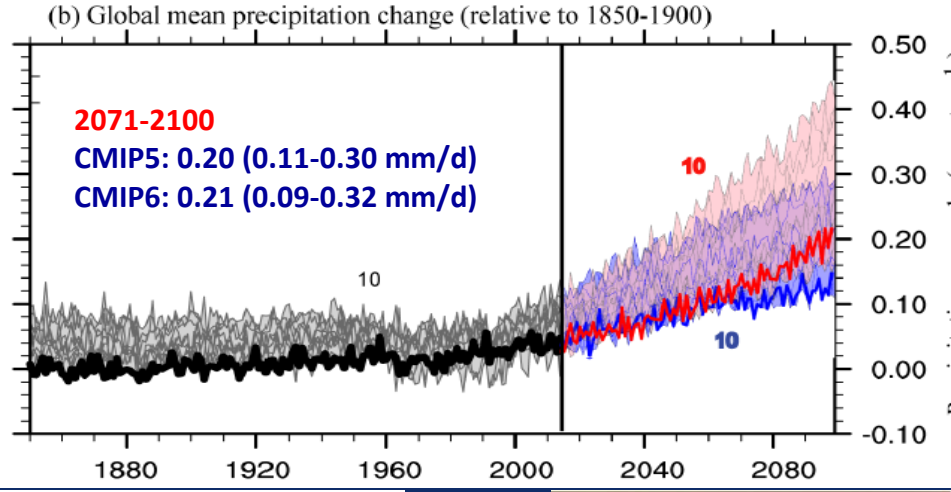

CMIP6 projected warming > CMIP5 more than 20%

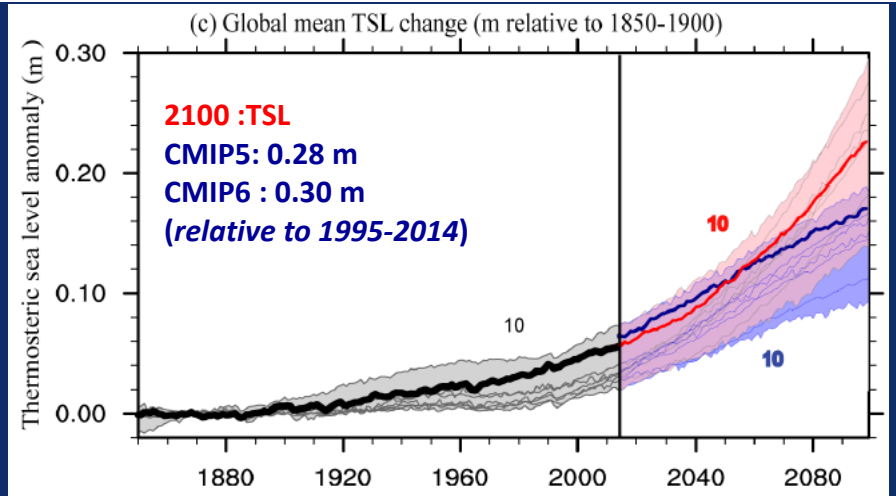

Climate Change Assessment Report over the Indian Region, MoES, Govt. of India (2020)

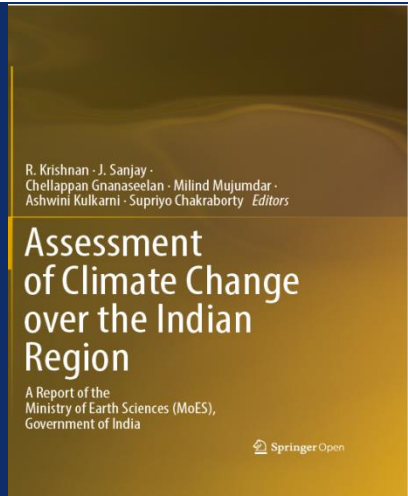

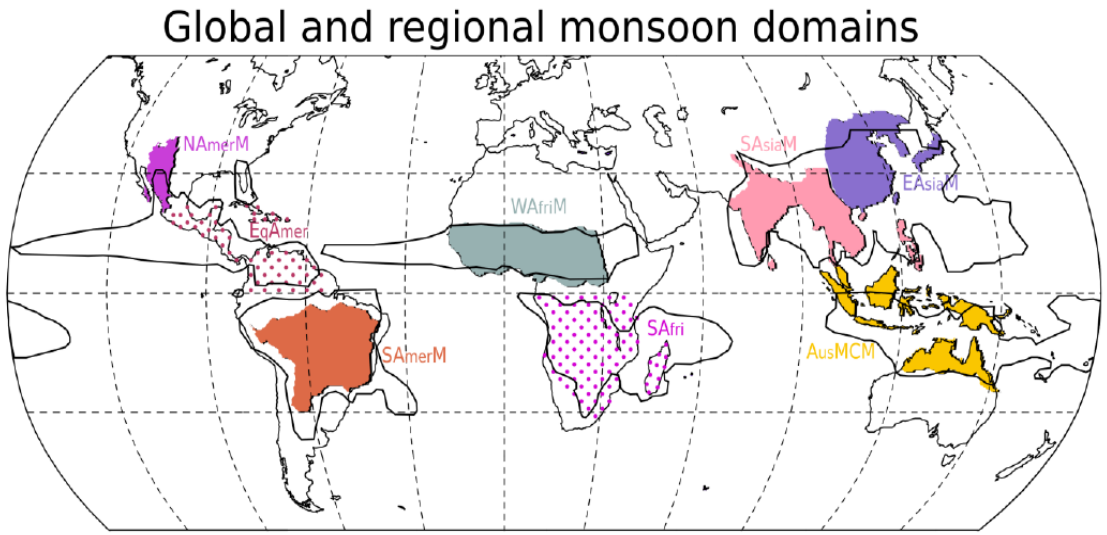

Figure AV.1 - **Annex V: Monsoons**

Global (black contour) and regional monsoons (color shaded) domains. The global monsoon (*GM*) is defined as the area with local summer-minus-winter precipitation rate exceeding 2.5 mm day^{-1}. The regional monsoon domains are defined based on published literature and expert judgement and also accounting for the fact that the climatological summer monsoon rainy season varies across the individual regions.

Box TS.13: Monsoons

- Global land monsoon precipitation decreased from the 1950s to the 1980s, partly due to anthropogenic aerosols, but has increased since then in response to GHG forcing and large-scale multi-decadal variability (*medium confidence*).
- During the 21st century, global land monsoon precipitation is projected to increase in response to GHG warming in all time horizons and scenarios (*high confidence*).
- In the long term, global monsoon rainfall change will feature a robust north-south asymmetry characterized by a greater increase in the Northern Hemisphere than in the Southern Hemisphere and an east-west asymmetry characterized by enhanced Asian-African monsoons and a weakened North American monsoon (*medium confidence*).

Trend and change in monsoon precipitation (1951-2014) for South & Southeast Asia (SAsiaM) and East Asia (EAsiaM)

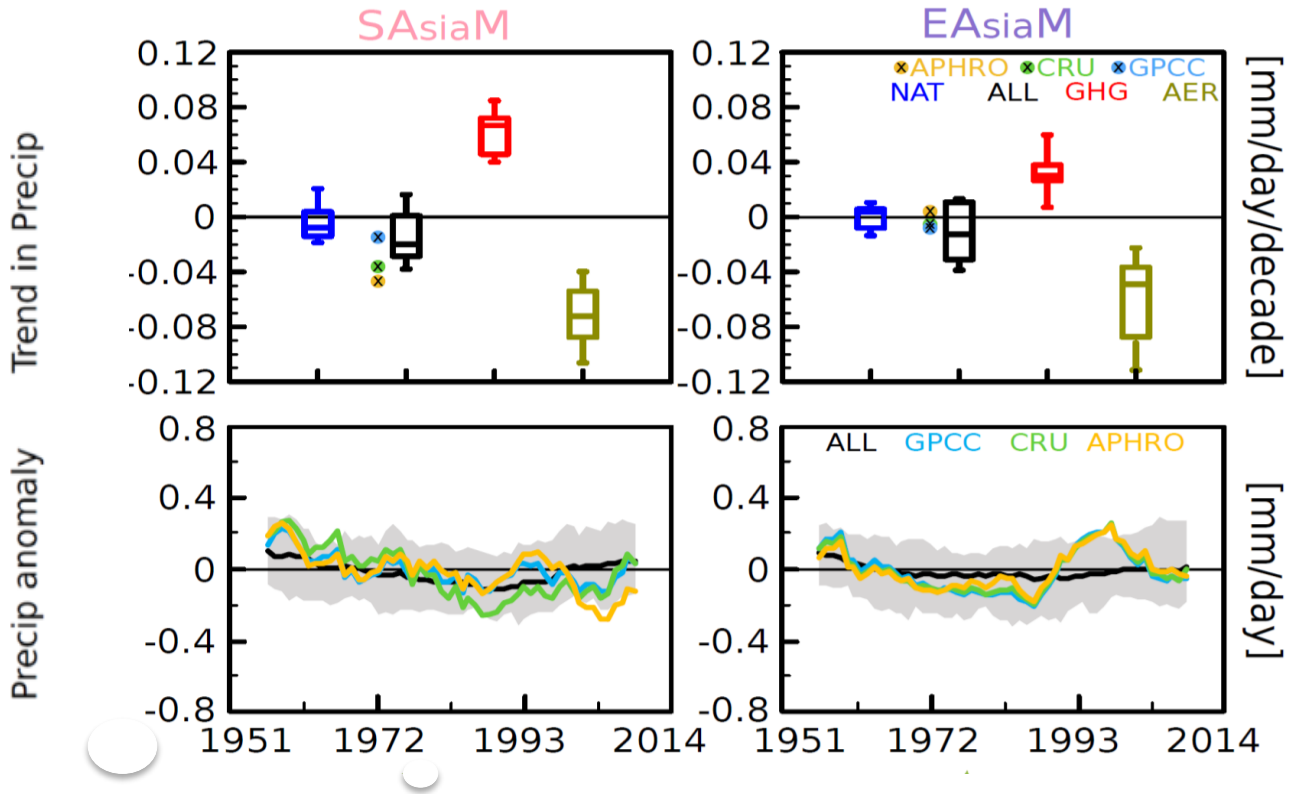

Figure 8.11

CMIP6 projected changes in monsoon precipitation for South and Southeast Asia (SAsiaM) and East Asia (EAsiaM)

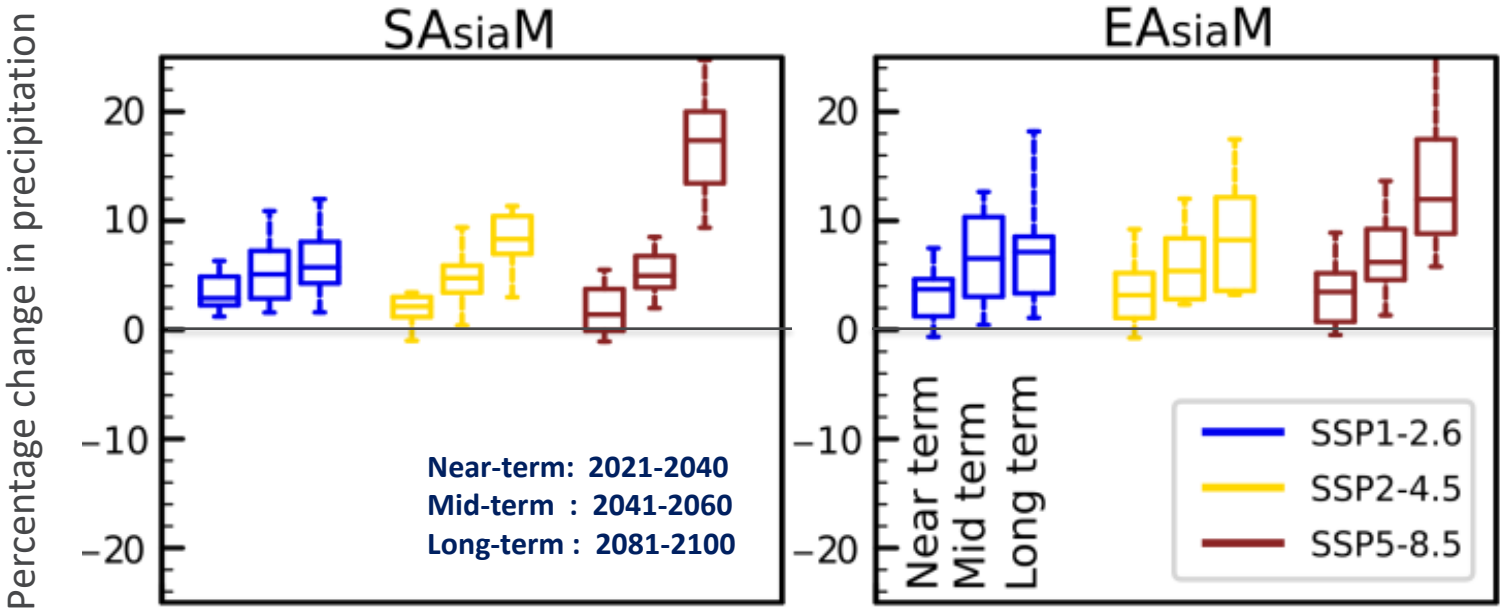

Figure 8.22

Asian Monsoons

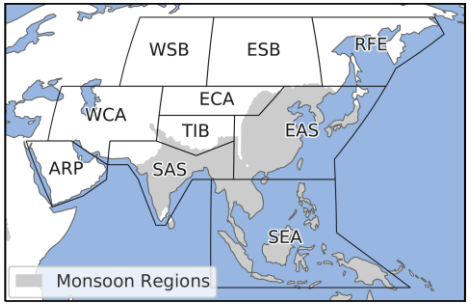

- The South and Southeast Asian monsoon precipitation decreased since the mid-20th century (*high confidence*), the dominant cause being anthropogenic aerosol forcing.
- The dry-north and wet-south pattern of East Asian summer monsoon precipitation change results from the combined effects of greenhouse gases and aerosols (*high confidence*).
- In the near-term (2021-2040), South and Southeast Asian monsoon and East Asian summer monsoon precipitation will be dominated by the effects of internal variability (*medium confidence*), but will increase in the long-term (2081-2100) (*medium confidence*).

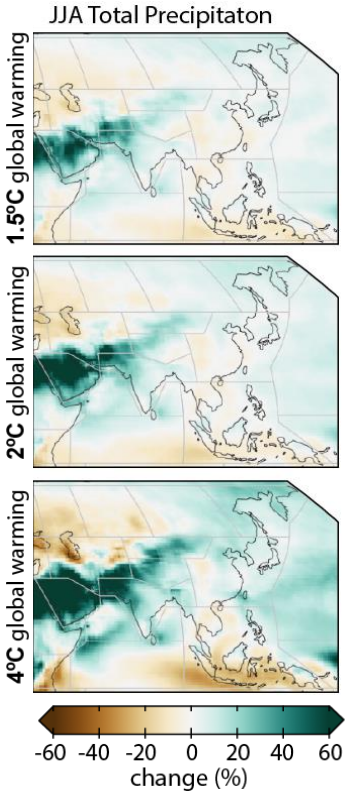

West African Monsoon

Trend and change in Precipitation (1951-2014)

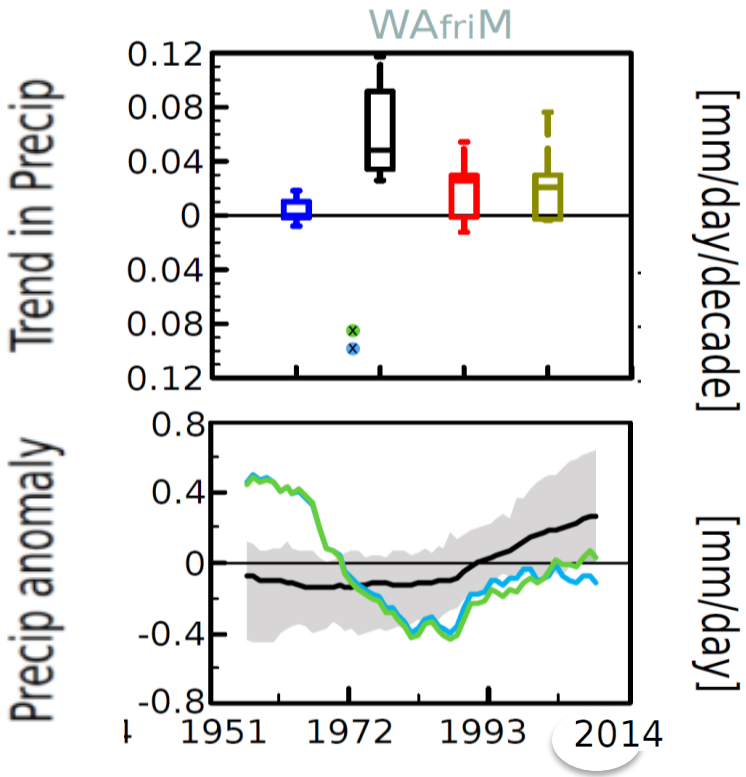

West African Monsoon

Projected changes in precipitation

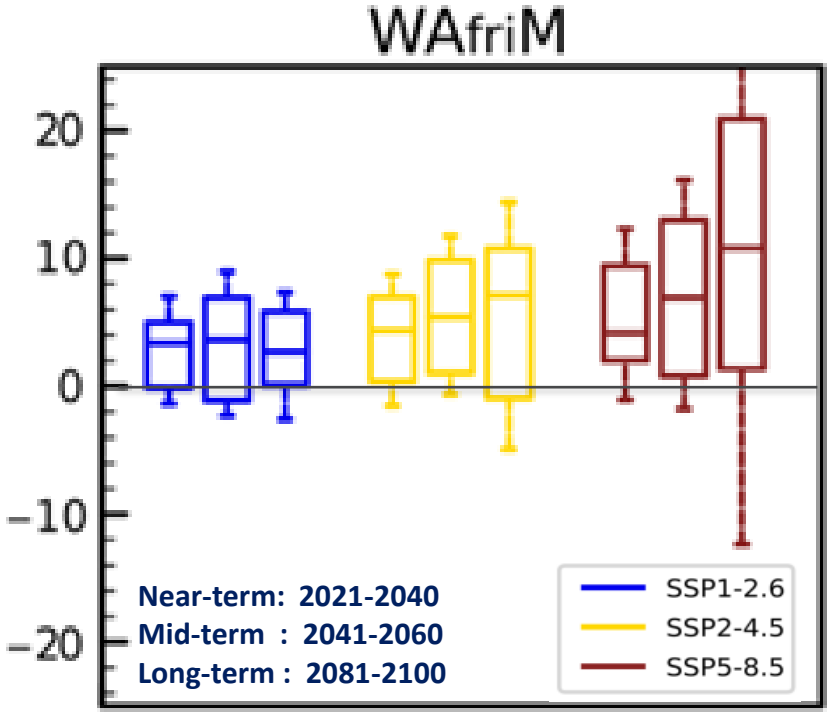

- **IITM ESMv1:** First version of IITM ESM was successfully developed at CCCR, IITM by incorporating MOM4P1 (with ocean biogeochemistry) component in CFSv2. Major improvements are seen in IITM ESMv1 vis-à-vis CFSv2 :
  - Significant reduction of cold bias of global mean SST by ~0.8^{o}C
  - ENSO & PDO are robust and spatially more coherent in ESM1.0
  - ENSO and monsoon links are well-captured
  - The IITM Earth System Model: Transformation of a seasonal prediction model to a long term climate model - *Swapna et al. 2015 (Bulletin of American Meteorological Society)*
- **IITM ESMv2:** Further improvements are incorporated in IITM ESMv1 *(Swapna et al. 2018*)
  - Reduced TOA radiation imbalance significantly
  - Improved mean monsoon precipitation, Indian Ocean Dipole (IOD) …
  - Improved sea-ice distribution in the Arctic and Antarctic
  - Improved Atlantic Meridional Overturning Circulation (AMOC)
  - Interactive ocean biogeochemistry
  - Included time-varying aerosol properties (3D fields) for the CMIP experiments
  - Included hydrological balance through discharge of runoff from land to ocean
- **IITM ESMv2:** Contributed to CMIP6, IPCC AR6 and National Climate Change Report (MoES)

Ongoing / Future Plans

•Development of High Resolution Global Model (~grid size 27 km) Atmospheric version of IITM-ESM for dynamical downscaling. Generation of high resolution global climate and monsoon projections. Timeline: 2019-2024

•Development of next-generation IITM-ESM Timeline: 2020-2025+

- New Dynamical Core (TCO Grid)
- Ice-sheets
- Interactive aerosols and atmospheric chemistry
- Carbon cycle

•Development of Community Indian Earth System Model **(CIESM)**: 2020-2025

•Participation in CMIP7

Ongoing & future work: High resolution (27 km grid) global climate model (T574)

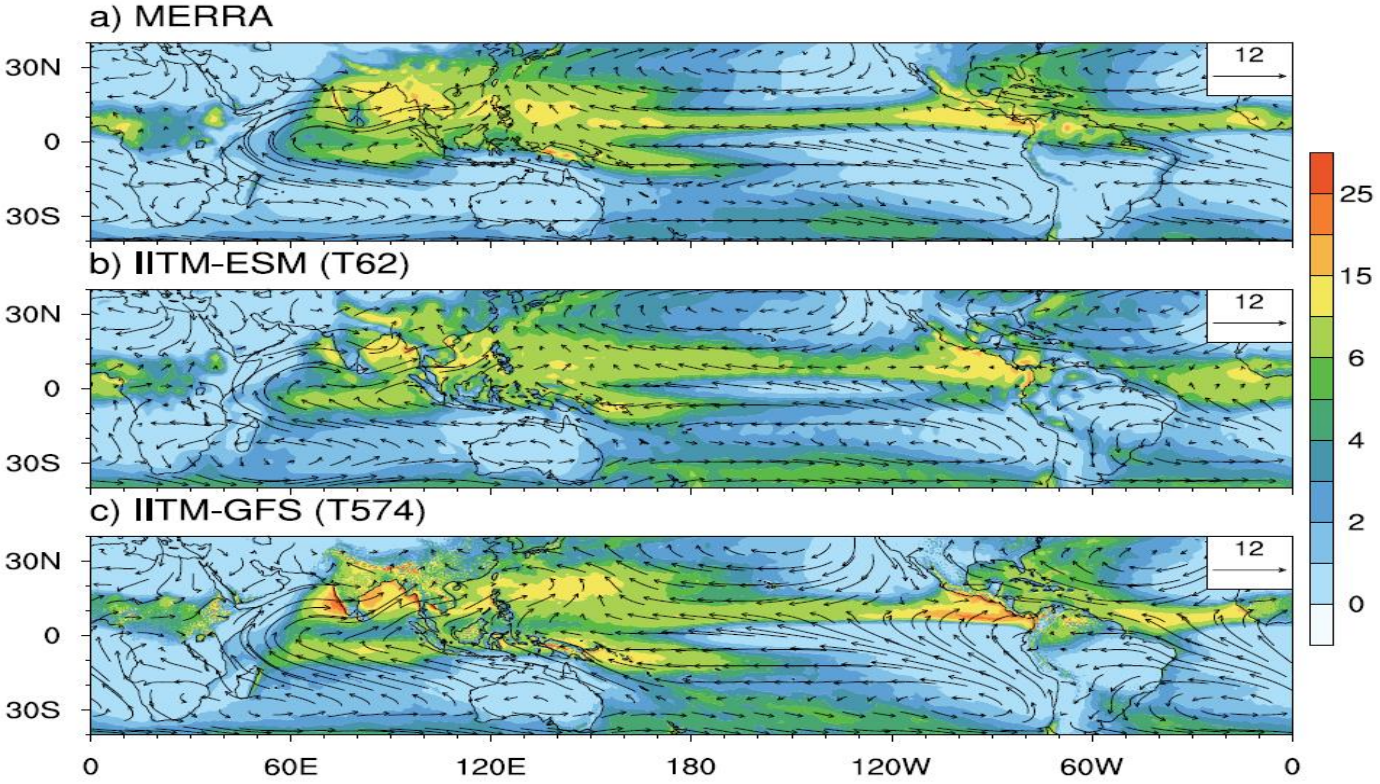

Fig. Spatial maps of climatological mean precipitation (mm day^{-1}) and 850 hPa winds during the boreal summer monsoon (June – September) season **(a)** TRMM precipitation and MERRA reanalysis winds **(b)** IITM-ESMv2 (PI control simulation) and **(c)** High-resolution (T574: 27 km grid) atmospheric-only version of IITM-ESMv2. The simulated means are based on the last 50 years of the PI Control experiment and 10 years from high-resolution atmospheric-only version of IITM-ESMv2.

Courtesy: Sabin

Land-Ice Sheet Model Experiments

Trend in ice surface temperature (1981-2010)

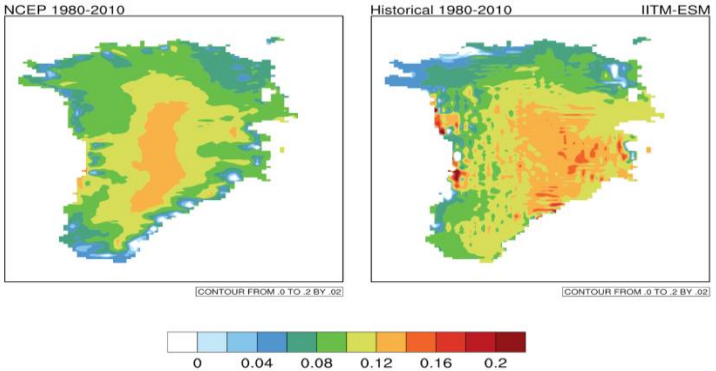

Trend in ablation (1981-2010)

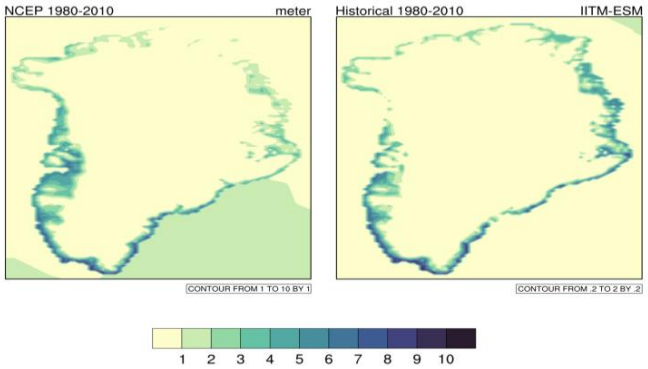

Courtesy: Sandeep, CCCR, IITM

NX x NY: **192 x 94**

T62

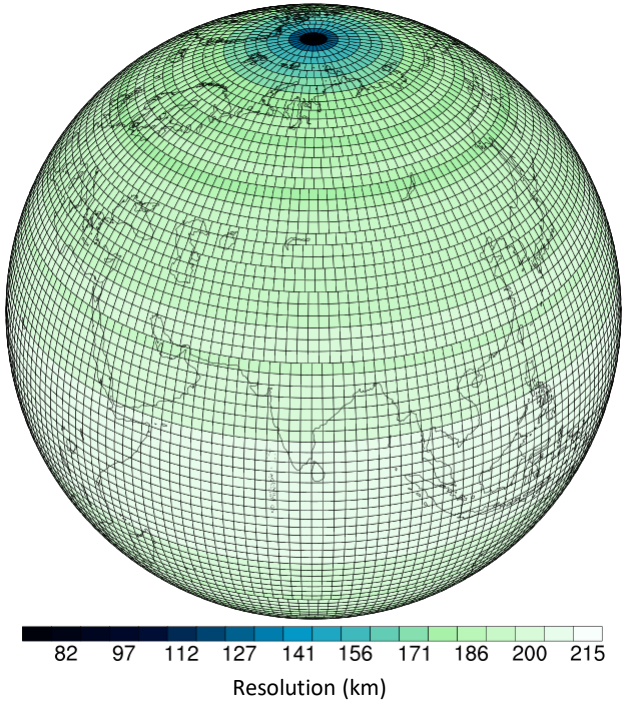

Triangular (T)

TCO62

NX x NY: **256 x 128**

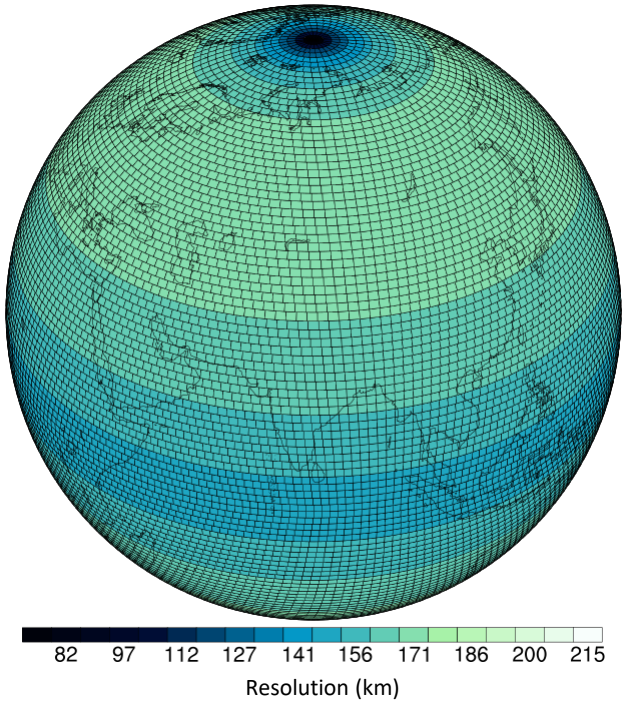

Triangular Cubic Octahedral (TCO)

Higher effective resolution

Higher resolution in tropics

Modified diffusion

30% less number of grid points (effective resolution): less memory requirement

Can be parallelized more efficiently: Lower computational cost

How to generate an octahedral reduced Gaussian grid

B

1. Imagine each hemisphere of the globe is divided into 4 quarters, with each quarter corresponding to one face of an octahedron (left).
2. Start with 20 points, i.e. 5 per quarter, at the Gaussian latitude closest to the pole (middle).
3. Add one point per quarter for each new Gaussian latitude towards the equator, i.e. 4 more points per Gaussian latitude circle.
4. Because of the curvature of the Earth, the spacing between the grid points along a latitude circle varies with the latitude. It is slightly wider in the mid-latitudes than at the equator and near the pole (right).

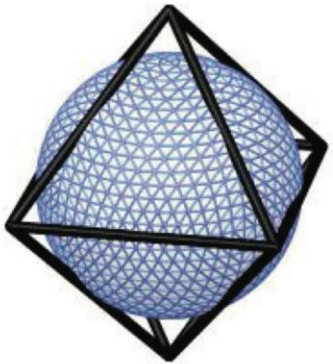

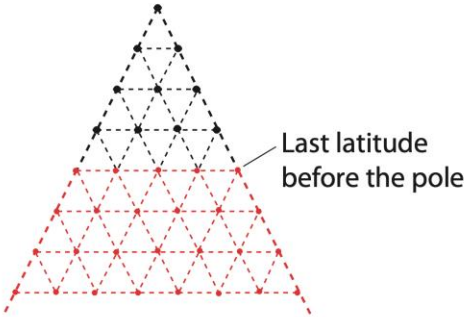

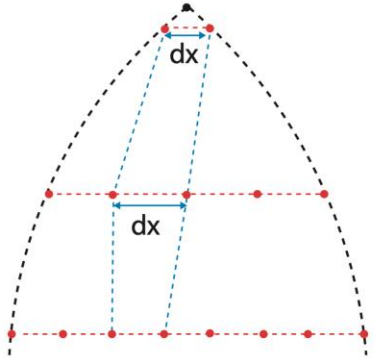

Malardel, S., et. Al., “A New Grid for the IFS,” 2016.

Thanks for your kind attention!